University of Alberta

Determination of Biokinetic Parameters of Wastewater Biofilms from Oxygen Concentration Profiles

by

Sabinus Ikemefule Okafor

A thesis submitted to the Faculty of Graduate Studies and Research
in partial fulfillment of the requirements for the degree of

Masters of Science

in

Environmental Science

Department of Civil & Environmental Engineering

Fall 2011
Edmonton, Alberta

This thesis is dedicated to my wife, ***Chinenye****, my parents,* ***Chief. Dennis O. Okafor and Mrs. Eunice Onyemaelu Okafor****, and my siblings-* ***Edus, Marcel, Verna, Franca, Bonny, Chinedu and Chigozie.***

I would not have reached this far in my career without your love, understanding, prayers, encouragement and support. I thank God for making me a part of you. I love you with all of my heart!

Abstract

The process of scale-up and rational optimization of biofilm processes for effective wastewater treatment and reuse require better understanding of the biokinetic behavior of microorganisms in the biofilms. At present, no fast and accurate methods exist for determining kinetic parameters for biofilm systems. This study presents a modified approach to quantify biofilm kinetic parameters from oxygen concentration profiles measured in membrane-aerated biofilms (MABs) and rotating biological contactors (RBC) biofilms.

The calculated values of Monod's half-saturation coefficient (K_s) for oxygen consumption and maximum utilization rate of oxygen (μ_m/Y) in MABs were estimated to be 2.01 mg O_2/cm^3 and 6.50×10^{-8} mgO_2/gVS·s, respectively. And, the values of first-order kinetic coefficient, $(\mu_m/Y)/K_s$, in MABs and RBC biofilms were in the range of $(0.62\text{-}1.43)\times10^{-6}$ and $(0.36\text{-}5.55)\times10^{-5}cm^3$/gVS·s, respectively. The biofilm kinetic parameters obtained in this study were found to differ from the same parameters in activated sludge systems, which show that more experimental data for kinetic parameters in biofilms are required.

Acknowledgements

To start with, I am highly grateful to my research supervisor, Dr. Tong Yu, for his excellent academic supervision and uninterrupted financial support throughout the course of my graduate work. I lack enough words to express my gratitude to you and if I have to do it all over again, you would still be my research supervisor. I am also grateful to the other members of thesis examining committee, Dr. Julia Foght and Dr. Ania Ulrich for their insights and suggestions on the revision of this thesis.

I am grateful to Maria Demeter, Jela Burkus and Jody Yu for providing me their technical assistance with the experiments and purchasing lab supplies. You were all parts of the vehicle that propelled my research to the stage that it formed a successful M.Sc. thesis.

This thesis would not have been completed without the assistance of my colleagues in Dr. Tong Yu's research group. First and foremost, I thank Shuying Tan for designing the membrane aerated biofilm reactors and teaching me how to successfully operate biofilm reactors. I also thank Kusumakar Sharma for helping me understood the engineering aspects of reactor operations and assisting with the microsensor measurements. I cannot forget to thank you, my teacher, Dr. Xiaohong Zhou for providing me with oxygen microsensors for my first microsensor measurements and the unalloyed support that you offered me throughout the course of my graduate program. I am equally grateful to Hong Liu for fabricating the microsensors and Shujie Ren for assisting me with the reactor operations.

I am grateful to the Canada (AB.AET)-China (MOST) Collaborative Project and Natural Sciences and Engineering Research Council of Canada (NSERC) for funding my research thesis project. I would also like to thank the Department of

Civil and Environmental Engineering for proving an excellent environment for graduate studies.

Finally, to the many friends I have made since I came to Edmonton, you are too numerous to mention, but I thank you for enriching my graduate experience.

Table of Contents

List of Tables

List of Figures

List of Symbols

A	Surface area of the oxygen microsensor tip
C	Oxygen concentration (mg/L or mg/cm^3)
D_{fl}	Local effective diffusivity of oxygen (cm^2/s)
$D_{e,z}$	Averaged effective diffusivity of oxygen in biofilm (cm^2/s)
D^*_{fz}	Surface-averaged relative effective diffusivity (dimensionless)
D_w	Effective diffusivity of oxygen in water (cm^2/s)
i	Limiting current density (A/cm^2)
I	Limiting current signal from the oxygen microsensor (amperes)
K_s	Monod half-saturation coefficient (mg/cm^3)
L_f	Distance travelled by the oxygen microsensor (cm)
R_s	Oxygen reaction rate (mg/cm^3·s)
μ_m/Y	Maximum specific rate of oxygen utilization (mgO_2/gVS·s)
$(\mu_m/Y)/K_s$	First-order kinetic coefficient (cm^3/gVS·s)
$\bar{X}_f$	Average biofilm density (gVS/L)
z	Biofilm depth (cm)
ζ	Average effective diffusivity gradient of oxygen in biofilm (cm/s)

List of Abbreviations

CSTR	Continuous Stirred Tank Reactor
FS	Flat-Sheet
HF	Hollow-Fiber
MAB	Membrane-Aerated Biofilm
MABs	Membrane-Aerated Biofilms
MABR	Membrane-Aerated Biofilm Reactor
MABRs	Membrane -Aerated Biofilm Reactors
RBC	Rotating Biological Contactors
WWTP	Wastewater Treatment Plant

Chapter 1

INTRODUCTION AND LITERATURE REVIEW

1.1 Overview of wastewater biofilms

A biofilm is a complex aggregation of microorganisms growing on a solid substrate. Biofilms are characterized by structural heterogeneity, genetic diversity, complex community interactions, and an extracellular matrix of polymeric substances. Formation of a biofilm begins with the attachment of free-floating microorganisms to a surface. These first colonists adhere to the surface initially through weak, reversible van der Waals forces. If the colonists are not immediately separated from the surface, they can anchor themselves more permanently using cell adhesion molecules such as pili, forming strong biofilm matrix. All the information on biofims, biofilm structure and formation were obtained from a textbook published by Lewandowski and Beyenal (2007).

There are two main systems in biological wastewater treatment processes, which are suspended-growth and attached growth systems. A biofilm system is defined as a group of compartments and their components determining biofilm structure and activity. A typical biofilm system consists of four basic properties, which are: (1) a surface to which the microorganisms are attached; (2) the biofilm (microbial community); (3) the solutions of nutrient and; (4) the gas phase.

Due to many advantages they offer over conventional activated sludge processes, biofilm-based processes are increasingly used in wastewater treatment. These advantages include the ability of biofilm-based processes to support the growth of mixed population microorganisms which may degrade different organic substrates. Another advantage is the sequestrating ability of the glycocalyx surrounding the microorganisms which protects them from harmful toxicants (Bishop 1997). Also, due to increased surface area for bacterial growth created by biofilm support materials, it is possible to achieve high treatment capacity with minimal space requirements and without increasing loadings to final clarifiers.

The basic principle of biofilm reactors in wastewater treatment is that biological processes take place inside a community of microorganisms (biomass) attached to an

inert support material. These biodegradation processes only take place when substrates have diffused through the biomass to reach the microorganisms in the biofilm and the products that diffuse out of the biofilm are said to be biologically treated. For a biofilm reactor to work properly, there are two basic principles that have to perform: (1) the substrates have to be transported to the biofilm and the products have to be transported away from the biofilm; and (2) the biomass produced has to be controlled to avoid clogging of the biofilm system, which may lead to inefficient wastewater treatment.

1.2 Importance of biofilm kinetic parameters in wastewater treatment

Models of microbial growth kinetics quantify the relationship between the specific growth rate of microorganisms and substrate concentration. The constants in these models are termed "biokinetic parameters", and in the Monod equation they are termed half-saturation coefficient (K_s) and maximum specific growth rate (μ_m/Y). As stated above, activated sludge processes and biofilm processes are the two major categories of bioreactors used in biological wastewater treatment. Kinetics-based bioreactor design has now been widely used in the design of activated sludge processes. It improves the performance and reliability of the bioreactors and is a major advance in the design of activated sludge processes. Accurate estimation of kinetic parameters for activated sludge processes is necessary for successful design that is based on kinetics; and the industry has accumulated sufficient knowledge of the kinetic parameters for activated sludge processes. However, kinetics-based bioreactor design for biofilm processes is still in a stage of early development due largely to the complexity of biofilms. Although modeling of wastewater biofilms has advanced significantly in past 20 years (Morgenroth et al. 2000; Eberl et al. 2000), study of kinetic parameters in biofilms lags behind. Kinetic parameters are essential for the calibration and improvement of biofilm models. Based on our current knowledge of biofilms, it is reasonable to expect that kinetic parameters in biofilms are different from those in activated sludge. More experimental data on the

kinetic parameters of biofilm are therefore needed to improve the modeling, designing and scaling-up of biofilm reactors for effective wastewater treatment.

1.3 Challenges of biofilm kinetic parameter measurements

It is difficult to measure the biokinetic parameters of biofilm systems due to diffusional resistance within the biofilm that masks its true biodegradation kinetics as well as the difficulty of replicating biofilm structure in a test vessel (Riefler and Smets 2003). Due to lack of data on biofilm kinetics, it became a practice to determine biokinetic parameters in suspended cultures and apply those values to model microbial growth and predict substrate concentration profiles in biofilms (Horn and Hempel 1997; Hsien and Lin 2005). However, using biokinetic parameters from suspended-growth cultures to predict microbial growth and substrate utilization in biofilms is questionable because both systems differ in microbial cell physiology and species compositions.

1.4 Previous measurements to determine biofilm kinetic parameters

To date, there have been few published studies on how to obtain biokinetic parameters in biofilms. However, due to the recognized importance of these kinetic parameters to the biofilm reactors' design, scale-up and operations, many researchers have undertaken studies aimed at estimating the two fundamental biokinetic parameters (K_s and μ_m/Y), which describe the process of microbial growth and substrate removal in biofilm systems designed for wastewater treatment. Though, in most of these studies, biokinetic parameters were successfully determined, it remains to be seen if these parameters are sufficiently accurate and reliable that they can truly represent the intrinsic biodegradation kinetic in the biofilm systems investigated because the studies assumed uniform biofilm structure and neglected the effects of diffusional resistance in biofilm processes. This following section reviews in detail previous experimental techniques that have been employed to estimate biokinetic parameters and their associated drawbacks.

1.4.1 Substrate concentrations analysis

Few research studies have been undertaken to measure biokinetic parameters in biofilms. To start with, an experimental approach was developed in which batch experiments were performed to determine biokinetic parameters in fluidized bed biofilm reactors (Chen et al. 2003; Hirata et al. 2000). In this study, the biofilms were developed under well-controlled conditions in biological fluidized bed reactors and kinetic models deduced to describe substrate removal rate at varying influent substrate concentrations. The biokinetic parameters were then determined by fitting experimental data to linear transformations of the Monod kinetic equation. This approach has several drawbacks: First, mass transfer effects were neglected in estimation of biokinetic parameters and as a result, the study could not represent the true reaction kinetics of the immobilized cells. The long re-colonization period of 6 to 7 d between batch experiments to allow the reactors to regain steady-state performance renders this method time-consuming and tedious. It is reasonable to also question the accuracy of the estimates due to errors in sample analysis and linearization method.

1.4.2 Substrate specific analysis

Another technique estimates biokinetic parameters and the diffusion coefficient of substrate in biofilm processes used in water treatment (Zhang and Huck 1996), by manipulating the steady–state biofilm model proposed by Rittmann and McCarty (1980). In this study, the biofilm kinetic model originally developed for wastewater treatment was applied to the drinking water treatment. Figure 1.1 illustrates the schematic diagram of continuous stirred tank reactor (CSTR) used for the study.

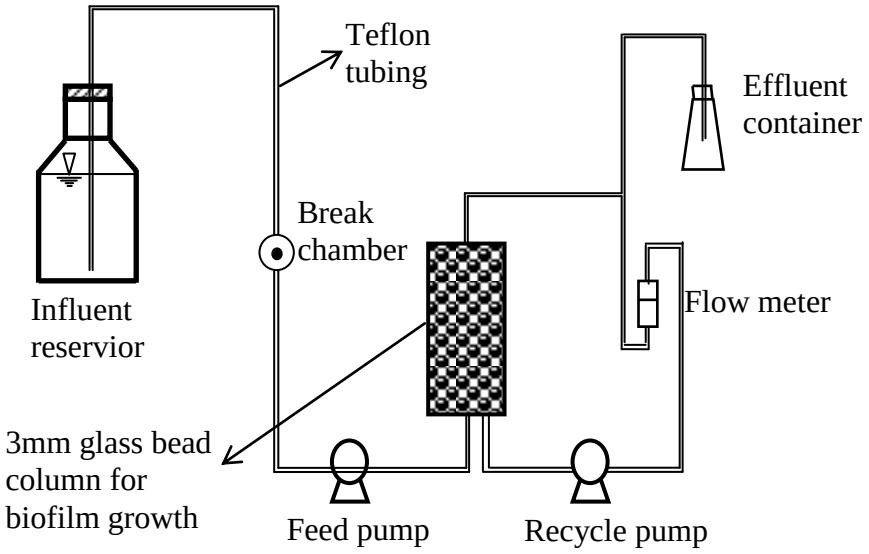

Figure 1.1 CSTR biofilm reactor adapted from Zhang and Huck (1996).

The authors were able to establish a mathematical relationship of the two main measurable variables: substrate flux into biofilm, *J,* and substrate concentration in the bulk liquid, S_b, with four model parameters: substrate diffusivity in biofilm, D_f ; the minimum substrate concentration to maintain a steady-state biofilm, S_{min}; the half-saturation coefficient, K_s; and the maximum growth rate lumped together as $k\mathrm{X_f}$ in which k is the maximum specific growth rate coefficient and X_f is the biofilm density. The best possible values of D_f, S_{min}, K_s, and kX_f were then obtained by iteration, with the values of J and S_b determined at different influent concentrations of the steady-state biofilm reactors. Unlike the previous study, this method took into account the diffusional mass transport limitations in interpreting the biokinetic parameters. This method is also time-consuming because each data point requires a different influent concentration condition, and the system must return to steady state between experiments.

1.4.3 Respirometric methods

Others have developed attached growth biofilm systems, but determined biokinetic parameters by measuring oxygen uptake profiles in the bulk liquid as a surrogate measure of substrate consumption. For instance, some researchers were able to determine bio-kinetic parameters in biofilms through the measured oxygen consumption profiles in the bulk liquid (Riefler et al. 1998; Plattes et al. 2007; Carvallo et al. 2002), which was similar to the experimental technique of respirometry in activated sludge (Kappeler and Gujer 1992). The studies have non-negligible drawbacks regardless of progress made with estimation of biokinetic parameters from cultures with intact biofilms. One drawback includes calculating the biokinetic parameters on the assumption that oxygen is not the microbial growth limiting factor when it is obviously difficult to justify this assumption due to oxygen diffusional limitations in biofilm systems. In the studies, however, models that were used in computing biokinetic parameters assumed that the biofilm consisted of uniform thickness, density, and structure, and that biofilm reactors were well-stirred (an indication of uniform substrate concentration at any point in the system). However, while these assumptions hold true for biofilms in pure culture, they certainly do not represent the biokinetic behavior of biofilms in mixed cultures such as those found in wastewater treatment and this flaw makes it difficult to conclude that estimated biokinetic parameters are reliable and accurate. Also, modeling substrate diffusion into the biofilm along with chemical reactions often complicates representation of the system parameters especially diffusion coefficient, which suggests that in-situ measurement is required in the determination of diffusion-controlled biokinetic parameters in thin layers containing microbial activity and not analysis of wastewater being treated in biofilm processes (Lewandowski et al. 1991).

1.4.4 Microsensor technology

The discussion above suggests that for accurate representation of biofilm system parameters, measurements inside the biofilms are necessary. It is encouraging to observe how improved microsensor technology has enabled in-situ chemical characterization of microbial activities including substrate concentration profiles in biofilms. To quantify biokinetic parameters from substrate concentration profiles, however, is still challenging due to lack of suitable computational procedures. Based on well-known reaction-diffusion equation, Yurt et al. (2003) developed computational procedures to quantify biokinetic parameters from oxygen concentration profiles in biofilms that were measured using a microsensor. The study was undertaken by growing pure culture biofilm, measuring oxygen concentration profiles and computing the biokinetic parameters based on mathematical models that described uniform structure. But the concept of uniform biofilm model contradicts several research findings, which have otherwise revealed the heterogeneity of biofilms (Zhang and Bishop 1994; Bishop and Rittmann 1995). As a result, the biokinetic parameters estimated from uniform biofilm models could not represent the biokinetic behavior of microorganisms in mixed cultures such as those found in wastewater treatment systems. Finally, technical challenges that would be encountered in using biokinetic parameters of pure culture biofilms strongly underscore the need for a computational technique that will take into account biofilm structural heterogeneity in quantifying biokinetic parameters from substrate concentration profiles while permitting accurate and reliable results.

1.5 Research goals

The main objective of this dissertation was to obtain kinetic parameters in biofilms based on the modification of existing computational procedures. Two types of biofilm were used in this study: membrane aerated biofilms (MABs) and rotating biological contactor (RBC) biofilms. It is hoped that information obtained from this

study would be useful in the process of modeling, designing and scaling-up biofilm reactors for effective wastewater treatment.

1.6 Research approach

In this research, a modified computational procedure was presented to quantify the biokinetic parameters from oxygen concentration profiles that were measured in mixed cultured biofilms grown in membrane-aerated biofilm reactors (MABRs) and RBC. The two types of biofilm were selected for this study for the following reasons: (1) RBC biofilm represents a conventional inert substratum and RBCs have been used extensively in the treatment of domestic wastewater and specific organic compound contaminants; and (2) MABs represent a new type of biofilm with a gas-permeable substratum, which allows oxygen to be supplied through the substratum to the biofilm for simultaneous COD removal, sulphate reduction, nitrification and denitrification.

1.7 Thesis outline

Chapter 2 of this thesis deals with the study to develop and examine process behavior of two MABRs with different membrane module configurations. The intent of studying this biofilm reactor was not to optimize it for wastewater treatment, but to develop biofilms under well-controlled conditions for kinetic parameter measurements.

Chapter 3 deals with quantification of intrinsic parameters relating biodegradation kinetics in MABs. The main focus of this chapter is on performing microsensor measurements on the mature biofilms to obtain oxygen concentration profiles and establishing a suitable computational procedure that would allow accurate and reliable estimation of biokinetic parameters in MABs.

Chapter 4 presents the experimental technique and computational procedure to quantify biokinetic parameters in RBC biofilms. This was done to obtain more experimental data on kinetic parameters in biofilms other than MABs.

Chapter 5 summarizes the conclusions of this study and states future work that is required to obtain more accurate and reliable experimental data on kinetic parameters in biofilms for improved biofilm reactors.

1.8 References

Bishop, P. L. 1997. Biofilm structure and kinetics. *Water Science and Technology* 36 (1):287-294.

Bishop, P. L., and B. E. Rittmann. 1995. Modelling heterogeneity in biofilms: Report of the discussion session. *Water Science and Technology* 32 (8):263-265.

Carvallo, L., J. Carrera, and R. Chamy. 2002. Nitrifying activity monitoring and kinetic parameters determination in a biofilm airlift reactor by respirometry. *Biotechnology Letters* 24 (24):2063-2066.

Chen, K. C., J. Y. Wu, W. B. Yang, and S. C. Hwang. 2003. Evaluation of effective diffusion coefficient and intrinsic kinetic parameters on azo dye biodegradation using PVA-immobilized cell beads. *Biotechnology and Bioengineering* 83 (7):821-32.

Eberl, H. J., C. Picioreanu, J.J. Heijnen, and M.C.M. van Loosdrecht. 2000. A three-dimensional numerical study on the correlation of spatial structure, hydrodynamic conditions, and mass transfer and conversion in biofilms. *Chemical Engineering Science* 55 (24): 6209-6222.

Hirata, A., T. Takemoto, K. Ogawa, J. Auresenia, and S. Tsuneda. 2000. Evaluation of kinetic parameters of biochemical reaction in three-phase fluidized bed biofilm reactor for wastewater treatment. *Biochemical Engineering Journal* 5 (2):165-171.

Horn, H., and D. C. Hempel. 1997. Growth and decay in an auto-/heterotrophic biofilm. *Water Research* 31 (9):2243-2252.

Hsien, T. Y., and Y. H. Lin. 2005. Biodegradation of phenolic wastewater in a fixed biofilm reactor. *Biochemical Engineering Journal* 27 (2):95-103.

Kappeler, J., and W. Gujer. 1992. Estimation of kinetic-parameters of heterotrophic biomass under aerobic conditions and characterization of waste-water for activated-sludge modeling. *Water Science and Technology* 25 (6):125-139.

Lewandowski, Z., G. Walser, and W. G. Characklis. 1991. Reaction-kinetics in biofilms. *Biotechnology and Bioengineering* 38 (8):877-882.

Lewandowski, Z., and H. Beyenal. 2007. Fundamentals of biofilm research. CRC Press. USA.

Morgenroth, E., H. Eberl H. and M.C.M van Loosdrecht. 2000. Evaluating 3-D and 1-D mathematical models for mass transport in heterogeneous biofilms. *Water Science and Technology* 41(4-5): 347-356.

Plattes, M., D. Fiorelli, S. Gille, C. Girard, E. Henry, F. Minette, O. O'Nagy, and P. M. Schosseler. 2007. Modelling and dynamic simulation of a moving bed bioreactor using respirometry for the estimation of kinetic parameters. *Biochemical Engineering Journal* 33 (3):253-259.

Riefler, R. G., D. P. Ahlfeld, and B. F. Smets. 1998. Respirometric assay for biofilm kinetics estimation: parameter identifiability and retrievability. *Biotechnology and Bioengineering* 57 (1):35-45.

Riefler, R. G., and B. F. Smets. 2003. Comparison of a type curve and a least-squared errors method to estimate biofilm kinetic parameters. *Water Research* 37 (13):3279-3285.

Rittmann, B. E., and P. L. Mccarty. 1980. Model of steady-state-biofilm kinetics. *Biotechnology and Bioengineering* 22 (11):2343-2357.

Yurt, N., H. Beyenal, J. Sears, and Z. Lewandowski. 2003. Quantifying selected growth parameters of Leptothrix discophora SP-6 in biofilms from oxygen concentration profiles. *Chemical Engineering Science* 58 (20):4557-4566.

Zhang, S. L., and P. M. Huck. 1996. Parameter estimation for biofilm processes in biological water treatment. *Water Research* 30 (2):456-464.

Zhang, T. C., and P. L. Bishop. 1994. Density, porosity, and pore structure of biofilms. *Water Research* 28 (11):2267-2277.

Chapter 2

STUDIES OF MEMBRANE-AERATED BIOFILMS (MABs)

2.1 Introduction

Stringent water quality standards have compelled many water and wastewater utilities to start investing in technologies that can lower the rising energy and operational costs of wastewater treatment and still provide efficient wastewater treatment. Many researchers have stated that MAB technology holds such promise for biological water and wastewater treatment in recent years (Timberlake et al. 1988; Brindle et al. 1998). Compared to conventional biofilm technologies, MABRs offer several advantages in advanced wastewater treatment because they deliver oxygen at high rate and increase oxygen transfer efficiencies, have small footprint requirements, and simultaneously achieve chemical oxygen demand (COD) and nitrogen removal, thereby enhancing the biofilm activity (Syron and Casey 2008).

In this study, two types of membrane module configured reactors were employed to develop biofilms for the kinetic studies. These included hollow-fiber (HF) and flat-sheet (FS) membranes: there are HF and FS membrane aerated biofilms (HF- and FS-MABs, respectively). Both membrane module configurations were used as a means of supplying oxygen and supporting biofilm growth. HF membrane modules have smaller diameter (< 1mm) and are cast as fine lumens and oxygen diffuses through the lumen of the HF membrane into the biofilm. On the other hand, FS membranes are flat in structure and have lower specific surface area when compared to the HF membranes. Oxygen diffuses through the bottom of the FS membrane into the biofilm.

In MABRs, the biofilm is attached to the gas permeable membrane. Unlike conventional biofilm where oxygen is supplied to the biofilm from the bulk liquid interface, in MABRs, oxygen diffuses through the membrane into the biofilm where the oxidation of pollutants supplied at the biofilm-liquid interface takes place. As illustrated in Figure 2.1, the oxygen and soluble wastewater constituents are supplied from opposite sides of the biofilm in the MABRs (Syron and Casey 2008).

The aerobic zone exists where both oxygen and nutrients are simultaneously available within the biofilm. In the context of nitrogen removal and sulfate reduction, the existence of an anaerobic zone at the biofilm-liquid interface is advantageous for denitrification and sulfate reduction process. Also, the counter-diffusion of oxygen and substrates creates various microenvironments within MABs that are capable of promoting stratification of metabolic processes across the depth of the biofilm (Bishop and Yu 1999). This stratification of microbial communities in MABs makes it possible to achieve simultaneous pollutant oxidation and nitrogen removal as demonstrated by Timberlake et al. (1988).

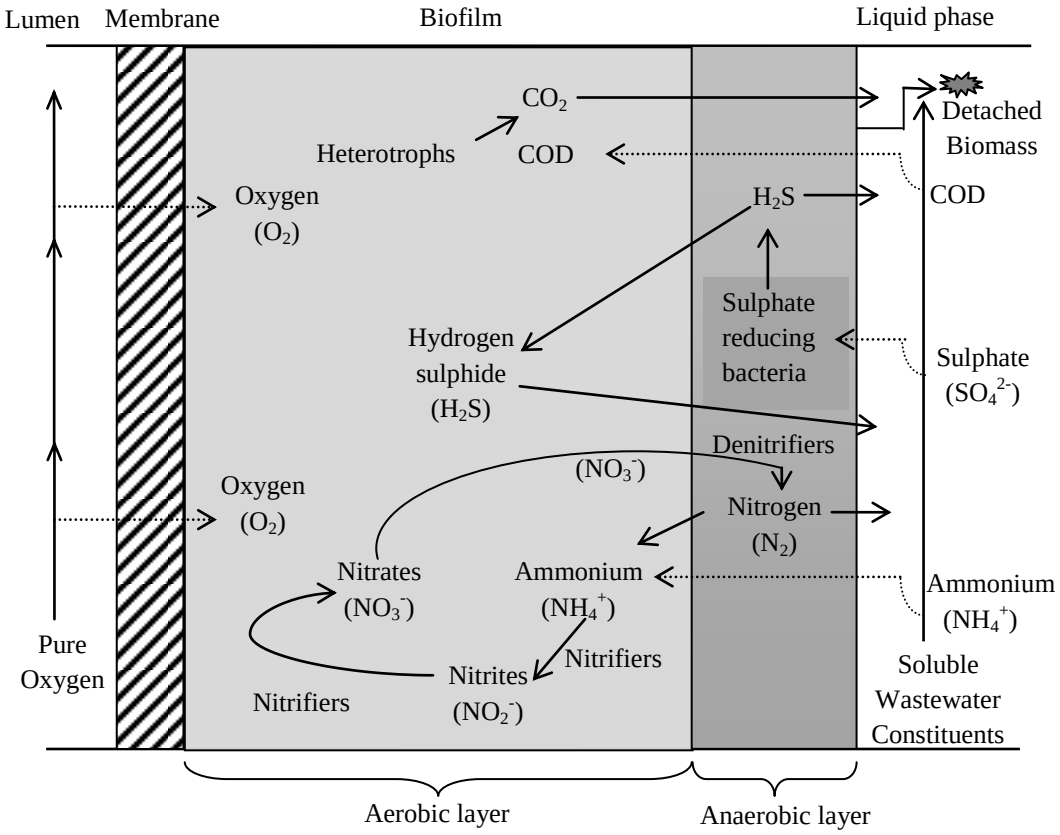

Figure 2.1 Schematic drawing showing the transport fluxes of soluble constituents and indicative microbial stratification in MABs in contact with wastewater.

The main objective of this study is to develop MABs under well-defined and controlled conditions. The biofilm is meant to be used for microsensor measurements that would reveal oxygen concentration profiles in the biofilm. In advancing this research, biokinetic parameters that describe microbial growth and substrate utilization in the biofilm would be determined from the measured oxygen concentration profiles. It is important to point out that the MABRs were not designed to study the efficiency or effectiveness of this type of biofilm systems in treating wastewater and as a result these MABRs were not optimized. Higher performance levels would have been expected with improved design and more membrane surface area.

2.2 Experimental

2.2.1 Experimental set-up and continuous operation

Two laboratory-scale MABRs were set up and operated for 310 days, with one reactor having HF membrane module configuration and the other a FS membrane configuration. These two reactors were designed by Shuying Tan in our research group. The FS-MABR consists of two membrane modules that offered a total of approximately 165.2 cm^2 membrane surface area for biofilm growth. Also, the HF-MABR consists of two membrane modules that offered a total of approximately 105.5 cm^2 membrane surface area for biofilm growth. Figure 2.2 shows the experimental set-up for continuous operation of the HF and FS-MABRs. Schematic diagrams of the assembled reactors are shown in the Figures 3.1 and 3.2 of Chapter 3. Biofilm in each reactor was then developed in a synthetic wastewater with same predetermined Chemical Oxygen Demand (COD), sulphate, ammonium and mineral salts nutrients at a room temperature of $23\pm2^{o}C$.

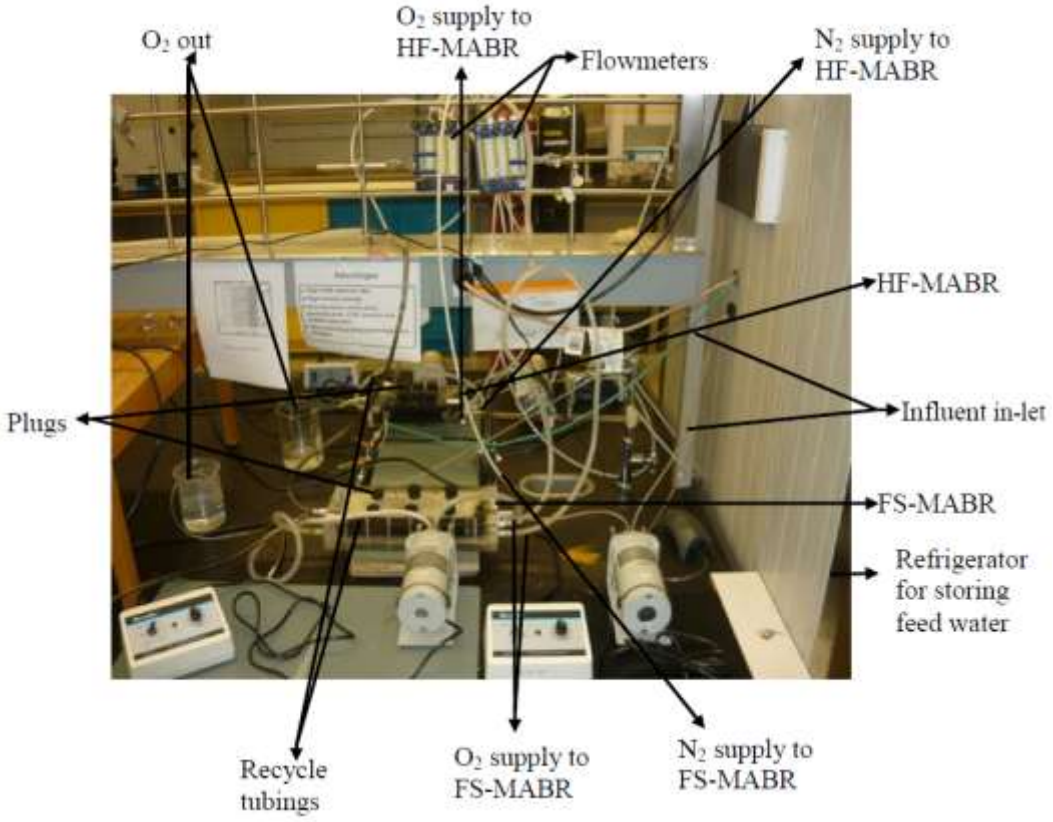

Figure 2.2 Experimental set-ups for continuous operation of the HF-and FS-MABRs.

Flow to the liquid compartment was re-circulated so that the hydraulic residence time within the two reactors and the average liquid velocity within the liquid compartments of the reactors could be varied independently. The effective volumes of the reactors were approximately 1.0 L and 1.2 L for FS and HF-MABRs, respectively. Influent wastewater feed was pumped into each of the MABRs with a peristaltic pump (Model #: 7553-80, 1-100 RPM, Cole Palmer, Montreal) at a flow rate of 2.0 mL/min and peristaltic pump (Model #: 7553-70, 6-600 RPM, Cole Palmer, Montreal) was used to recycle the effluent at flow rate of 200 mL/min. The effluent overflowed via effluent tubing to waste containers positioned on the floor of lab room. Table 2.1 shows the composition of the synthetic wastewater for the MABRs.

Table 2.1. Composition of synthetic wastewater for MABRs

	Specific component	
Constituents *	**Name**	**Concentration , mg/L**
$C_6H_{12}O_6$	COD	250
KH_2PO_4	PO_4	5
NH_4Cl	NH_4	20
Na_2SO_4	SO_4	277.5
$MgCl_2.6H_2O$	Mg	12.86
$FeSO_4.7H_2O$	Fe	2.57
$CoCl_2.6H_2O$	Co	0.2572
$CaCl_2.2H_2O$	Ca	0.7716
$CuSO_4.H_2O$	Cu	0.2572
$MnCl_2.4H_2O$	Mn	0.2572
$ZnSO_4.7H_2O$	Zn	0.2572
Yeast Extract	-	1

**All chemicals were purchased from Fisher Scientific Inc.*

High sulphate concentration in the synthetic wastewater was intended for the study of sulphate reduction by the sulphate-reducing bacteria in the anaerobic zone of the biofilm by Shuying Tan in our research group. As this biofilm also contains aerobic layer, this thesis is focused on the determination of kinetic parameters from oxygen concentration profiles measured in the aerobic zone of the biofilm.

2.2.2 Cultivation of MABs

Before the start of operation, each reactor was seeded with fresh mixed microbial culture obtained from the aeration tank of a municipal wastewater treatment plant (Gold Bar Wastewater Treatment Plant, Edmonton, Alberta, Canada). Before seeding the reactors, about 20 mL of culture sample was acclimatized in 250 mL conical flask containing the same synthetic wastewater prepared for the reactors and the suspension was placed in an incubator in the lab for 14 d under anaerobic conditions with nitrogen headspace (to stimulate the growth of anaerobic

bacteria). The nitrogen headspace was created by sparging nitrogen gas into an air-tight conical flask containing synthetic wastewater to remove dissolved oxygen. Synthetic wastewater free of dissolved oxygen was then used to acclimatize the culture sample. At same time, another 20 mL of culture sample was acclimatized in 250 mL conical flask containing the same synthetic wastewater prepared for the reactors and the solution was placed under laboratory conditions for 14 d under aerobic conditions with the supply of oxygen (to stimulate the growth of aerobic bacteria). Every two-day interval until expiration of 14 day-period of acclimatization, both cultures were allowed to settle for about 5 h, the supernant was decanted, and the flasks were re-filled with the same wastewater used in the MABR operations. After the bacterial culture was acclimatized, the reactors were then seeded with about 10 mL of a homogenized sample from each of the bacterial culture grown in anaerobic and aerobic conditions. The two reactors were then subsequently operated continuously with constant supply of pure oxygen for aerating the biofilm systems. The bulk wastewater was maintained in anaerobic conditions by sparging with nitrogen gas and maintaining air-tight condition in the upper compartment of the reactors. The pH in each of the reactors was maintained at 7.6±0.5 by buffering the feed water with 8.6 g Na_2CO_3 per 20 litre (0.0811 mol/litre) before it was fed into the reactors. Reactor operation was shut down for maintenance and cleaning protocol on a periodic basis (once every 3 months). This maintenance and cleaning protocol involved mainly: cleaning the influent, effluent and recycle tubing and removing excess sludge from the reactors.

2.2.3 Sampling and analytical methods

Intermittent sampling was carried out by collecting about 300 mL of the influent and effluent samples from each of the MABRs at least three times per week. Dissolved oxygen concentration in the bulk liquid and effluent samples were recorded daily with dissolved oxygen probes (Model #: Orion 97-08, Thermo Electro Corporation). Also, the pH and oxygen reduction potential (ORP) were

recorded daily with pH meter (Model #: AR 15, Fisher Scientific Inc.). The ammonia nitrogen (NH_3-N) in the influent and effluent samples were measured using the ammonia combination ion selective electrode (Model #: 13-620-508, Fisher Scientific Inc.). The NH_3-N analysis was conducted based on the known addition technique, which required that the NH_3-N concentration of standard solution, the electrode slope (obtained through calibration of known standards) and the volumes of both the standard and sample solutions be known. The potential (mV) of the sample was measured, the potential of the sample plus standard was also measured, and the sample NH_3-N concentration was derived from an established equation.

For COD and sulphate analysis, extra care was given to influent and effluent samples from both reactors by filtering them with a 0.22 µm membrane filters to remove particulates and microbes before the samples were subjected to these analyses. The analysis of sulphate was based on U.S Environmental Protection Agency (EPA) Method 300.0. The COD was analysis according to standard method 5220 D (APHA 1998). Sulfate and COD measurements were then performed on filter-sterilized (0.22 µm) reactor samples. Sulfate ion measurement was separated from the measurement of other ions in the sample by ion chromatograph and then detected and quantified with a conductivity detector. A Dionex model 2000 ion chromatograph (IC) with an IonPac AS4A-SC column (Dionex) was used for this analysis of sulphate. The mobile phase was 1.7 mM sodium biocarbonate and 1.8 mM sodium carbonate.

2.3 Reactor performance

Both reactors were operated for 310 days until pseudo-steady state performance was achieved and the biofilm attained a thickness of 1.5-2 mm and was ready for microsensor measurements. Figure 2.3 shows mature pieces of biofilm that were harvested from the MABRs for density measurements.

Figure 2.3 Samples of mature MABs.

Throughout the operation of the MABRs, dissolved oxygen (DO) concentrations in the influent and effluent reactor feeds were in the range of 7 - 8 mg/L and below 1.5 mg/L, respectively. The ORP were around an average of +350 mV for reactor influent and -250 mV for the effluent. The influent NH_3-N concentration was maintained at an average value of 20 mg/L and effluent NH_3-N concentration varied within the range of 7-15 mg/L depending on the reactor performance and conditions. The pH in each of the reactors was adjusted as appropriate by either adding a dilute solution of sodium hydroxide (NaOH) when effluent pH readings indicated minor acidic wastewater in the reactors or by adding a dilute solution of hydrochloric acid (HCL) when effluent pH readings indicated minor alkaline wastewater in the reactors. With consistent pH of wastewater in the reactor and constant pressure of oxygen supply to the MABRs, it was possible to maintain the DO, ORP and NH_3-N concentrations in the influent feed and effluent around the targeted operational parameters.

The results of the COD analysis of samples collected from HF and FS-MABRs from 3 to 310 days of operation are shown in Figures 2.4 and 2.5, respectively. Similarly, the results of the sulphate analysis of samples from HF and FS-MABRs from 3 to 310 days of operation are shown in Figures 2.6 and 2.7, respectively.

The experimental data for reactor performance are presented in Appendices A1-A4. The results of the DO, ORP, NH_3-N and pH parameters of the MABRs from 3 to 310 days of operation were not presented in this thesis as the monitoring of these parameters were only intended to ensure that the MABRs were operated under well-controlled and defined laboratory conditions.

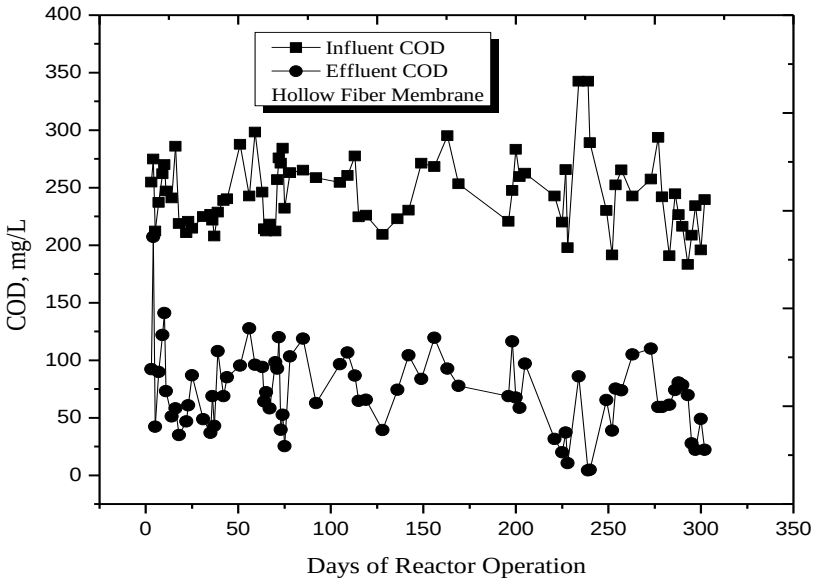

Figure 2.4 Process performance for COD removal by HF-MAB from Day 3 through Day 310.

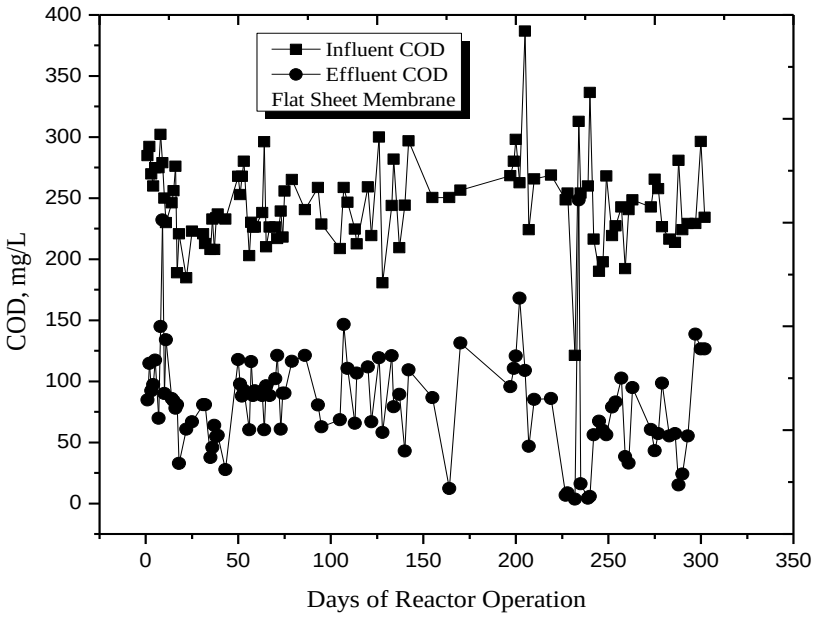

Figure 2.5 Process performance for COD removal by FS-MAB from Day 3 through Day 310.

Influent COD concentration was on average 245 mg/L for both the reactors. The COD removal differed based on the type of reactor membrane module configurations. The average effluent COD concentration of the HF-MABR was 72 mg/L. The FS-MABR experienced an average effluent COD concentration of 82 mg/L. The average removal rate for the HF-MABR was approximately 70%, the averaged removal rate for the FS-MABR was approximately 67%. This indicates that the HF-MABR is operating at around the same efficiency as the FS-MABR based on removal of COD from the synthetic wastewater.

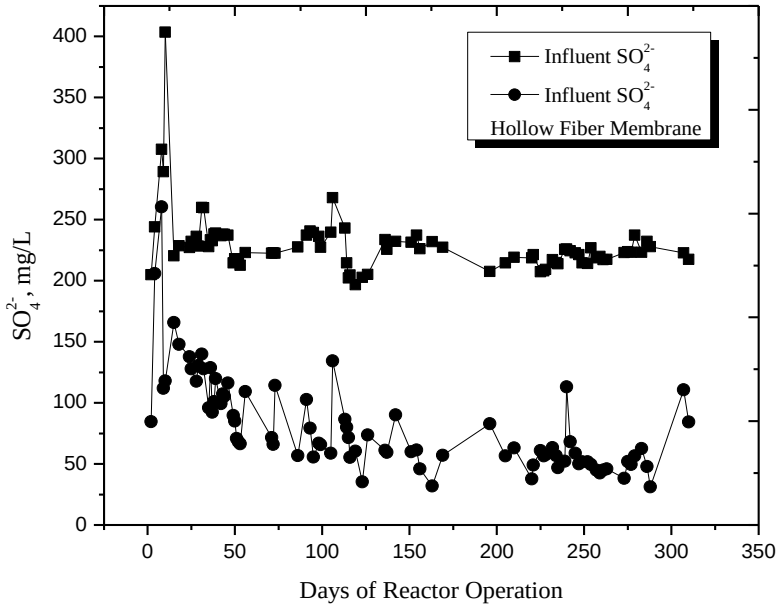

F**igure 2.6** Process performance for sulphate removal by HF-MAB from Day 3 through Day 310.

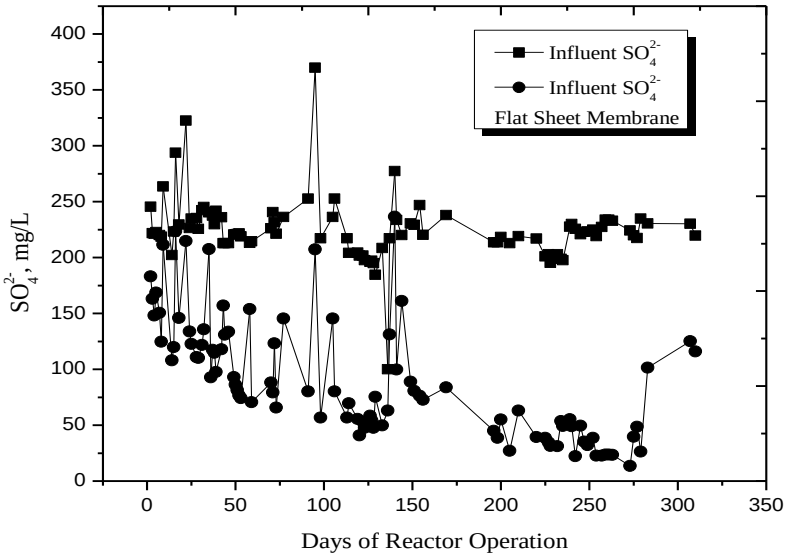

Figure 2.7 Process performance for sulphate removal by FS-MAB from Day 3 through Day 310.

Influent sulphate concentration was on average 227 mg/L for both the reactors. The sulphate removal differed based on the type of reactor membrane module configurations. The average effluent sulphate concentration of the HF-MABR was 81 mg/L. The FS-MABR experienced an average effluent sulphate concentration of 90 mg/L. The average sulphate removal rate for the HF-MABR was approximately 65%, and 61% for FS-MABR. This indicates that the HF-MABR was operating at around the same efficiency as the FS-MABR based on removal of sulphate from the synthetic wastewater.

Both reactors operated at pseudo-steady state in the later period of the operation. There were some noticeable varations in the trend of COD and sulphate removal in both of the reactors. These were isolated events and were most likely caused by errors in filtering or by the degradation of organic matter in the samples during storage for 4 d due to non-avalilability of analytical instruments at the time this analysis was required. Sample filteration was part of the procedure for the sulphate and COD analysis. The magnitude and impact of these errors on the reactors' samples analytical results was determined to be minimal as these isolated events occurred not more than four times over the entire period of the reactors' operation, which lasted for 310 days prior to the microsensor measurements. Also, these errors were later eliminated by proper filtration of the samples and storage of samples for not more than a day prior to analysing them for COD and sulphate. Another source of variation in the reactors sample analytical results could also be related to the maintenance and cleaning of the reactors. These events could have caused changes in expected COD and sulphate values, but as the reactor was allowed to operate over time the results returned to expected values due to normailization of reactor performance.

2.4 Summary

This study was conducted to develop and examine the process behaviour of two MABRs under well-defined and controlled laboratory conditions. All these studies were performed in preparation for the microsensor measurements of

oxygen concentration profiles in the biofilms. Kinetic parameters in MABs will be later extracted from the measured oxygen concentration profiles.

In general, the removal rates for COD and sulphate were low for typical biological reactors, but the MABRs were not designed for the study of treatment performances. Instead, they were designed for growing the type of biofilms required for the kinetic study and the reactors' performance and the biofim growth conditions were good for this purpose. The COD and sulphate analysis, as well as the other parameters, are to ensure microbial processes inside the biofilms did remove COD and used sulphate as electron acceptors in biological sulfate reduction and organic pollutant oxidation. It is important to note that the kinetic study was focused on the aerobic zone and these biofilms did have aerobic zones. Studying and determining biokinetic parameters that describe the microbial growth and substrate removal in any other layers of MABs other than the aerobic were not parts of the objective of this thesis.

2.5 References

American Public Health Association (APHA), 1998. Eaton, A.D., Clesceri, L.S., and Greenberg, A.E (eds), Standard methods for the examination of water and wastewater, 20th edition, American Water Works Association; Water Pollution Control Federation, Washington, D.C.

Bishop, P. L., and T. Yu. 1999. A microelectrode study of redox potential change in biofilms. *Water Science and Technology* 39 (7):179-185.

Brindle, K., T. Stephenson, and M. J. Semmens. 1998. Nitrification and oxygen utilisation in a membrane aeration bioreactor. *Journal of Membrane Science* 144 (1-2):197-209.

Environmental Protection Agency (EPA), Environmental Monitoring Systems Laboratory, Office of Research and Development, USEPA Method 300.0, "Determination of Inorganic Anions by Ion Chromatography," EPA-600/R-93-100, August 1993.

Syron, E., and E. Casey. 2008. Membrane-aerated biofilms for high rate biotreatment: Performance appraisal, engineering principles, scale-up, and development requirements. *Environmental Science & Technology* 42 (6):1833-1844.

Timberlake, D. L., S. E. Strand, and K. J. Williamson. 1988. Combined aerobic heterotrophic oxidation, nitrification and denitrification in a permeable-support biofilm. *Water Research* 22 (12):1513-1517.

Chapter 3

DETERMINATION OF KINETIC PARAMETERS IN MEMBRANE-AERATED BIOFILMS (MABs)

3.1 Introduction

Among the most obstacles for public wastewater utilities is developing a high-rate and cost-effective wastewater treatment technology that can degrade target pollutants to produce a waste stream that meets compliance requirements. Biofilm-based processes such as MABs have gained increased application in the treatment of waste streams containing organic and inorganic contaminants. Compared to other conventional biofilm technologies, MABRs are leading innovative technology that can offer several advantages in advanced wastewater treatment because it can deliver oxygen at high rate and increase oxygen transfer efficiencies therefore enhancing the biofilm activity (Syron and Casey 2008).

Inadequate understanding of the biodegradation kinetics of biofilms is one of the unresolved problems that have hampered rational optimization of biofilm reactor design and operation. In order to understand the biokinetic behaviors of microorganisms in biofilms, accurate, fast and in-situ measurements are required to quantify biokinetic parameters from wastewater constituents' biodegradation process. Mathematical models have been developed that can predict COD and inorganic nitrogen removal behavior (Shanahan and Semmens 2004) and investigate organic substrate utilization rates under co-diffusion and counter-diffusion reactor configurations (Syron et al. 2009) in MABRs. However, successful application of these models would require direct measurements in the biofilm to be able to accurately quantify mass transfer coefficients and biokinetic parameters that describe the process of substrate diffusion, bacterial growth and substrate removal. To date there have been no reports of suitable computational procedures to determine these parameters in structurally heterogeneous biofilm-based reactors that perform at high oxygen concentration such as MABRs.

There have been few previous attempts to quantify biokinetic parameters in biofilm from oxygen concentration profiles that were measured using oxygen microsensor. In a remarkable paper, Yurt et al. (2003) developed an algorithm

and a computational procedure to determine biokinetic parameters from oxygen concentration profiles. By fitting an oxygen concentration profile measured vertically across *Leptothrix discophora* SP-6 biofilms into Monod or Tessier growth kinetics, they successfully calculated the Monod half-saturation coefficient for oxygen consumption in the biofilm to be 0.333±0.077 mg/L. While their study provided a useful method to determine biokinetic parameters characterizing microbial growth of biofilm in pure culture, it may not allow quantitative determination of biokinetic parameters in mixed culture biofilm. Like other previous studies that determined biokinetic parameters from oxygen concentration profiles based on the well-known reaction-diffusion equation (Zhou et al. 2008; Hooijmans et al. 1990), the method assumed uniform biofilm structure despite a growing body of experimental evidence of biofilm heterogeneity (Zhang and Bishop 1994; Bishop and Rittmann 1995). The computational method as developed by Yurt et al. (2003) only works well for ideal biofilms with uniform structure. It would be challenging to apply the same method to most biofilms with heterogeneous structure, which with microsensor measurements give an imperfect experimental data set of substrate concentration profiles. The other weakness of the technique is that parameter estimation routinely determines average biofilm density, $\bar{X}_f$. But, the density of biofilm involved in the degradation of the test compound needs to be determined experimentally in order to obtain an accurate assessment of the maximum specific rate of oxygen uptake, μ_m / Y.

Also, microsensor technology was employed by Zhou et al. (2009) to determine biokinetic parameters from oxygen concentration profiles measured at several locations in the biofilms. However, their method provided non-reproducible kinetic parameter estimates that were dependent on the concentration of the organic carbon substrate injected. With this approach, the oxygen gradient effect caused by mass transfer was neglected in the calculation of oxygen uptake rate for kinetic parameters at a specified substrate concentration. This method is based on batch respirometric procedure that use low oxygen concentrations; but high

oxygen concentrations affect oxidation rates (Hibiya et al. 2004). Also Lewandowski et al. (1991) determined K_s in mixed population biofilm grown in RBC to be 0.25 mg/L by a graphical method involving linear transformations of the non-linear Michaelis-Menten equation; however, this method introduces errors in the parameter estimation step.

We therefore present a modified approach to quantify the biokinetic parameters in the MABs from the oxygen concentration profiles. The approach is more reliable with improved stability compared with the existing model proposed by the previous above researchers, which only works for a perfect experimental dataset which is common to pure biofilms and uncommon to mixed culture biofilm systems for wastewater treatment. In order words, it cannot be used for experimental data from a biofilm that has some fluctuations in the substrate concentration profiles due to the heterogeneous nature of biofilm structure.

The study was conducted on HF-and FS-MABs developed under well-defined and controlled laboratory conditions. Oxygen microsensors were fabricated and used to obtain oxygen concentration profiles along the vertical depth at several locations in the MABs.

3.2 Materials and methods

3.2.1 Experimental set-up

Section 2.2.1 of Chapter 2 explains the MABR process, including the membrane materials, modular design and operation parameters. The reactors were seeded with the fresh mixed liquor obtained from the aeration tank of Goldbar wastewater treatment plant (Edmonton, Canada). Biofilm in each reactor was then developed in a synthetic wastewater with same predetermined COD, ammonium and mineral salts nutrients at a room temperature of 23±2^{o}C. Table 2.1 of Chapter 2 shows the composition of the synthetic wastewater for the MABRs.

The two MABRs were operated continuously with constant supply of pure oxygen to the biofilm. The synthetic water was maintained under anaerobic conditions by sparging with nitrogen gas and maintaining air-tight conditions. About 9-10 months after the start of reactors' operation, the biofilm had attained a thickness of 1.5-2 mm and was ready for microsensor measurements. The upper compartments of both reactors consist of plugs that can be removed when needed to allow the measurement of oxygen concentration profiles in the biofilms using microsensors. These plugs are shown in the schematic diagram of assembled reactors in Figures 3.1 and 3.2 for HF- and FS-MABRs, respectively.

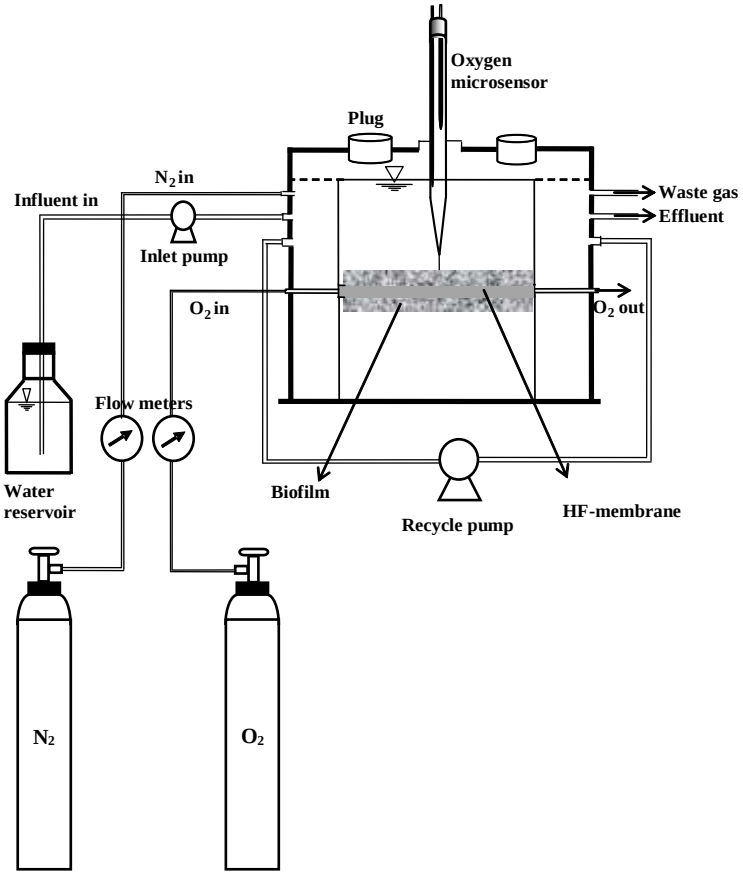

Figure 3.1 The schematic diagram of the experimental setup for in-situ measurement of oxygen concentration profiles in HF-MABR.

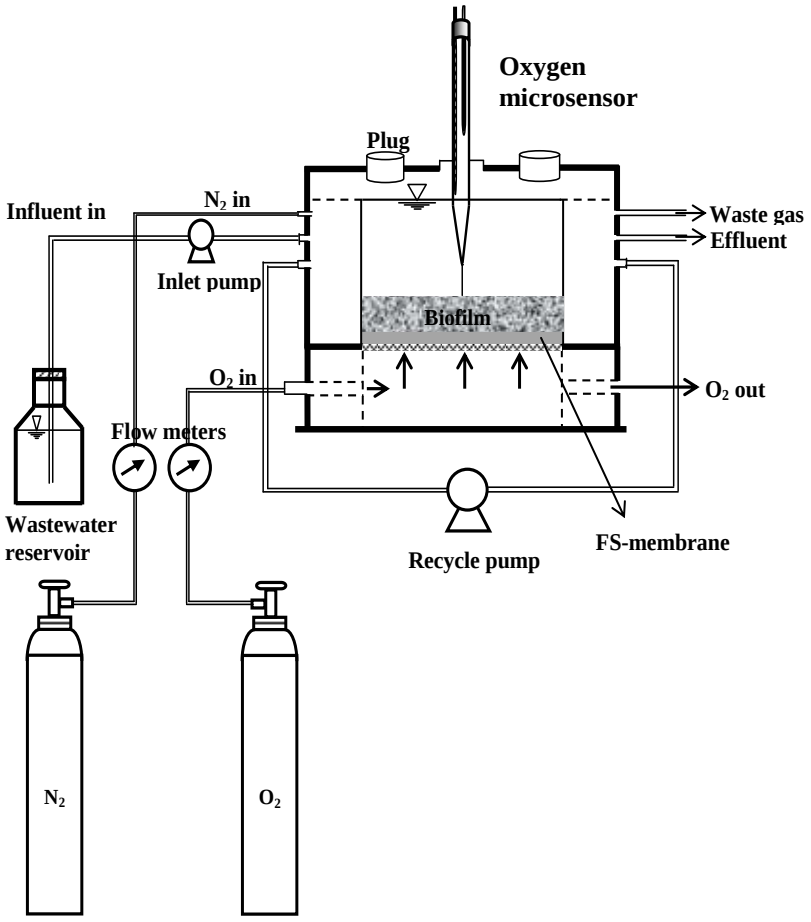

Figure 3.2 The schematic diagram of the experimental setup for in-situ measurement of oxygen concentration profiles in FS-MABR.

3.2.2 Calibration of oxygen microsensor

A combined oxygen microsensor was used to obtain oxygen concentration profiles in the MABs. The type of oxygen microsensor was constructed in our lab based on the method described by Lu and Yu (2002). The tip of microsensor was approximately 30 μm in diameter. The microsensor has 90 % response time of less than 5 s and effect of stirring is only 0.5% of the signal. The microsensor was connected to a picoammeter (Unisense, Denmark, Model No. PA2000) and the working cathode was polarized at -0.75V versus an internal Ag/AgCl reference electrode. After polarization to achieve stable signals, the oxygen

microsensor was calibrated before it was used for biofilm measurements. For each measurement cycle, a three-point calibration process was carried out at 100 % O_2 saturation in atmospherically equilibrated water aerated with standard pure oxygen (O_2, 100%), 21% O_2 saturation with compressed air (O_2, 21%) and 0% saturation in anoxic water aerated with nitrogen (O_2, 0%). Figure 3.3 illustrates calibration curves for combined oxygen microsensors used in HF- and FS-MABs.

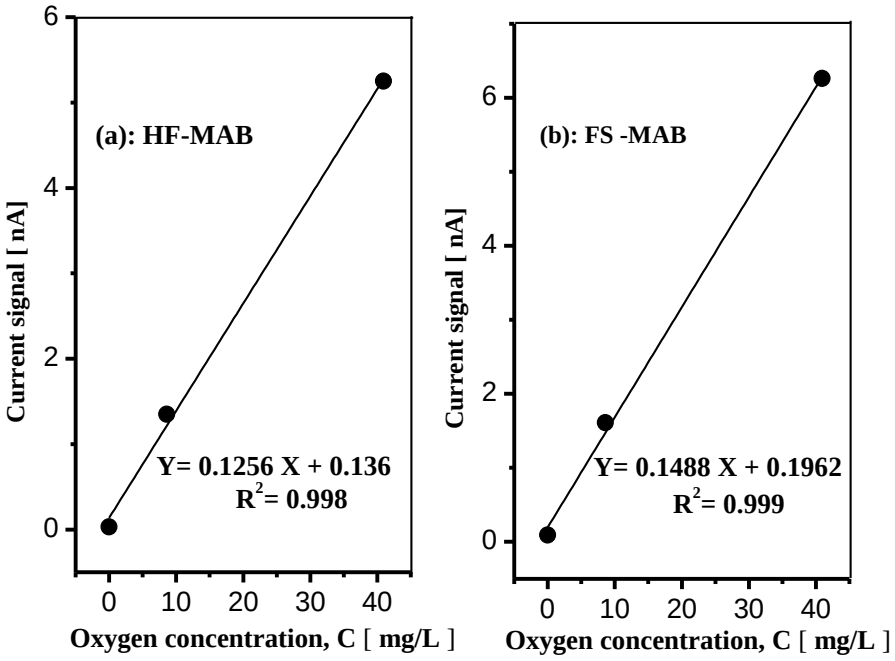

Figure 3.3 Calibration curves of combined oxygen microsensors used in HF-and FS-MABs.

The microsensor calibration curves for the combined oxygen microsensor were obtained by plotting the oxygen saturation concentrations of the gas introduced into the calibration chamber against current signals measured by the microsensor. The calibration data for the combined oxygen microsensor and procedure for calculating maximum dissolved pure oxygen in water are presented in Appendix B1.

3.2.3 Oxygen profile measurements

The schematic diagram of the experimental setup for in-situ measurement of oxygen concentration profiles in the biofilm is illustrated in Figures 3.1 and 3.2. The microsensor was first mounted on micromanipulator (World Precision Instruments Inc., Sarasota, Florida, Model #: M3301R). The measurement for dissolved oxygen was carried out by moving the microsensor from the bulk liquid through the biofilm in 20 and 25 μm increments (for FS-and HF-MAB, respectively) until the oxygen concentration became constant (close to the membrane substratum). All the microsensor measurements were performed at random locations approximately 1 mm apart from one another.

3.2.4 Measurements of MAB density

In order to estimate the concentration of microorganisms responsible for the biodegradation activities (biofilm density), several pieces of biofilms (approximately 1.0 cm × 1.5 cm and 1.0 cm × 1.0 cm for FS- and HF-MABs, respectively) were sampled from the reactors after microsensor measurements had been performed. Based on a method already developed by some researchers (Zhou et al. 2009; Zhang and Bishop 1994), these biofilm samples were subjected to gravimetric analysis to obtain data for the density calculations. The biofilm depth was measured by microsensor as described by Zhang et al. (1995). The values of the biofilm depth of the biofilms sampled were 0.15 and 0.10 cm for HF and FS-MABs, respectively. Crucibles containing biofilms were weighed after drying at 105^{o}C and combusting at 550^{o}C for 2 h to determine the biofilm dry cell mass. The biofilm volume was obtained by multiplying the biofilm thickness and the biofilm area. The average biofilm density $\overline{X}_f$ was thus calculated by dividing the total dry cell mass of the biofilm samples, by the total volume of the biofilm samples, as expressed below:

$$\overline{X}_f = \frac{W_d}{V_b} \Big/ n \qquad (3.1)$$

where; W_d is the total dry cell mass of the biofilm samples in terms of volatile solids (g VS); V_b is the total volume of the biofilm samples, and *n* is the number of biofilm pieces that were sampled.

As this study is focused on the aerobic zone of the MABs, values of the biofilm densities of the MABs obtained from above calculations were therefore approximate as they may have included the densities of microorganisms existing in both aerobic and anaerobic layers of the MABs.

3.3 Results

3.3.1 Biofilm at pseudo-steady state

Microsensor measurements were performed only when the biofilm had attained pseudo-steady state performance, which is one of the assumptions of Monod kinetic model used in this work. The pseudo steady-state nature of the biofilm was also investigated by taking oxygen concentration profiles measurements three times at the same location in 12-h time interval in one biofilm sample. As shown in Figure 3.4, these profiles were similar based on their trends. This phenomenon implied that the biofilm was at pseudo-steady state at the time the microsensor measurements were conducted. The data used in plotting Figure 3.4 are presented in Appendix B2.

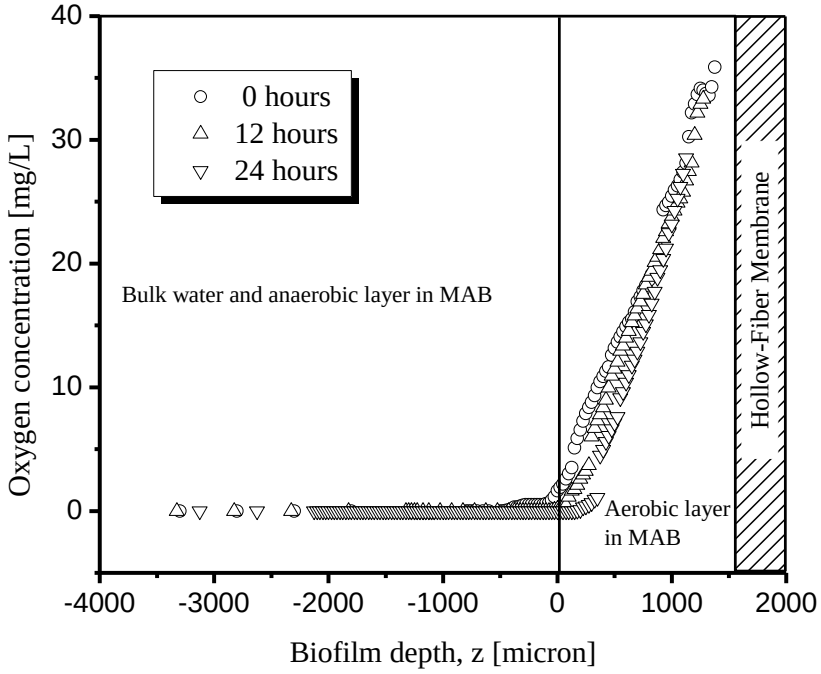

Figure 3.4 Oxygen concentration profiles measured in 12-h interval at the same position in the HF-MAB.

3.3.2 Oxygen concentration profile along the biofilm depth

With the use of an oxygen microsensor, oxygen concentration profiles in the MABs were measured. Figure 3.5 show the oxygen concentration profiles in the two different module configurations of MAB (HF and FS membrane modules). Data for plotting Figure 3.5 are presented in Appendix B3.

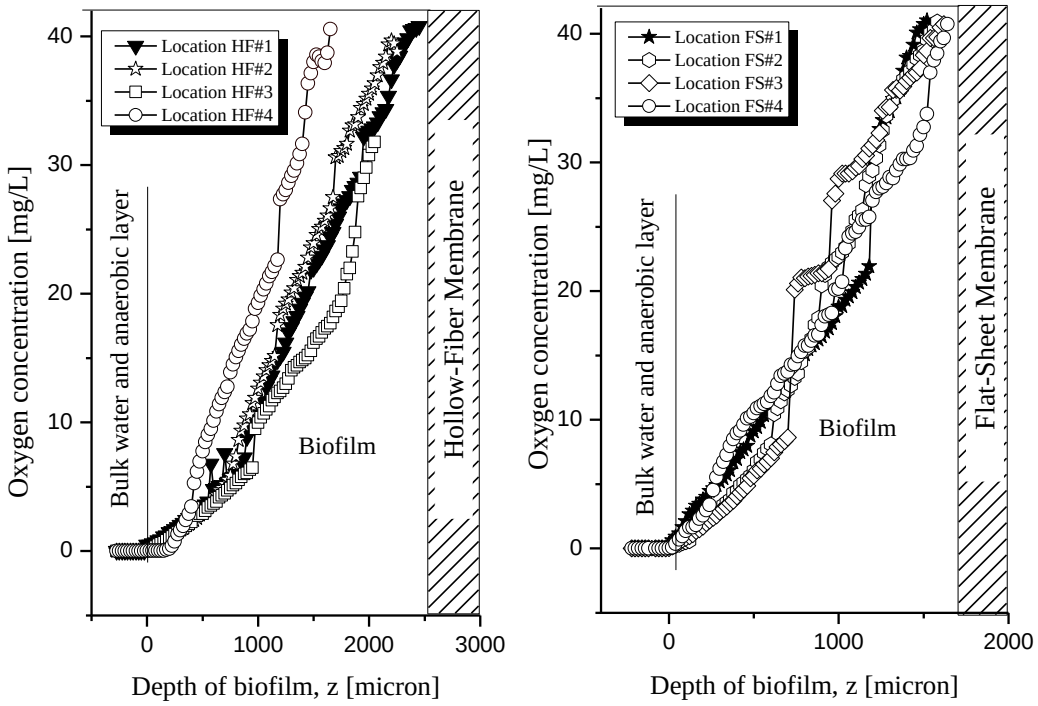

Figure 3.5 Oxygen concentration profiles in the aerobic zone of biofilm grown in the HF-MABR (location 1 to 4) and the FS-MABR (location 1 to 4).

As shown in the Figure 3.5, concentration profiles in the biofilm grown in the two MABR configurations (HF and FS) follow the same trend of decreasing oxygen concentration from the membrane inert support materials to the biofilm surface. Both biofilm systems were subjected to the same growth conditions, such as influent substrate loading rates and substrates types. The only difference in the two reactor systems was the mode of oxygen supply. However, there are no reports of experimental comparisons between various membrane module configurations as it affects the oxygen transfer rates in biofilm. This study is the first of its kind to explore the difference in biokinetic parameters in HF and FS membrane module configurations of MABRs.

3.3.3 Biofilm model

The Monod model is a popular kinetic expression that describes microbial growth in suspension (Yurt et al. 2002). In a previous study to extract biokinetic parameters from substrate concentration profiles (Yurt et al. 2003), it was demonstrated that a single substrate Monod model adequately describes the growth of pure culture microorganisms in biofilms. Therefore, we used this growth model to examine the growth of mixed micro-organisms population in MABs. The assumptions of the Monod model are described below:

1. This model considers oxygen as the single limiting substrate and the oxygen in biofilm is consumed at a rate described by Monod equation.

2. There is no substrate removal or oxygen consumption in the bulk liquid in the reactor.

3. Oxygen is the growth-limiting parameter for the metabolic activities of the heterotrophic bacteria.

4. Oxygen and biodegradable organic matter are transported perpendicularly through the biofilm to an inactive and impermeable substratum.

5. Mass transport oxygen in the biofilm is one-dimensional.

By assuming one-dimensional mass transport, the mass transfer of oxygen within the biofilm unit area is described by Fick's first law (Williamson and McCarty 1976):

$$\frac{\partial C}{\partial t} = - AD_{e,z}\left(\frac{\partial C}{\partial z}\right) \qquad (3.2)$$

where $\frac{\partial C}{\partial t}$ is the rate of oxygen mass transfer (mgO_2/s); $D_{e,z}$ is the diffusion coefficient (cm^2/s); A is cross-sectional area of the biofilm through which flux is

occurring; $D_{e,z}$ is the diffusion coefficient of oxygen at biofilm depth z (cm^2/s)and $\frac{\partial C}{\partial z}$ is the concentration gradient of oxygen in the vertical direction, z (mg/cm^4).

The rate of oxygen utilization at any point within the biofilm is assumed to follow the Monod relationship (Monod 1949):

$$-\frac{dC}{dt} = \frac{\mu_m}{Y}\bar{X}_f\left(\frac{C}{K_s + C}\right)_f \tag{3.3}$$

Where $-\frac{dC}{dt}$ is the utilization rate of the rate-limiting oxygen substrate, ($mgcm^{-3}\cdot s^{-1}$); $\frac{\mu_m}{Y}$ is the maximum specific growth rate of oxygen utilization, mgO_2/g VS·s; K_S is the Monod half-saturation coefficient, mg/L; C is the oxygen concentration in the biofilm at a given depth z, mg/L; $\overline{X}_f$ is the averaged biofilm density (g VS/L) and subscript $_f$ stands for inside the biofilm.

Applying Equations 3.2 and 3.3 to the differential element of biofilm width, dz, the mass transfer terms become (Williamson and McCarty 1976):

$$\text{Inflow of oxygen} = -AD_{e,z}\left(\frac{\partial C}{\partial z}\right) \tag{3.4}$$

$$\text{Outflow of oxygen} = -AD_{e,z}\left(\frac{\partial C}{\partial z} + \frac{\partial}{\partial z}\cdot\frac{\partial C}{\partial z}dz\right) \tag{3.5}$$

$$\text{Oxygen utilization} = -A\frac{\mu_m}{Y}\bar{X}_f\left(\frac{C}{K_s + C}\right)_f dz \tag{3.6}$$

Combining above Equations 3.4, 3.5 and 3.6 for the mass balance gives a steady-state equation:

$$D_{e,z}\left(\frac{d^2C}{dz^2}\right)_f = \frac{\mu_m}{Y}\bar{X}_f\left(\frac{C}{K_s + C}\right)_f \tag{3.7}$$

However in discrete biofilms, the mass balance above is expressed as follows:

$$D_{e,z}\left(\frac{d^2C}{dz^2}\right)_f + \zeta\left(\frac{dC}{dz}\right)_f = \frac{\mu_m}{Y}\bar{X}_f\left(\frac{C}{K_s + C}\right)_f \qquad (3.8)$$

Equation 3.8 takes into account the variable diffusivity, $D_{e,z}$, and diffusivity gradient, ζ, due to the experimental evidence demonstrating that: (1) the effective diffusivity in the biofilms varies across the biofilm and (2) the effective diffusivity in biofilms depends on the flow velocity at which the biofilms were grown (Beyenal and Lewandowski 2002).

3.3.4 Determination of mass transfer coefficients

The mass transfer coefficients in the biofilm model are variable diffusivity $D_{e,z}$ and diffusivity gradient, ζ. The steps involved in the determination of these mass transfer coefficients starts with calculation of the limiting current density, *i* (measured from the oxygen microsensor) by using the following relation:

$$i\,(A/cm^2) = \frac{I}{A} = \frac{Limiting\ current\ measured\ by\ microsensor\,(A)}{Microsensor\ tip\ \ surface\ area\ (cm^2)} \qquad (3.9)$$

The local effective diffusivity, D_{fl} (cm/s), is related to the limiting current density by the following equation (Beyenal and Lewandowski 2000):

$$D_{fl} = 1.12\times10^{-10} + 3.69\times10^{-12}\,(i) \qquad (3.10)$$

where D_{fl} is the effective diffusivity (cm^2/sec) and *i* is the limiting current density (A/cm^2)

The local relative effective diffusivity, D^*_{fz} (dimensionless), was estimated from the following relation (Beyenal and Lewandowski 2002):

$$D_{fz}^{*} = \frac{D_{fl}}{\left(D_{K_3Fe(CN)_6}\right)_e} \tag{3.11}$$

where $\left(D_{K_3Fe(CN)_6}\right)_e$ is the molecular diffusivity of ferricyanide in the electrolyte, equal to 7×10^{-6} cm^2/s at room temperature (Gao et al. 1995). The molecular diffusivity of ferricyanide serves a common factor to obtain a dimensionless D_{fz}^{*} (Beyenal and Lewandowski 2002).

Finally, effective diffusivity gradient, ζ (cm/sec), was determined by multiplying the diffusion coefficient of water, D_w , at 21°C of 2.0×10^{-5} cm^2/sec (Revsbech et al.1986) by the slope of a plot of local relative effective diffusivity versus biofilm depth, *z* (cm) as follows:

$$\zeta = D_w\left(\frac{\Delta D_{fz}^{*}}{\Delta z}\right) \tag{3.12}$$

The average effective diffusivity of oxygen is, therefore, calculated using the following relation (Beyenal and Lewandowski 2002):

$$D_{e,z} = 0.252\times\left(2\times10^{-5}\right)+\left(\frac{\zeta L_f}{2}\right) \tag{3.13}$$

L_f in the Equation 3.13 above is the average biofilm thickness.

The plots for the determination of effective diffusivity gradient are shown in Figures 3.6 and 3.7 for HF- and FS-MABs, respectively. The data points for the plot in the Figures 3.6 and 3.7 are presented in Appendices B4 and B5, respectively. These data were taken from aerobic layer of the MABs, starting from the depth in the MABs where oxygen was first detected.

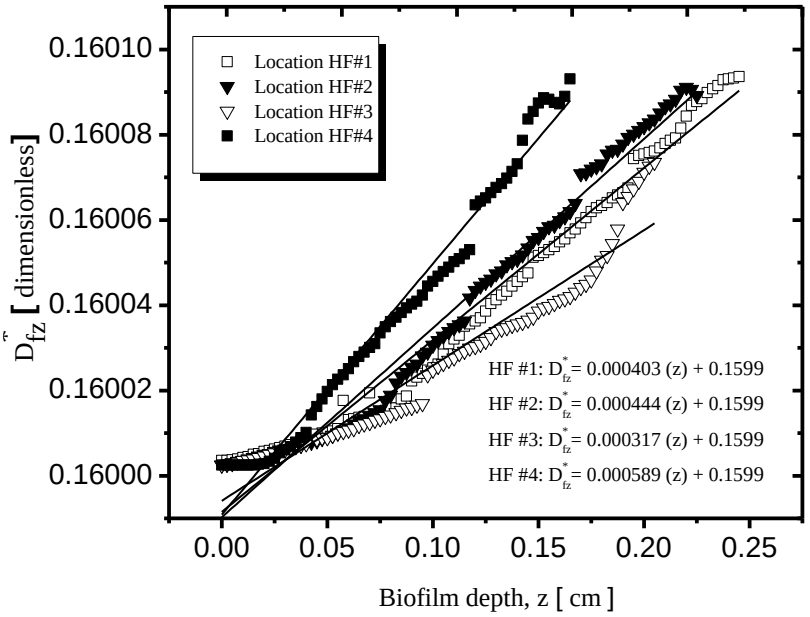

Figure 3.6 Effective diffusivity gradient of oxygen transport in the HF-MAB.

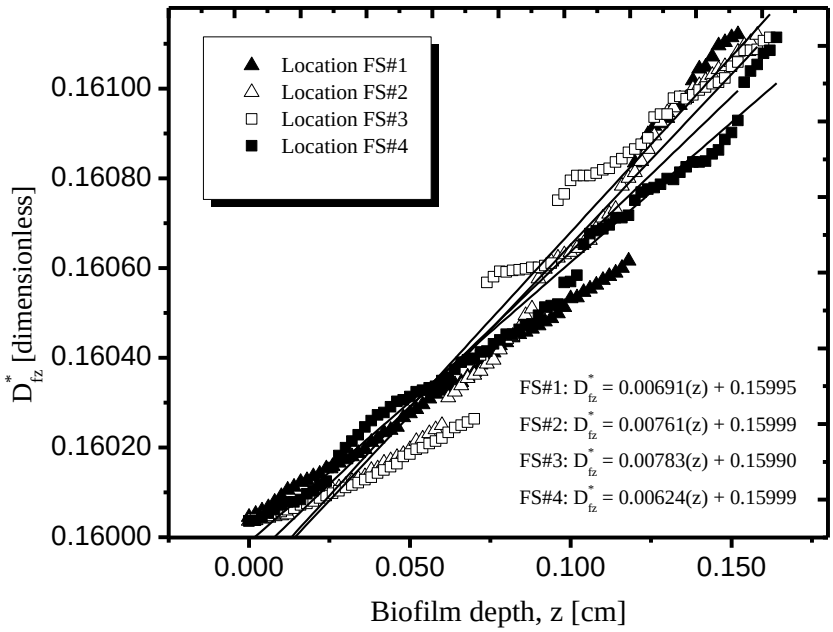

Figure 3.7 Effective diffusivity gradient of oxygen transport in the FS-MAB.

Table 3.1 contains a summary of the calculated values of $D_{e,z}$ and ζ of oxygen in the biofilms in two different module configurations of MABRs as well as the values of their respective average biofilm densities.

Table 3.1 The average biofilm density and mass transfer coefficients of oxygen in the HF- and FS-MABs

Biofilms	Locations	$\overline{X}_f$ (gVS/L)	ζ (cm/s)	$D_{e,z}$ (cm^2/s)	Correlation Coeffient[a]
Hollow-Fiber	1		8.00×10^{-9}	5.04×10^{-6}	0.97
	2		8.00×10^{-9}	5.04×10^{-6}	0.98
	3		6.00×10^{-9}	5.04×10^{-6}	0.93
	4		1.20×10^{-8}	5.04×10^{-6}	0.98
	Average	147.00	8.50×10^{-9}	5.04×10^{-6}	
Flat-Sheet	1		1.38×10^{-7}	5.08×10^{-6}	0.93
	2		1.52×10^{-7}	5.09×10^{-6}	0.97
	3		1.56×10^{-7}	5.09×10^{-6}	0.96
	4		1.24×10^{-7}	5.08×10^{-6}	0.99
	Average	104.67	1.43×10^{-7}	5.09×10^{-6}	

[a] *Correlation coefficient for D^*_{fz} and z*

The experimentally determined values of biofilm densities for HF and FS-MABs are 147.00 and 104.67 gVS/L, respectively. The effective diffusivity, D_{fl} calculated from the current signal measured by the oxygen microsensor were used to compute the local effective diffusivities D^*_{fz}, which were plotted against the biofilm depth (Figures 3.6 and 3.7). The local diffusivity profiles in Figures 3.6 and 3.7 were fitted to linear relationship to obtain a function (D^*_{fz} = slope$\times z$ + intercept), which was used to correlate local effective diffusivity,

D^*_{fz} with the biofilm depth, *z*. The slope of the effective diffusivity profile (Figures 3.6 and 3.7) can be multiplied by the diffusivity of oxygen in water to calculate the effective diffusivity gradient, ζ. Having determined ζ, respective effective diffusivity, $D_{e,z}$ values were calculated using Equation 3.13. As shown in Table 3.1, the average effective diffusivity of oxygen of 5.04×10^{-6} and 5.09×10^{-6} cm^2/s were obtained in biofilms of HF and FS module membrane configurations, respectively. In the same vein, average diffusivity gradient of 8.50×10^{-9} and 1.43×10^{-7} cm/s was obtained in biofilms of HF and FS module membrane configurations, respectively. The values obtained for effective diffusivity in both biofilms are a few orders of magnitude higher than that of diffusivity gradient, suggesting that mass transfer diffusion limitations had a more pronounced effect on the transport of oxygen in the biofilm than variations in flow velocities of bulk water.

3.3.5 Determination of the biokinetic parameters in biofilms

To start with, first derivatives $(dC/dz)_f$, and second derivatives $(dC^2/dz^2)_f$, of oxygen concentration respect to the biofilm depth were calculated from polynomial equation approximation, which fits the experimental profile of oxygen concentration in the biofilms (Lewandowski et al. 1994). The polynomial fits are shown in Appendices B6 and B7 for HF- and FS-MABs, respectively.

Then, the oxygen concentration profiles in Figure 3.5, mass transfer coefficients and biofilm density in Table 3.1 were used to estimate the Monod kinetic parameters in the HF- MAB and first-order kinetic coefficients in HF - and FS- MABs.

As presented in Figures 3.8, the regression relationship between oxygen utilization rate and oxygen concentration in one measurement location in HF-MAB exhibits the saturation kinetics of Monod model. Therefore, non-linear regression of Monod model was used to fit the experimental data. Kinetic models have been fitted using nonlinear regression. Examples in the literature include

specific cellular growth rate as a function of liquid phase substrate concentration to study growth rate of microorganism in suspension (Bakke et al. 1984) and photosynthetic rate as a function of irradiance to study the rate of enzymatic reactions in the photosynthesis in alga *Chlorella* (Dabes et al. 1973). We therefore use the nonlinear regression technique to fit the reaction rate and oxygen concentration data obtained from this particular location in HF-MABs.

The fitting formula for the non-linear regression analysis is (Monod 1949):

$$R_s = \frac{V_{max} C^n}{K_s^{\ n} + C^n} \tag{3.14}$$

where $R_s = D_{e,z}\left(\frac{\partial^2 C}{\partial z^2}\right)_f + \zeta\left(\frac{\partial C}{\partial z}\right)_f$ at pseudo steady-state in the biofilm and $V_{\max} = \frac{\mu_m}{Y}\overline{X}_f$. With the results of non-linear regression, $\frac{\mu_m}{Y}$ can be calculated successfully since $\overline{X}_f$ has been determined experimentally. K_s is the Monod half-saturation coefficient which can be read directly from the plot of oxygen utilization rate in biofilm as a function of oxygen concentration in Figure 3.8 and n is the number of substrates investigated which in this study is 1 (only oxygen in MABs).

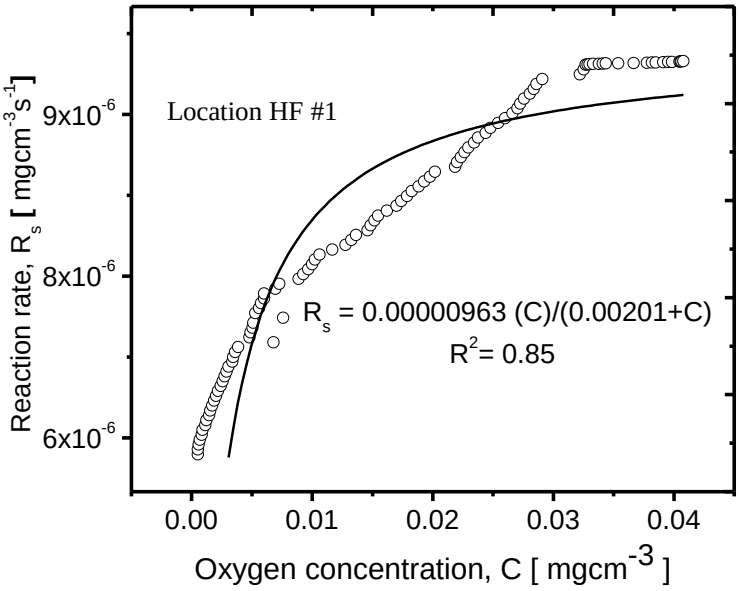

Figure 3.8 Monod kinetic relationship between oxygen concentration and its utilization rate from one measurement location in the HF-MAB.

The Monod kinetic parameters determined from microsensor measurements at one location in HF-MAB are summarized in Table 3.2. The data for plotting Figure 3.8 are presented in Appendix B8.

Table 3.2 The Monod kinetic parameters determined from experiment at one location in HF-MAB ($\overline{X}_f$ for HF=147.00 gVS/L)

Biofilm	Locations	K_s (mg O_2/cm^{-3})	μ_m/Y ($mgO_2/gVS \cdot s$)	Correlation Coeffient[a]
Hollow-fiber	1	0.00201	6.50×10^{-8}	0.85

[a] *Correlation coefficient of nonlinear regression for estimation of μ_m/Y and K_s*

As presented in Figures 3.9 and 3.10, the regression relationship between oxygen utilization rate and oxygen concentration in MABs was linear which is

characteristic of first-order kinetics. Therefore, the Monod kinetic equation (3.8) was simplified to first order kinetics assuming that the apparent K_s is of magnitude much greater than the concentration of limiting substrate, C (oxygen in this case) due to oxygen mass transport limitations in the biofilms. In this case, K_s >> C, the concentration term (C), in the denominator of the Monod equation 3.8 can be neglected such that $(K_s + C) \approx K_s$ and the resulting rate equation is:

$$R_s = \frac{V_{max} C}{K_s + C} = \frac{(\mu_m / Y)}{K_s} \bar{X}_f [C] \tag{3.15}$$

where $\frac{(\mu_m / Y)}{K_s} \bar{X}_f$ is equal to the slope of the plot of oxygen reaction rate in the biofilm as a function of oxygen concentration as shown in Figures 3.9 and 3.10. The first-order kinetic coefficient, $\frac{(\mu_m / Y)}{K_s}$ can be determined from the slope of the plot since the biofilm density, $\bar{X}_f$ has been determined experimentally. Further explanation on the first-order fit of the experimental data is provided in Section 3.4.2.

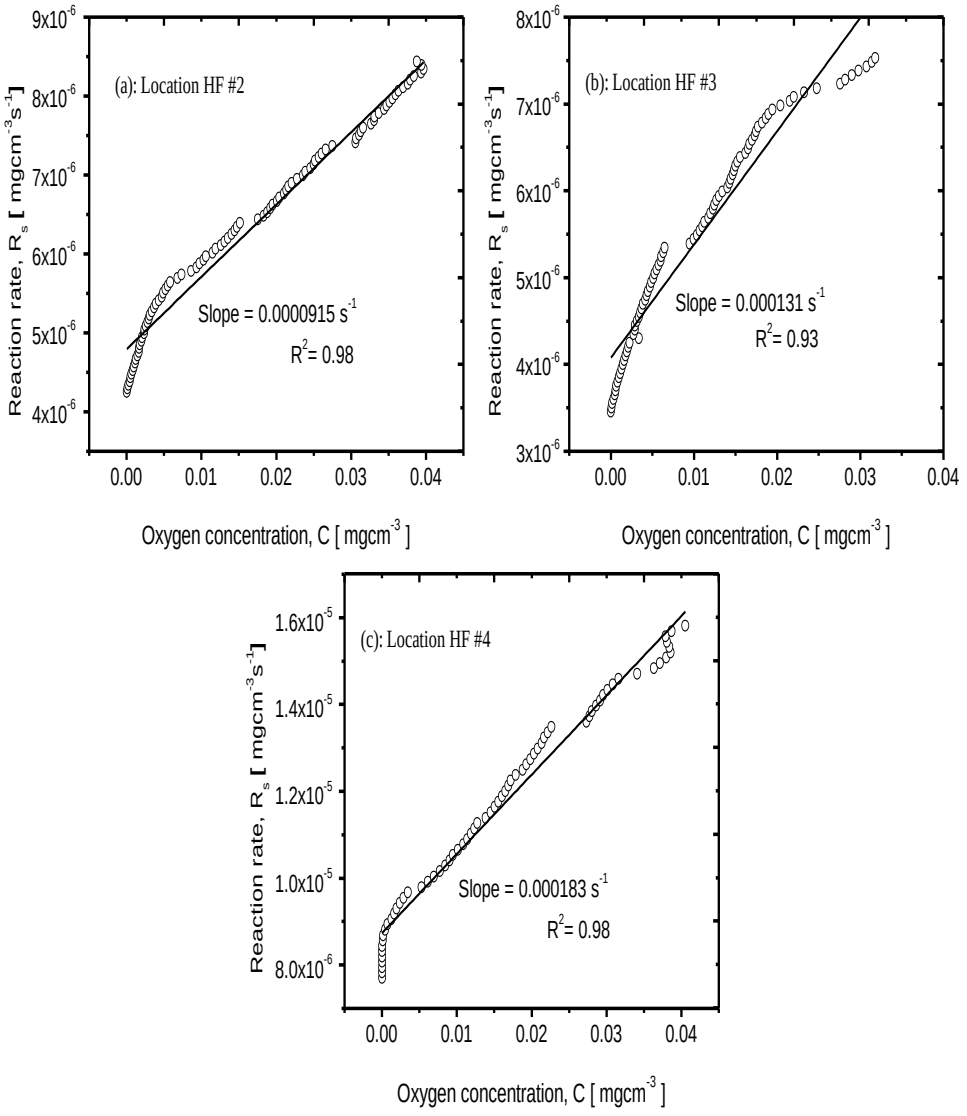

Figure 3.9 First-order kinetic relationship between oxygen concentration and its utilization rate in the HF-MAB.

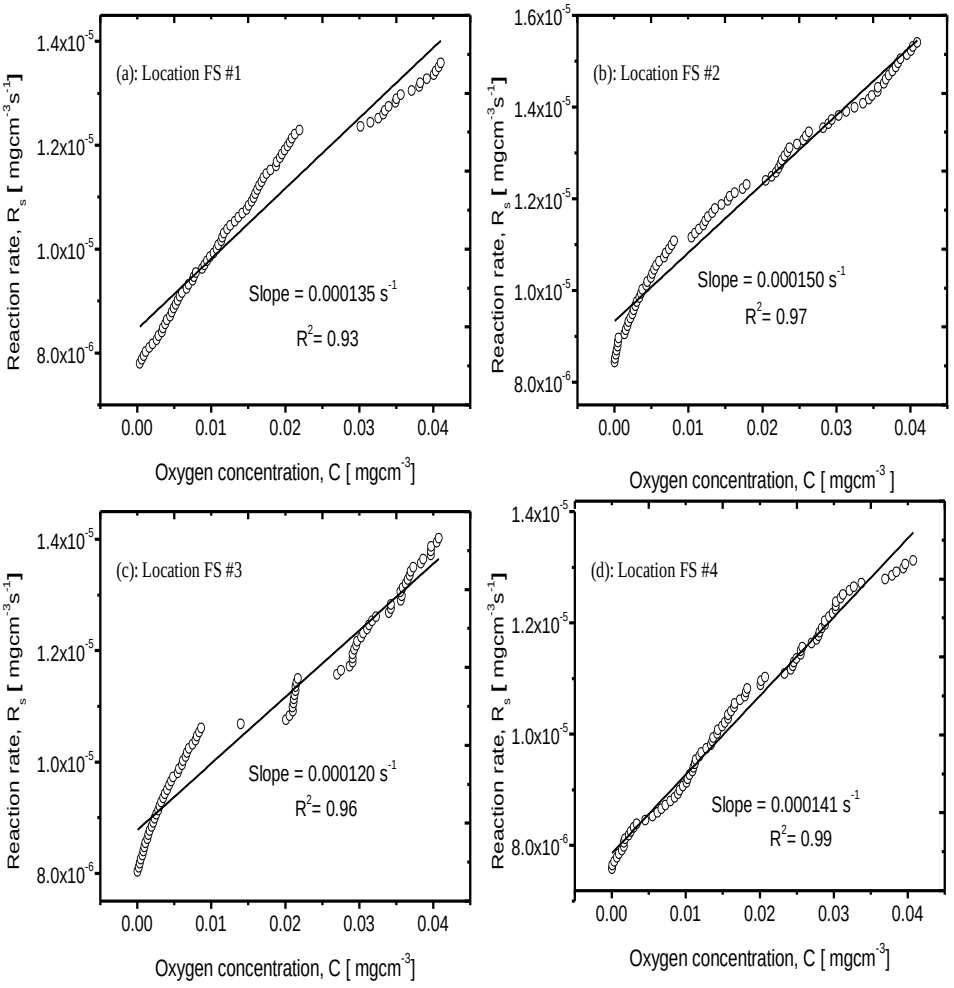

Figure 3.10 First order kinetic relationship between oxygen concentrations and its utilization rate in the FS-MAB.

The kinetic parameter determined from microsensor measurements with varying locations in the two different module configurations of MABRs are presented in Table 3.3. The data for plotting Figure 3.9 and 3.10 are presented in Appendices B9 and B10, respectively.

Table 3.3 The first order kinetic coefficient determined from experiments with varying locations in HF-and FS-MABs ($\overline{X}_f$ for HF=147.00 gVS/L and $\overline{X}_f$ for FS = 104.67 gVS/L)

Biofilms	Locations	$(\mu_m/Y)/K_s$ (cm^3/gVS·s)	Correlation Coeffient
Hollow-fiber	2	6.22×10^{-7}	0.98
	3	8.91×10^{-7}	0.93
	4	1.24×10^{-6}	0.98
		Mean = 9.18×10^{-7}	
		S.D = 3.09×10^{-7}	
Flat-sheet	1	1.29×10^{-6}	0.93
	2	1.43×10^{-6}	0.97
	3	1.15×10^{-6}	0.96
	4	1.35×10^{-6}	0.99
		Mean = 1.31×10^{-6}	
		S.D = 1.18×10^{-7}	

A statistical analysis of F-and t-tests were employed to investigate the effects of membrane module configuration of MABRs on the estimated first-order kinetic parameter. The results of this statistical analysis indicate that the values of $(\mu_m/Y)/K_s$ in biofilms obtained in HF- and FS- MABs were statistically different. Details of this statistical analysis are presented in Appendix C1.

3.4 Discussion

3.4.1 Estimated kinetic parameters

The calculated Monod's half-saturation coefficient (K_s) for oxygen consumption from measurement location in the HF-MAB was 0.00201 mg O_2/cm^3 (2.01 mg O_2/L) and maximum utilization rate of oxygen (μ_m/Y) was 6.50×10^{-8} mgO_2/gVS·s. Even though, these Monod kinetic parameters were obtained from experimental

data from one location in the biofilms out of eight locations investigated, it is important to compare the values to kinetic constants for activated sludge process. In this regards, biokinetic parameters of biofilms from this study were found to differ from published data on kinetic constants for activated sludge process at room temperature, suggesting that physiology and microbial species composition of biofilm systems are different from suspended growth systems. For instance, the computed maximum specific growth rate, μ_m/Y in the HF-MAB of 6.50×10^{-8} $mgO_2/gVS\cdot s$ is several times smaller than those reported in suspended cultures (0.56-2.44) $\times10^{-2}$ $mgO_2/gSS\cdot s$ by Jørgensen et al. (1992). On other hand, the calculated Monod's saturation coefficient for oxygen, K_S, was 0.00201 mg O_2/cm^3 (2.01 mg O_2/L). This K_S value is, therefore, higher than those obtained for biomass grown in suspended cultures (0.25 mg/L by Kappeler and Gujer (1992); 0.237 mg/L by Yurt et al. (2002)), which is in close agreement with the conclusion reached by Perez et al. (2005) that the effects of mass transport limitations is reflected by the Monod's saturation coefficient, which are one order of magnitude greater for activated sludge flocs than those reported for single suspended cells. Also, pure oxygen was used in the MABs while other activated sludge systems used air. The difference between kinetic parameters measured in MABs and other reported numbers in activated sludge cannot be attributed entirely to the difference in physiology and microbial species composition between these two systems. The difference between pure oxygen and air is another reason.

Similarly, the calculated K_S values for microbial growth in HF-MAB was higher than those reported for other biofilm systems (0.25 mg/L by Lewandowski et al. (1991); 0.333 mg/L by Yurt et al. (2003) and 0.16-0.75 mg/L by Zhou et al. (2008). Like the activated sludge systems described above, air was used in these other biofilm systems. It is possible that the observed difference between the kinetic parameters in MABs and other biofilm systems is also related to the use of pure oxygen in MABs.

In HF-and FS-MABs, the first-order kinetic coefficient, $(\mu_m/Y)/K_s$ were in the range of $(0.62 - 1.24)\times10^{-6}$ and $(1.15 - 1.43)\times10^{-6}$ $cm^3/gVS\cdot s$, respectively. These values of $(\mu_m/Y)/K_s$ obtained by first-order kinetics are also several times smaller than those reported for biodegradation of organic compounds in activated sludge (0.21– 0.40 $m^3/gVSS\cdot d$ converting to 2.31 - 4.63 $cm^3/gVSS\cdot s$) by Namkung and Rittmann (1987).

3.4.2 Kinetic analysis of MABs

This study did achieve the goal of estimating kinetic parameters in MABs. Based on the results of this study, it was demonstrated that the approach for estimating kinetic parameters worked. The experimental data obtained from one measurement location in HF-MAB exhibited the saturation kinetics of Monod model and therefore the data fitted to Monod model with the correlation coefficient, R^2 of 0.85, which is significant for non-linear estimates of kinetic parameters in biofilms. However, first-order relationship, a special case of Monod relationship was encountered in several measurements and the situation is analyzed in this section.

The Monod model states that the relationship between the rate of substrate removal and microbial growth can be best described by a "saturation type of curve" where at high concentration of the substrate, the microorganisms grow at a maximum rate independent of substrate utilization (Monod 1949). This means that for maximum utilization of the substrate to be attained, the substrate has to be in a sufficient quantity for microbial utilization. The experimental data plotted in Figures 3.9 and 3.10 show that oxygen utilization rate in the biofilm increases with the increase in oxygen concentration and maximum utilization rate of oxygen was not attained. Based on this observation and Monod relationship described above, it could be possible that oxygen concentration in the biofilm was not in a sufficient quantity to reach saturation surrounding the microbial cells in the biofilms and cause them to exhibit the saturation kinetics that is characteristics

of Monod model. Since oxygen was continuously supplied to the biofilm from external source, a possible explanation for limited oxygen conditions in the biofilm might have something to do with the rate of oxygen transport by diffusion within biofilm and biological oxygen demand in the biofilms. If the rate of oxygen mass transport is slower than the biological demand in biofilm, limited oxygen conditions will exist and increase in oxygen concentration will result in increased utilization rate. Maximum oxygen utilization rate can only be attained if the oxygen is available in sufficient quantity to the microorganisms in the biofilm, but this was not the case in this study due to the diffusion resistance of oxygen transport in biofilm that might have created unsaturated oxygen conditions in the biofilms.

The observed kinetics of oxygen utilization in the biofilms in this study as a result of oxygen transport limitations can be related to the phase-transfer model that was put forward by Robinson and Tiedje (1982) to describe the kinetics of hydrogen consumption in anaerobic habitat. Due to phase transfer limitations, this model used first-order kinetics to describe substrate consumption in anaerobic habitat when the rate at which a gaseous crosses the gas-liquid interphase is slower than the rate of biological consumption. However, in the absence of phase-transfer limitations, this model assumes that the rate of substrate transfer will be rapid enough to supply the biological demand and kinetic pattern will be controlled by biological process. This model also states that, in the absence of phase-transfer limitations, a Michaelis-Menten progress curve will be observed for gaseous substrate consumption assuming the biological processes exhibit saturation kinetics. Applying the same principles of this phase-transfer model in activated sludge processes to the biofilms processes, it is reasonable to assume that under oxygen mass transport limitations, the kinetics of oxygen utilization is of first order. This assumption is supported by better fit of the experimental data with first-order kinetic model. Similar biofilm model has been proposed by Atkinson et al. (1963), which assumes that the intrinsic reaction rate in the biofilm is of first order in substrate limiting system (as a simplification of the Michaelis-Menten or

Monod kinetics). First-order diffusion reaction model was also applied by Vieira and Melo (1992) to study the intrinsic kinetics of biofilm formed under turbulent flow and low substrate concentrations. It is important to note that Michaelis-Menten kinetics described here is mathematically analogous to the Monod model.

Researchers have also reported close relationship between the biokinetic parameters, in particular the K_s, and the substrate transport limitation in attached growth systems (Plattes et al. 2007; Chen et al. 2003). The K_s value has also been proposed as a manifestation of mass transfer effects on microbial growth kinetics (Logan and Dettmer 1990). In Monod kinetics, K_s determines how rapidly specific substrate (oxygen) utilization rate approaches maximum substrate (oxygen) utilization rate. The K_s is also defined as the substrate concentration at one-half of the maximum specific substrate utilization rate. This means that the higher the maximum specific substrate utilization rate, the higher the K_s value. Based on the curve fittings in Figures 3.9 and 3.10, it seems that the oxygen utilization in the biofilm was at early stage of Monod relationship and maximum oxygen utilization rate was not attained, which suggests high apparent K_s value. This observation is in agreement with research by Grasso et al. (1995) which demonstrated that when mass transfer limits the availability of the substrate, the apparent value of K_s would appear to be greater than its actual value. This means that the value of K_s under oxygen mass transport limitation appears very high compared to the actual value in the absence of this constraint. Therefore, under substrate mass transport limitations (oxygen in this case) in the biofilm, the apparent K_s is of magnitude much greater than the concentration of limiting oxygen concentration ($K_s >> C$), therefore the concentration term (C), in the denominator of the Monod equation 3.14 can be neglected such that $(K_s + C) \approx K_s$. The resulting equation is first-order kinetics, indicating that the rate of oxygen utilization is directly proportional to the available oxygen concentration in the biofilm and this relationship is manifested in the curve fittings of Figures 3.9 and 3.10.

3.5 Conclusions

We have presented a computational procedure to determine kinetic parameters in MABs from the oxygen concentration profiles, and that the following conclusions are drawn:

1. The approach presented in this study successfully measured the kinetic parameters in MAB as intended. The values of Monod's half-saturation coefficient (K_s) for oxygen consumption and maximum utilization rate of oxygen (μ_m/Y) in MAB were 2.01 mg O_2/cm^3 and 6.50×10^{-8} $mgO_2/gVS\cdot s$, respectively.

2. Oxygen mass transfer limitation was encountered in several measurements. It allowed first-order relationship, a special case of Monod kinetic model, which limited the number of kinetic parameter estimate to one. And, the range and average values of first-order kinetic coefficient, $(\mu_m/Y)/K_s$ in MABs were $(0.62 - 1.43)\times10^{-6}$ and 1.14×10^{-6} $cm^3/gVS\cdot s$, respectively.

3.6 References

Atkinson, B., A.W. Busch, and G. S. Dawkins. 1963. Recirculation, reaction kinetics and effluent quality in a trickling filter model. *Journal Water Pollution Control Federation* 35 (10):1307-1321.

Bakke, R., M. G. Trulear, J. A. Robinson, and W. G. Characklis. 1984. Activity of pseudomonas-aeruginosa in biofilms - Steady-State. *Biotechnology and Bioengineering* 26 (12):1418-1424.

Beyenal, H., and Z. Lewandowski. 2000. Combined effect of substrate concentration and flow velocity on effective diffusivity in biofilms. *Water Research* 34 (2):528-538.

Beyenal, H., and Z. Lewandowski. 2002. Internal and external mass transfer in biofilms grown at various flow velocities. *Biotechnol Prog* 18 (1):55-61.

Bishop, P. L., and B. E. Rittmann. 1995. Modelling heterogeneity in biofilms: Report of the discussion session. *Water Science and Technology* 32 (8):263-265.

Chen, K.-C, J.-Y. Wu, W.-B.Yang, and S-C. J. Hwang. 2003. Evaluation of effective diffusion coefficient and intrinsic kinetic parameters on azo dye biodegradation using PVA-immobilized cell beads *Biotechnology and Bioengineering* 83(7):821-832.

Dabes, J. N., R. K. Finn, and C. R. Wilke. 1973. Equations of substrate-limited growth - case for blackman kinetics. *Biotechnology and Bioengineering* 15 (6):1159-1177.

Gao, X. P., J. Lee, and H. S. White. 1995. Natural-Convection at Microelectrodes. *Analytical Chemistry* 67 (9):1541-1545.

Grasso, D., K. Strevett, and R. Fisher. 1990. Uncoupling mass transfer limitations of gaseous substrates in microbial systems. *The Chemical Engineering Journal and the Biochemical Engineering Journal* 59 (2):195-204.

Hibiya, K., J. Nagai, S. Tsuneda, and A. Hirata. 2004. Simple prediction of oxygen penetration depth in biofilms for wastewater treatment. *Biochemical Engineering Journal* 19 (1):61-68.

Hooijmans, C. M., S. G. M. Geraats, and K. C. A. M. Luyben. 1990. Use of an oxygen microsensor for the determination of intrinsic kinetic-parameters of an immobilized oxygen reducing enzyme. *Biotechnology and Bioengineering* 35 (11):1078-1087.

Jorgensen, P. E., T. Eriksen, and B. K. Jensen. 1992. Estimation of viable biomass in waste-water and activated-sludge by determination of ATP, oxygen utilization rate and FDA hydrolysis. *Water Research* 26 (11):1495-1501.

Kappeler, J., and W. Gujer. 1992. Estimation of kinetic-parameters of heterotrophic biomass under aerobic conditions and characterization of waste-water for activated-sludge modeling. *Water Science and Technology* 25 (6):125-139.

Lewandowski, Z., P. Stoodley, S. Altobelli, and E. Fukushima. 1994. Hydrodynamics and kinetics in bioifilm kinetics in biofilm systems - recent advances and new problems. *Water Science and Technology* 29 (10-11):223-229.

Lewandowski, Z., G. Walser, and W. G. Characklis. 1991. Reaction-kinetics in biofilms. *Biotechnology and Bioengineering* 38 (8):877-882.

Logan, B. E., and J. W. Dettmer. 1990. Increased mass transfer to microorganisms with fluid motion. *Biotechnology and Bioengineering* 35(11):1135-1144.

Lu, R. and Yu, T. 2002. Fabrication and evaluation of an oxygen microelectrode applicable to environmental engineering and science. *Journal of Environmental Engineering and Science* 1(3):225-235.

Monod, J. 1949. The growth of bacterial cultures. *Annual Review of Microbiology* 3:371-394.

Namkung, E., and B. E. Rittmann. 1987. Estimating volatile organic compound emissions from publicly owned treatment works. *Journal Water Pollution Control* 59 (7):670-678.

Plattes, M., D. Fiorelli, S. Gille, C. Girard, E. Henry, F. Minette, O. O'Nagy, and P. M. Schosseler. 2007. Modelling and dynamic simulation of a moving bed bioreactor using respirometry for the estimation of kinetic paramters. *Biochemical Engineering Journal* 33(3):253-259.

Perez, J., C. Picioreanu, and M. van Loosdrecht. 2005. Modeling biofilm and floc diffusion processes based on analytical solution of reaction-diffusion equations. *Water Research* 39 (7):1311-1323.

Revsbech, N. P., B. Madsen, and B. B. Jørgensen. 1986. Oxygen production and consumption in sediments determined at high spatial-resolution by computer-simulation of oxygen microelectrode data. *Limnology and Oceanography* 31 (2):293-304.

Robinson, J. A., and J. M. Tiedje. 1982. Kinetics of hydrogen consumption by rumen fluid, anaerobic digestor, and sediment. *Applied and Environmental Microbiology* 44 (6):1374-1384.

Shanahan, J. W., and M. J. Semmens. 2004. Multipopulation model of membrane-aerated biofilms. *Environmental Science & Technology* 38 (11):3176-3183.

Syron, E., and E. Casey. 2008. Membrane-aerated biofilms for high rate biotreatment: Performance appraisal, engineering principles, scale-up, and development requirements. *Environmental Science & Technology* 42 (6):1833-1844.

Syron, E., H. Kelly, and E. Casey. 2009. Studies on the effect of concentration of a self-inhibitory substrate on biofilm reaction rate under co-diffusion and counter-diffusion configurations. *Journal of Membrane Science* 335 (1-2):76-82.

Vieira, M.J, and L.F. Melo. 1999. Intrinsic kinetics of biofilms formed under turbulent flow and low substrate concentrations *Bioprocess Engineering* 20(4):369-375.

Williamson, K., and P.L. McCarty. 1976. A Model of Substrate Utilization by Bacterial Films. *Journal Water Pollution Control* 48 (1):9-24.

Yurt, N., H. Beyenal, J. Sears, and Z. Lewandowski. 2003. Quantifying selected growth parameters of *Leptothrix discophora* SP-6 in biofilms from oxygen concentration profiles. *Chemical Engineering Science* 58 (20):4557-4566.

Yurt, N., J. Sears, and Z. Lewandowski. 2002. Multiple substrate growth kinetics of *Leptothrix discophora* SP-6. *Biotechnology Progress* 18 (5):994-1002.

Zhang, T. C., and P. L. Bishop. 1994. Density, Porosity, and Pore Structure of Biofilms. *Water Research* 28 (11):2267-2277.

Zhang, T. C., Y. C. Fu, and P. L. Bishop. 1995. Competition for substrate and space in biofilms. *Water Environment Research* 67 (6):992-1003.

Zhou, X. H., Y. Q. Qiu, H. C. Shi, T. Yu, M. He, and Q. Cai. 2009. A new approach to quantify spatial distribution of biofilm kinetic parameters by in situ determination of oxygen uptake rate (OUR). *Environmental Science & Technology* 43 (3):757-763.

Zhou, X. H., H. C. Shi, Q. Cai, M. He, and Y. X. Wu. 2008. Function of self-forming dynamic membrane and biokinetic parameters' determination by microelectrode. *Water Research* 42 (10-11):2369-2376.

Chapter 4

DETERMINATION OF KINETIC PARAMETERS IN ROTATING BIOLOGICAL CONTACTORS BIOFILMS

4.1 Introduction

Due to many advantages they offer over conventional activated sludge processes, biofilm-based processes are increasingly used in wastewater treatment. These advantages include mixed microbial populations in bioiflms that can degrade organic substrates and the ability of microorganisms in biofilm to produce glycocalyx surface coatings which protect them from harmful effects of toxicants (Bishop 1997).

Inadequate understanding of the biodegradation kinetics of biofilms is one of the unresolved problems that have hampered rational optimization of biofilm reactor design and operation. In order to understand the biokinetic behaviors of microorganisms in biofilms, accurate, fast and in-situ measurements are required to quantify biokinetic parameters from wastewater constituent biodegradation process. At present, there are several models describing the microbial growth kinetics in activated sludge processes and the computational procedures for determining the biokinetic parameters are well-developed. There are existing mathematical models, which have been used successfully in simulating substrate degradation and biomass growth in biofilms (Namkung and Rittmann 1987; Rittmann and McCarty 1982). But, there is lack of biokinetic parameters for the calibration of these biofilm models to verify that the solutions of the models predict the behaviour of real biofilms (Riefler et al.1998).

It is difficult to measure the biokinetic parameters of biofilm systems due to diffusional resistance within the biofilm that masks its biodegradation kinetics as well as the difficulty of replicating biofilm structures in a test vessel (Riefler and Smets 2003). Due to lack of data on biofilm kinetics, it became practice to determine biokinetic parameters in suspended cultures and apply those values to model microbial growth and predict substrate concentration profiles in biofilms (Horn and Hempel 1997; Hsien and Lin 2005). However, using biokinetic parameters from suspended-growth cultures to predict microbial growth and

substrate utilization in biofilms is questionable because the two systems differ in microbial cell physiology and species compositions.

Other researchers have developed attached growth biofilm systems, but determined biokinetic parameters by measuring oxygen uptake profiles in the bulk liquid as a surrogate measure of substrate consumption. For instance, Riefler et al. (1998), Plattes et al. (2007), and Carvallo et al. (2002) were able to determine bio-kinetic parameters in biofilms through the measured oxygen consumption profiles in the bulk liquid, which was similar to the experimental technique of respirometry in activated sludge (Kappeler and Gujer 1992). The studies have non-negligible drawbacks regardless of progress made with estimation of biokinetic parameters from cultures with intact biofilms. One such drawback includes using a kinetic expression, which assumes that oxygen is not the microbial growth limiting factor when it is obviously difficult to justify this assumption due to oxygen diffusional limitations in biofilm systems. In the studies, however, models that were used in computing biokinetic parameters assumed that the biofilm consisted of uniform thickness, density, and structure and biofilm reactors were well-stirred (an indication of uniform substrate concentration at any point in the system). However, while these assumptions hold true for biofilms in pure culture, they certainly do not represent the biokinetic behavior of biofilms in mixed cultures such as those found in wastewater treatment and this flaw makes it difficult to conclude that estimated biokinetic parameters are reliable and accurate. Also, successful modeling of biofilm reactors for effective wastewater treatment requires kinetic parameters obtained from measurements inside biofilms and not from chemical analysis of substrate removal in the bulkwater phase of biofilm reactors (Lewandowski et al.1991).

The discussion above suggests that for accurate representation of biofilm system parameters, measurements inside the biofilms are necessary. It is encouraging to observe how improved microsensor technology has enabled in-situ chemical characterization of microbial activities including substrate concentration profiles

in biofilms. To quantify biokinetic parameters from substrate concentration profiles, however, is still challenging due to lack of suitable computational procedures. Based on well-known reaction-diffusion equation, Yurt et al. (2003) developed computational procedures to quantify biokinetic parameters from substrate concentration profiles in biofilms that were measured using microsensors. The study was undertaken by growing pure culture biofilm, measuring substrate concentration profiles and computing the biokinetic parameters based on a mathematical model that describes uniform structure. But, the concept of uniform biofilm model contradicts several research findings, which have otherwise revealed the heterogeneity of biofilms (Zhang and Bishop 1994; Bishop and Rittmann 1995). As a result, the biokinetic parameters estimated from uniform biofilm models could not represent the biokinetic behavior of microorganisms in mixed cultures such as those found in wastewater treatment systems. Finally, technical challenges that would be encountered in using biokinetic parameters from pure culture biofilms strongly underscores the need for a computational technique that will take into account biofilm structural heterogeneity in quantifying biokinetic parameters from substrate concentration profiles while permitting accurate and reliable results. The current study provides such a technique.

The objective of this research is to estimate biokinetic parameters of substrate biodegradation in RBC biofilm. RBC biofilm represents a conventional inert substratum and has been used extensively in the treatment of domestic wastewater and specific organic compound pollutants. Mature biofilms grown on a 4-stage rotating biological contactors (RBCs) were sampled from a municipal wastewater treatment plant for laboratory-scale experiments. An oxygen microsensor was constructed to measure oxygen concentration profiles at different locations in the biofilms.

4.2 Materials and methods

4.2.1 Biofilm used

Mature biofilms were taken from a 4-stage RBC system with acrylic circular dics treating municipal wastewater in the town of Devon in Alberta, Canada. Table 4.1 lists the characteristics of the RBC system.

Table 4.1. Main characteristics of RBC system in Devon Wastewater Treatment Plant

Parameters	**Value**
Number of stages	4
Disc diameter (m)	3.7
Disc thickness (mm)	1
Total surface area per stage (m^2)	9290
Effective tank volume (m^3)	51
Percentage immersion of disk (%)	45
Influent flow rate (L/sec)	8-80
Hydraulic retention time (min)	11-106
BOD concentration in influent (mg/L)	100-200

The schematic diagram of 4-stage RBC system is shown in Figure 4.1. Biofilm samples of various thicknesses together with their substratum were randomly sampled from stage 2 and stage 4 of the RBC system and moved immediately to the lab under well-moisturized conditions.

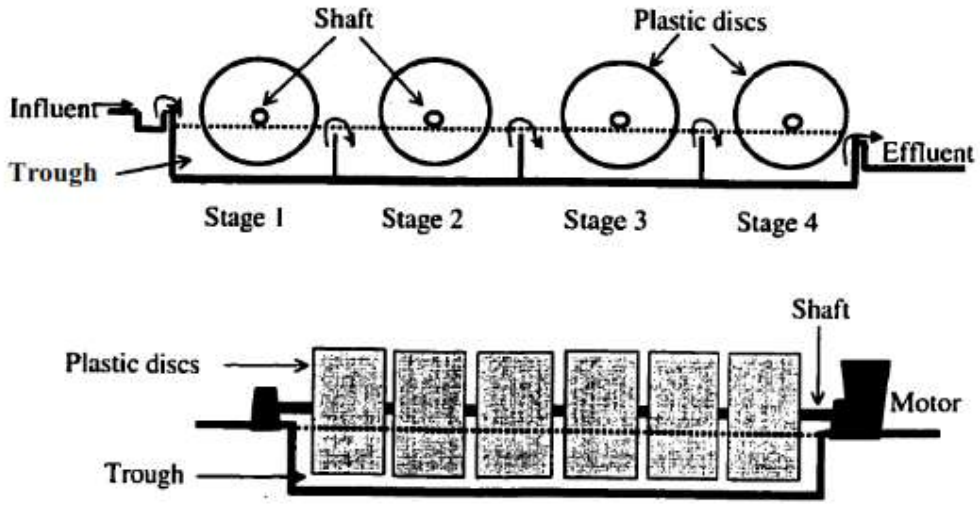

Figure 4.1 Schematic diagram of a four-stage RBC system (adapted from Chun Lu, M.Sc. Thesis, University of Alberta, 2001). (Above: cross-section of a four-stage RBC system; below: cross-section of one stage).

4.2.2 Calibration of oxygen microsensor

A microsensor was connected to a picoammeter (Unisense, Denmark, Model No. PA2000) and polarized at -0.75V versus a Ag/AgCl reference microsensor. For each measurement cycle, a two-point linear calibration was carried out at 100% saturation in atmospherically equilibrated water aerated with standard air (O_2, 21%) and at 0% saturation in anoxic water aerated with nitrogen (O_2, 0%). A three-point calibration in our lab using compressed air with 21% oxygen, a mixed gas with 10.5% oxygen balanced with nitrogen, or nitrogen gas (0% oxygen) produced a typical calibration curve for a combined oxygen microsensor as shown in Figure 4.2 (Lu and Yu 2002). Since it has been observed from practical experience in our lab that such a linear calibration curve of current signal and dissolved oxygen concentration, with $R^2 = 1$ could always be achieved from this type of oxygen microsensor, normally, a two-point (21% oxygen and oxygen free) calibration is sufficient and reliable for routine use of oxygen microsensor. As shown in Figure 4.3, the calibration curve for a combined oxygen microsensor used in this RBC biofilm measurements had the same linear relationship of

$R^2 = 1$. This type of microsensor has 90% response time of less than 5 s and low stirring effect of 0.5% of the signal. The calibration data are presented in Appendix D1.

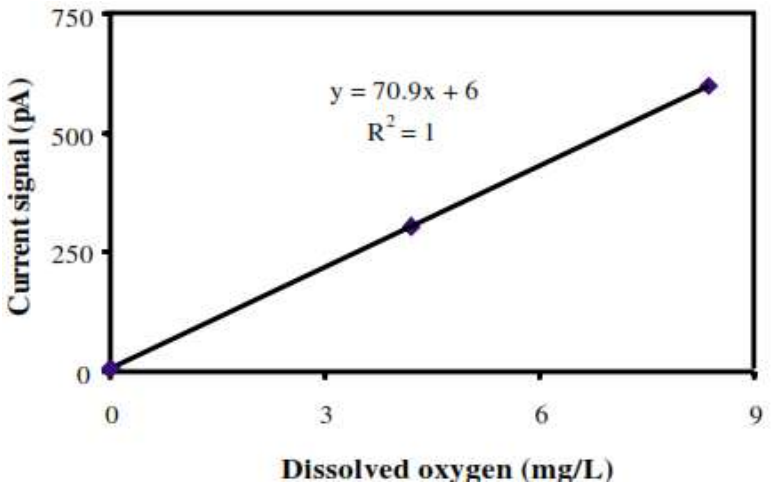

Figure 4.2 Calibration curve of a typical combined oxygen microsensor (Lu, and Yu 2002).

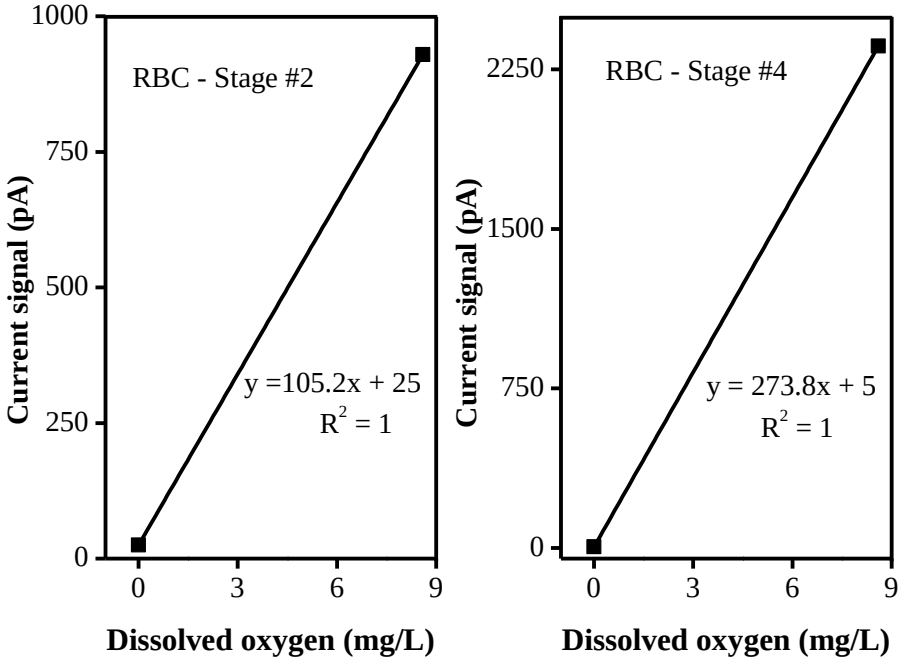

Figure 4.3 Calibration curves of combined oxygen microsensors used in RBC biofilms.

The calibration process in this case is more of a way to re-check the microsensor function and reliability for the biofilm measurements. For this purpose, a two-point calibration of the oxygen microsensor is sufficient and reliable. Conversely, with the use of microsensor to measure pure oxygen concentrations in biofilms as in the case of MABs (discussed in Chapter 3), three-point calibration process using pure oxygen (100% oxygen), compressed air (21% oxygen) and nitrogen (0% oxygen) was necessary because the behavior of oxygen microsensor in pure oxygen microenvironment is relatively new in biofilm research.

Additionally, two-point calibration process for routine use of microsensors to measure substrate concentration profiles in microbial environment has been employed by several researchers (Lorenzen et al. 1998; Meyer et al. 2001; Revsbech et al.1988; Zhou et al. 2008)

4.2.3 Microsensor measurements for oxygen concentration profiles

The schematic diagram of the experimental setup for measurement of oxygen concentration profiles in the biofilm is illustrated in Figure 4.4. The microsensor was mounted on micromanipulator (World Precision Instruments Inc., Sarasota, Florida, Model #: M3301R). A sample of RBC biofilm was placed in a testing chamber and was exposed to the same wastewater under which it was grown in the Devon RBC municipal wastewater treatment plant. Effluent wastewater from the testing chamber outflows into a holding chamber where it is continuously aerated and recycled back to the testing chamber. The measurement for dissolved oxygen was carried out by moving the microsensor from the bulk liquid through the biofilm in 50 μm increments until the oxygen concentration in the RBC biofilm became zero. All the microsensor measurements were performed at several locations approximately 1 mm apart from one another in the biofilm having surface area of 2×2 cm^2.

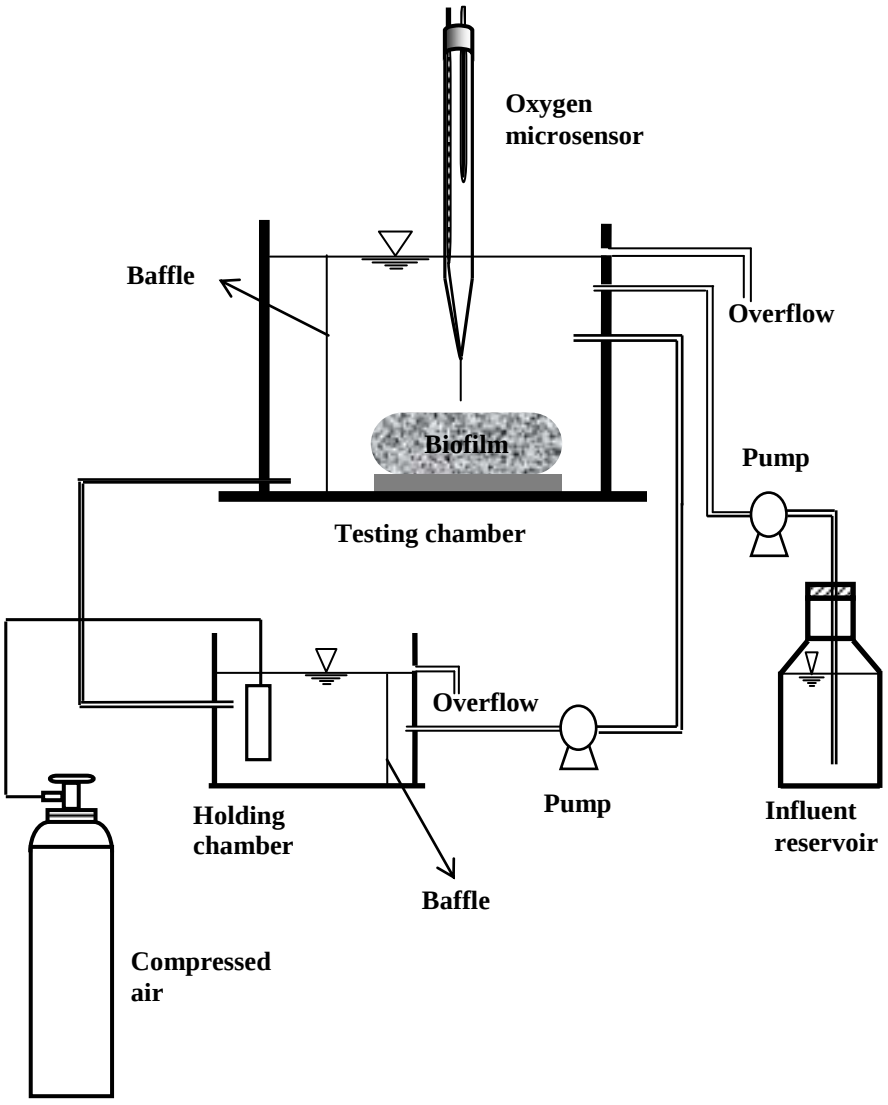

Figure 4.4 Schematic diagram of microsensor measurement in the RBC biofilms.

4.2.4 Biofilm model

The details of the biofilm model used in this study have been presented in Section 3.3.3 of Chapter 3. Figure 4.5 shows the hypothetical oxygen concentration profiles in the bulk water, diffusion layer and biofilm.

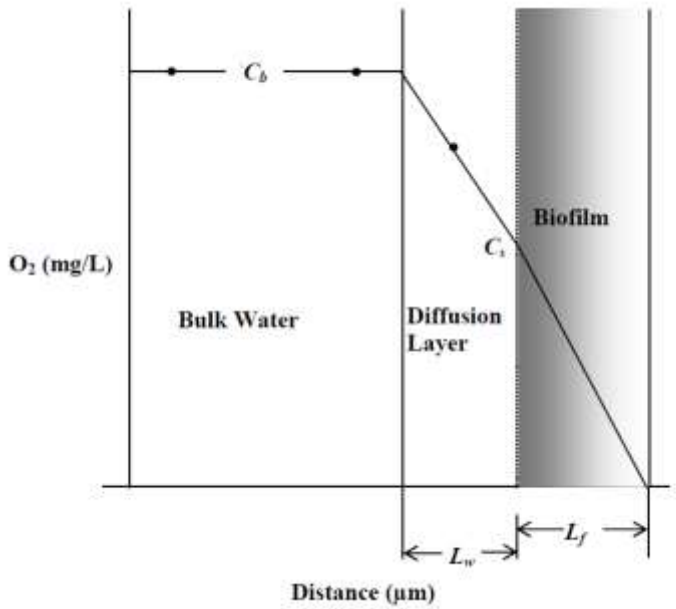

Figure 4.5 Hypothetical model of RBC biofilm system adapted from Nishidome et al. (1994).

In Figure 4.5, C_b stands for concentration of oxygen (mg/L) in the bulk water interface; C_s is the concentration of oxygen (mg/L) at the biofilm-bulk water interface; L_w is the thickness of the diffusion layer (µm); and L_f is the thickness of the biofilm (µm).

The oxygen consumption at any point in the biofilm is described by Monod relationship (Monod 1949):

$$R_s = \frac{\mu_m}{Y}\overline{X}_f \left(\frac{C}{K_s + C}\right)_f \qquad (4.1)$$

where $\frac{\mu_m}{Y}$ is the maximum specific growth rate of oxygen utilization, $mgO_2/gVS \cdot s$; K_S is the Monod half-saturation coefficient, mg/L; R_s is the reaction rate of oxygen consumption in the biofilms, ($mgcm^{-3}s^{-1}$); $\overline{X}_f$ is the average

biofilm density (g VS/L) and *C* is the concentration of the limiting substrate (oxygen in this case) at given biofilm depth *z*, mg/L.

The Monod equation 4.1 considers two special cases: zero order when the oxygen concentration is high enough (C>>K_S) and first-order when the oxygen concentration is smaller (K_S >> *C*). The steady-state mass balance on the limiting substrate at the any depth in the biofilm is described by the equation (Beyenal and Lewandowski, 2002):

$$D_{e,z}\left(\frac{d^2C}{dz^2}\right)_f + \zeta\left(\frac{dC}{dz}\right)_f = \frac{\mu_m}{Y}\bar{X}_f\left(\frac{C}{K_s + C}\right)_f \qquad (4.2)$$

$D_{e,z}$ is the diffusion coefficient of oxygen at biofilm depth *z* (cm^2/s); and ζ is the diffusivity gradient of oxygen in the biofilm, cm/s.

The mass balance equation (Equation (4.2)) takes into account the variable diffusivity, $D_{e,z,}$ and diffusivity gradient, ζ, due to the experimental evidence demonstrating that: (1) that effective diffusivity in the biofilms varies vertically across the biofilm depth and (2) that effective diffusivity in biofilms depends on the flow velocity at which the biofilms were grown (Beyenal and Lewandowski, 2002).

It was assumed that the kinetics of oxygen utilization inside the biofilm is of first-order in relation to the oxygen concentration in the biofilm (in the case where the value of K_S is much higher than the concentration of the limiting substrate (oxygen in this case). Therefore, the equation 4.2 can be approximated to first-order kinetic equation:

$$R_s = \frac{V_{max}C}{K_s + C} = \frac{(\mu_m/Y)}{K_s}\bar{X}_f[C] \qquad (4.3)$$

where $\frac{(\mu_m/Y)}{K_s}\bar{X}_f$ is equal to the slope of the plot of oxygen utilization rate in the biofilm as a function of oxygen concentration as shown in Figures 4.10 and 4.11. The first-order kinetic coefficient, $\frac{(\mu_m/Y)}{K_s}$ can be determined from the slope of the plot since the biofilm density, $\bar{X}_f$ has been determined experimentally.

4.2.4.1 Determination of mass transfer coefficients

Equation (4.1) can be solved analytically to estimate the biokinetic parameters from oxygen concentration profiles following successful determination of the mass transfer coefficients ($D_{e,z}$ and ζ) and average biofilm density ($\overline{X}_f$) as outlined in the following mathematical procedures:

4.2.4.1.1 Effective diffusivity gradient

The followings are the steps involved in the determination of mass transfer coefficients:

1. The limiting current density, i can be calculated by using the following relation:

$$i\ (A/cm^2) = \frac{I}{A} = \frac{Limiting\ current\ measured\ by\ microsensor\ (A)}{Microsensor\ tip\ surface\ area\ (cm^2)} \qquad (4.4)$$

2. The local effective diffusivity, D_{fl}, (cm/s) is related to the limiting current density by the following equation (Beyenal and Lewandowski, 2000):

$$D_{fl} = 1.12\times10^{-10} + 3.69\times10^{-12}\ (i) \qquad (4.5)$$

where D_{fl} is the effective diffusivity (cm^2/sec) and i is the current density (A/cm^2)

3. The local relative effective diffusivity, D_{fz}, (dimensionless) was estimated from the following relation (Beyenal and Lewandowski, 2002):

$$D_{fz} = \frac{D_{fl}}{\left(D_{K_3Fe(CN)_6}\right)_e} \tag{4.6}$$

where $\left(D_{K_3Fe(CN)_6}\right)_e$ is the molecular diffusivity of ferricyanide in the electrolyte and it is equal to 7×10^{-6} cm^2/s at room temperature (Gao et al. 1995). The molecular diffusivity of ferricyanide serves as a common factor to obtain a dimensionless D_{fz} (Beyenal and Lewandowski, 2002).

4. Finally, the effective diffusivity gradient, ζ, (cm/sec) was determined by multiplying the diffusion coefficient of oxygen in water, D_w, at 21°C of 2.0×10^{-5} cm^2/sec (Revsbech et al., 1986) by the slope of a plot for local relative effective diffusivity versus biofilm depth, z (cm) as follows:

$$\zeta = D_w\left(\frac{\Delta D_{fz}}{\Delta z}\right) \tag{4.7}$$

5. The averaged effective diffusivity of oxygen is therefore calculated using the following relation (Beyenal and Lewandowski, 2002):

$$D_{e,z} = 0.252\times\left(2\times10^{-5}\right)+\left(\frac{\zeta L_f}{2}\right) \tag{4.8}$$

4.2.4.1.2 Average biofilm density

$\overline{X}_f$ (g VS/L) was calculated as follows:

$$\overline{X}_f = \frac{W_d}{V_b}\Big/ n \tag{4.9}$$

where W_d is the total dry cell mass of the biofilm samples in terms of volatile solids (g VS); V_b is the total volume of the biofilm samples (equal to the biofilm area multiplied by the depth of biofilm); n is the number of biofilm pieces that were sampled.

4.3 Results and discussions

4.3.1 Biofilm density

After measurements of oxygen concentration profiles, the biofilm samples were cut into small pieces and ten of the small pieces were used for biofilm density determination. Crucibles containing the small biofilm samples were weighed after drying at 105^{o}C and combusting at 550^{o}C for 2 h to determine the biofilm dry cell mass. The biofilm depth was measured by microsensor as described by Zhang et al. (1995). The measured values were in the range of 1.05-2.59 mm. The biofilm volume was obtained from the biofilm thickness (1.05-2.59 mm) and the biofilm area (6 mm^2). The average biofilm density thus calculated by dividing the biofilm dry cell mass by the biofilm volume for stage 2 and stage 4 of the RBC system was 15.24±1.34 and 13.55±1.34 g VS/L, respectively.

4.3.2 Oxygen concentration profiles in the biofilm

With the use of an oxygen microsensor, the oxygen concentration profiles in the biofilms were measured. The plots of oxygen concentration profiles versus biofilm depth in the biofilm samples collected from stage 2 and stage 4 of RBC system are shown in Figure 4.6. The data for plot of Figure 4.6 are presented in Appendix D2.

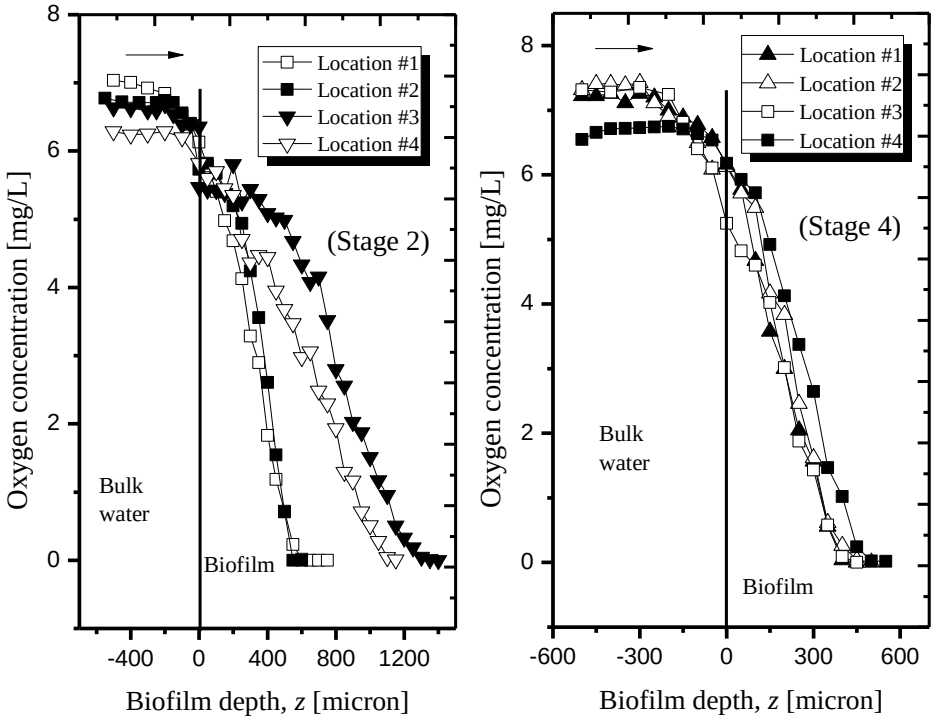

Figure 4.6 Oxygen concentration profiles at different locations in RBC-stage 2 and stage 4 biofilms.

The oxygen concentration curves in Figure 4.6 were fitted to polynomial mathematical functions to estimate the first $(dC/dz)_f$ and second derivatives $(dC^2/dz^2)_f$ of oxygen concentration variation with respect to depth in the biofilms (Lewandowski et al. 1994). The polynomial fits are presented in the Appendix D3. Using the method of Horn et al. (2002) for the determination of concentration boundary layer thickness in biofilms from oxygen profiles, the approximately linear region of the concentration profiles with a constant gradient $(dC/dz)_f$ was assumed to be inside the biofilm. On the other side, the nearly vertical part of the profile (perpendicular to the biofilm surface) belonged to the completely mixed bulk phase. Therefore, the interface between the biofilm and the bulk solution was located as shown in Figure 4.6. The biofilm-water interface was positioned at around 100 to 250 μm from the starting point of the bulk water phase.

As oxygen diffuses into the biofilm, it is consumed by the hetetrophic bacteria. As a result of this microbial oxygen utilization process, the aerobic region in the biofilm was limited to the surface layer in the biofilms of 0.4-1.35 mm in thickness. Comparing the oxygen concentration profiles that were measured in the biofilms from different stages of RBCs, the following was observed: (1) higher heterogeneity in oxygen distribution occurred in the biofilm from stage 2 versus stage 4 of the RBC systems. This could be explained by the difference in biofilm growth conditions, such as influent substrate loading rates and substrate types in two stages; (2) in all measurements conducted, the oxygen penetration depths in the biofilm taken from stage 4 were higher than those from stage 2 of the RBC system. Therefore, it can be concluded that the deeper oxygen penetration observed in stage 4 was primarily due to the reduced organic loading rate in stage 4 of the RBC system, which does not necessary indicate greater microbial activity.

The steady-state nature of the biofilms was investigated by measuring oxygen profiles at the same location three times in 13 and 14-hour interval, as shown in Figure 4.7.

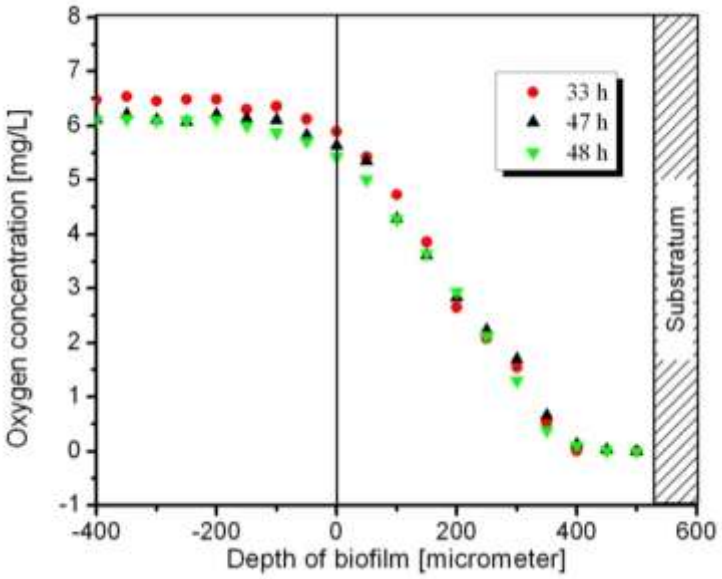

Figure 4.7 Oxygen concentration profiles measured in 14 and 15-h interval at the same position in RBC-stage 4 biofilm.

The profiles did not change much and, therefore, we concluded that for this time interval the oxygen profile change caused by the intervention of microsensor is negligible compared with that caused by the chemical heterogeneity. The data for the plot of Figure 4.7 are presented in Appendix D4.

4.3.3 Mass transfer coefficients

The mass transfer coefficients in the biofilm model are variable diffusivity $D_{e,z}$ and diffusivity gradient, ζ. Figures 4.8 and 4.9 illustrates graphical plots required for the determination of $D_{e,z}$ and ζ. The data points for the plot in the Figures 4.8 and 4.9 are presented in the Appendices D5 and D6.

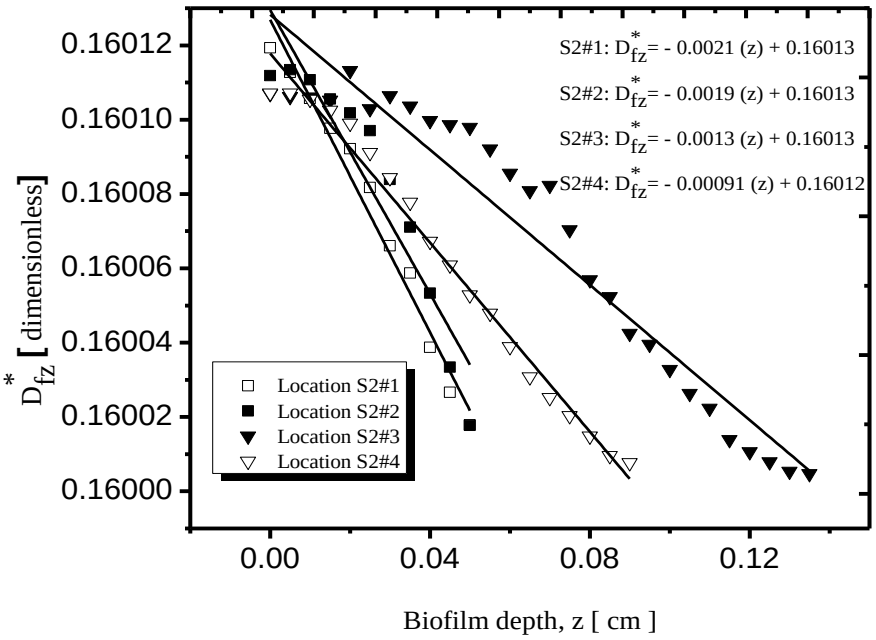

Figure 4.8 Effective diffusivity gradient of oxygen in RBC-stage 2 biofilm during biodegradation process of wastewater constituents.

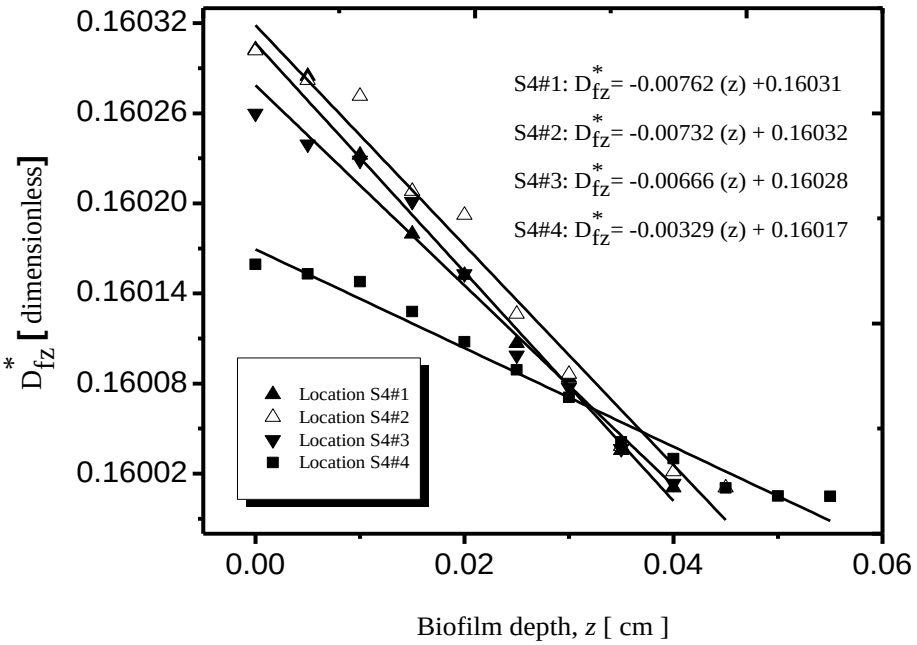

Figure 4.9 Effective diffusivity gradient of oxygen in RBC-stage 4 biofilm during biodegradation process of wastewater constituents.

The slopes obtained from the plots in Figures 4.8 and 4.9 represent $\left(\Delta D^{*}_{fz}/\Delta z\right)$ in Equation 4.7, which was used to estimate ζ at various locations in biofilms from stage 2 and stage 4 of the RBC system, respectively. Having determined ζ, respective $D_{e,z}$ values were calculated using Equation 4.8. Table 4.2 contains a summary of the calculated values of diffusion coefficient and diffusivity gradient of oxygen in the biofilms in the two treatment stages of the RBC biofilms. As shown in Figures 4.8 and 4.9, the effective diffusivity gradient has a negative value. This indicates that the substrate flux goes from regions of high oxygen concentration (biofilm top layer) to regions of low oxygen concentration (biofilm bottom layer), with a magnitude that is proportional to the concentration gradient $(dC/dz)_f$ based on Fick's first law of diffusion.

Table 4.2 The average density of microorganism and local mass transfer coefficients of oxygen in the RBC biofilms

Biofilms	**Locations**	X_f	ζ	$D_{e,z}$	[a]**Correlation Coefficient**
		(gVS/L)	**(cm/s)**	**(cm^2/s)**	
Stage #2	1		4.20×10^{-8}	5.04×10^{-6}	0.98
	2		3.80×10^{-8}	5.04×10^{-6}	0.87
	3		1.80×10^{-8}	5.04×10^{-6}	0.93
	4		2.60×10^{-8}	5.04×10^{-6}	0.99
	Average	15.24	3.10×10^{-8}	5.04×10^{-6}	
Stage #4	1		1.52×10^{-7}	5.04×10^{-6}	0.99
	2		1.53×10^{-7}	5.04×10^{-6}	0.98
	3		1.26×10^{-7}	5.04×10^{-6}	0.98
	4		6.66×10^{-8}	5.04×10^{-6}	0.97
	Average	13.55	1.24×10^{-7}	5.04×10^{-6}	

[a] *Correlation coefficient between D^{*}_{fz} and z*

The same variable average $D_{e,z}$ of 5.04×10^{-6} cm^2/s were obtained in biofilms from stage 2 and 4 of the RBC systems. Conversely, average ζ of 3.10×10^{-8} and 1.24×10^{-7} cm/s were calculated for biofilms from stage 2 and stage 4 of the RBC system, respectively. The value obtained for $D_{e,z}$ in both biofilms is few orders of magnitude higher than that of ζ, suggesting that mass transfer diffusion limitations had a more pronounced effect on the transport of oxygen in the biofilm than variations in flow velocities of bulk water.

4.3.4 Estimation of biokinetic parameters

Figures 4.10 and 4.11 show the linear relationship between R_S and C in determining first-order kinetic coefficient, $(\mu_m/Y)/K_s$ from the single Monod relationship. The biofilm kinetic parameters were determined from experimental data from four different locations in each of the biofilms collected from stage 2 and stage 4 of the RBC system.

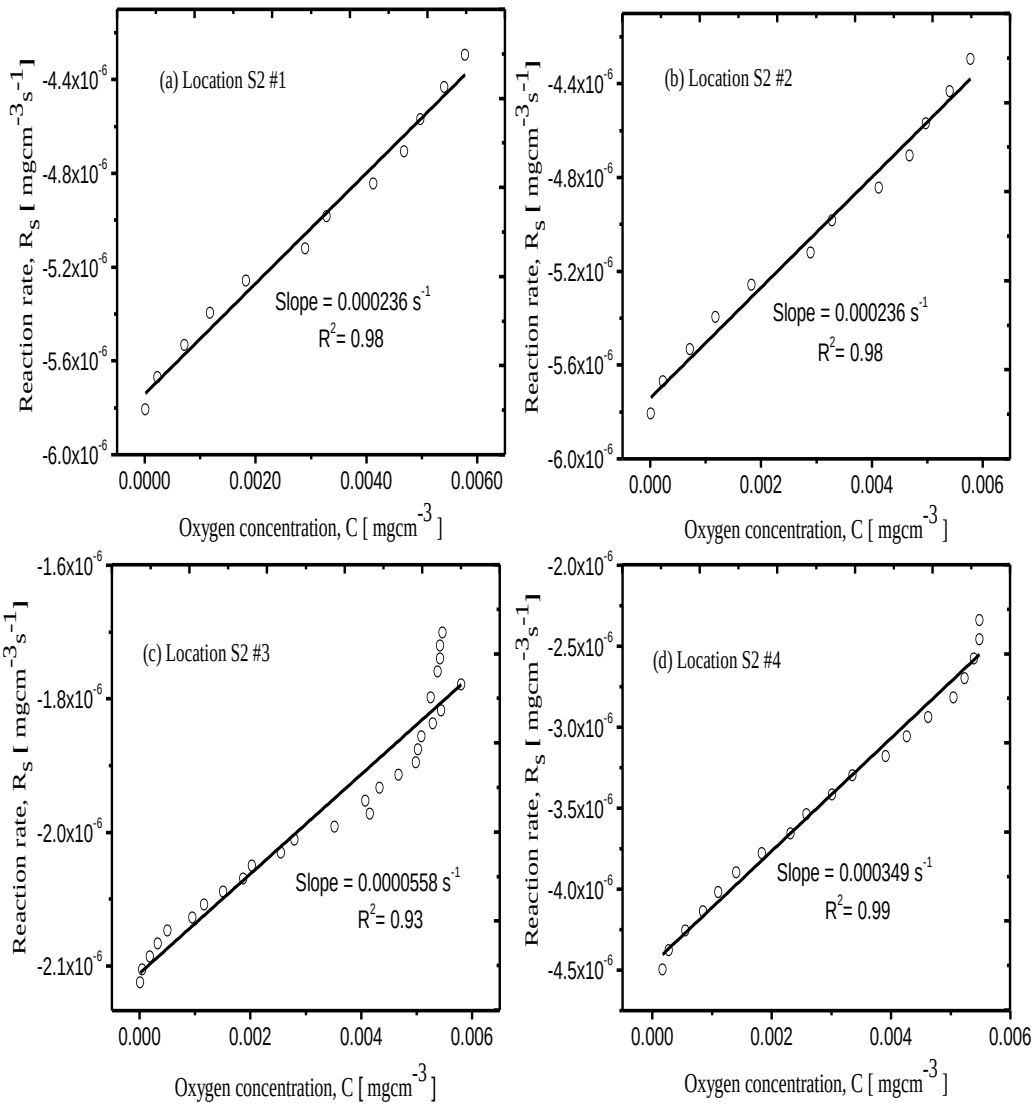

Figure 4.10 Determination of $(\mu_m/Y)/K_s$ in RBC-stage 2 biofilm.

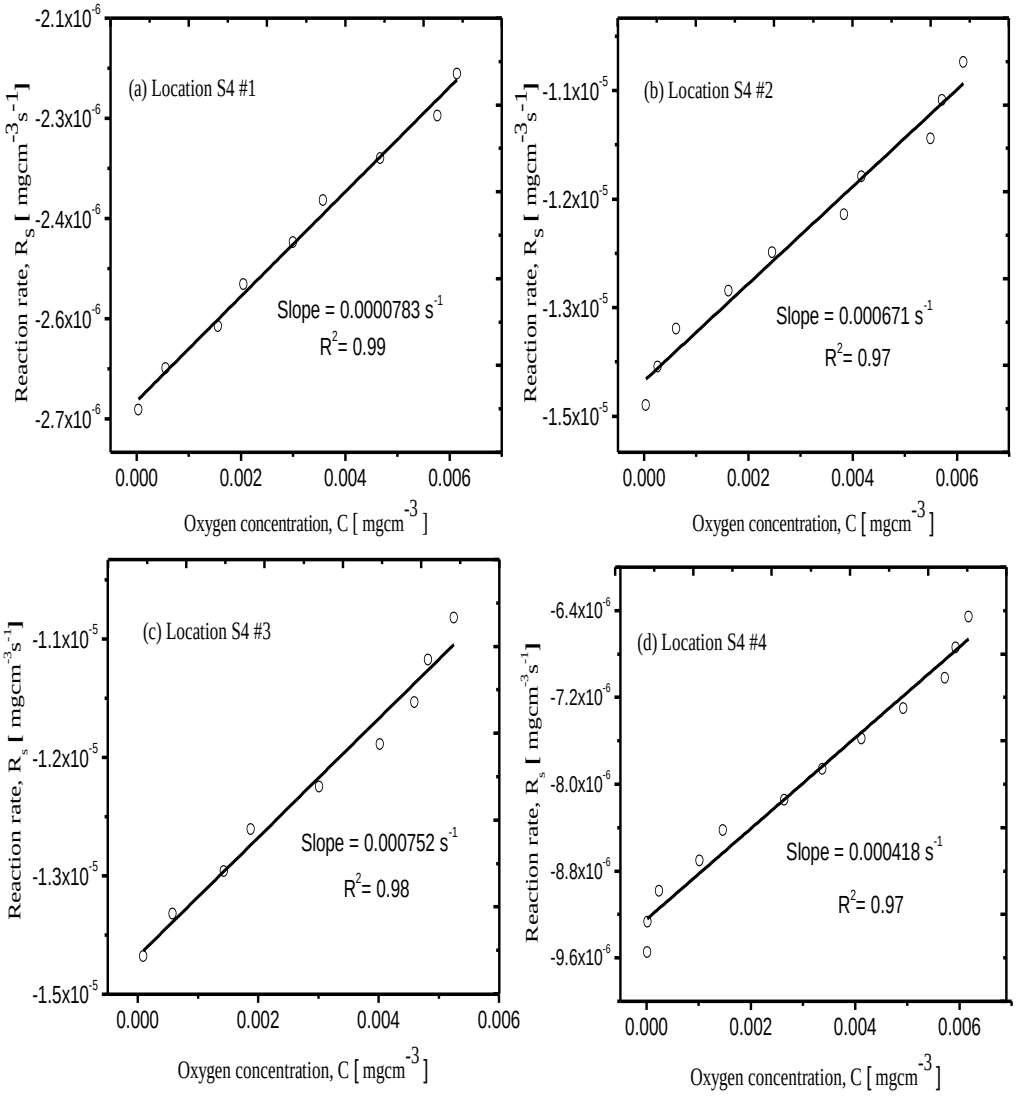

Figure 4.11 Determination of $(\mu_m/Y)/K_s$ in RBC-stage 4 biofilm.

From linear regression analysis in Figures 4.10 and 4.11, the values of R_s were negative and this is explained by the decreasing oxygen concentration due to biofilm utilization in the biofilm from biofilm-bulk water interface (z = 0) to the substratum. The results of the linear regression of the reaction rate and oxygen concentration data in Figures 4.10 and 4.11 are presented in Table 4.3. It is important to note that the kinetic parameters were obtained from oxygen

concentrations measured in the aerobic zone biofilm and not those of bulk water or anaerobic layer. The data for plotting Figure 4.10 and 4.11 are presented in Appendices D7 and D8, respectively.

Table 4.3 The first-order kinetic coefficient determined from experiments with varying locations in two different treatment stages of RBC biofilms ($\overline{X}_f$ of biofilms from stage 2 and stage 4 of the RBC system are 15.24 and 13.55 gVS/L)

Biofilms	**Locations**	$(\mu_m/Y)/K_s$ **(cm^3/gVS·s)**	**Correlation Coeffient[a]**
	1	1.55×10^{-5}	0.98
	2	1.55×10^{-5}	0.98
	3	3.66×10^{-6}	0.93
RBC-Stage #2	4	2.29×10^{-5}	0.99
		Mean = 1.44×10^{-5}	
		S.D = 7.96×10^{-6}	
	1	5.78×10^{-6}	0.99
	2	4.95×10^{-5}	0.97
	3	5.55×10^{-5}	0.98
RBC-Stage #4	4	3.08×10^{-5}	0.97
		Mean = 3.54×10^{-5}	
		S.D = 2.24×10^{-5}	

[a]*Correlation coefficient of linear regression for estimation of* $(\mu_m/Y)/K_s$

As shown in Table 4.3, The ratio of Monod kinetic terms, $(\mu_m/Y)/K_s$ were in the range of (0.36-2.29) $\times10^{-5}$ and (0.58-5.55) $\times10^{-5}$ cm^3/gVS·s for stage 2 and stage 4 of the RBC system, respectively. These values of $(\mu_m/Y)/K_s$ obtained by first-order kinetics are also several times smaller than those reported for

biodegradation of organic compounds in activated sludge (0.21– 0.40 m^3/gVSS·d converting to 2.31 - 4.63 cm^3/gVSS·s) by Namkung and Rittmann (1987).

A statistical analysis of F- test and t-test was used to investigate the effects of treatment stages of the RBC system on the estimated kinetic parameters. The results of this statistical analysis indicate that the values of $(\mu_m/Y)/K_s$ in biofilms collected from stage 2 and stage 4 of the RBC system were statistically different. Details of this statistical analysis are presented in Appendix E1.

Due to oxygen mass transport limitations, the kinetics of oxygen utilization in biofilm is of first-order as shown in Figures 4.10 and 4.11. The effects of oxygen mass transport limitations on the kinetics of oxygen utilization are discussed in Section 3.4.2 of Chapter 3.

4.4 Conclusions

This study presents a computational procedure for estimating biokinetic parameters in biofilms that were collected from RBC system. In particular, this procedure enables the determination biofilm kinetic parameter such as first-order kinetic coefficient, $(\mu_m/Y)/K_s$. We conclude that:

1. This study presents useful experimental information on biofilm kinetic parameters. The experimental results obtained suggest possible effects of oxygen mass transport limitations on the biofilm kinetics. As a result, the kinetic relationship between oxygen utilization in biofilm and oxygen concentration was of first-order. The use of first-order kinetics to fit the experimental data reduces the number of estimable kinetic parameters to one, $(\mu_m/Y)/K_s$. It is therefore expected that, more kinetic parameters can be extracted from the oxygen concentration profiles in biofilms in the absence of oxygen mass transport limitations.

2. With the computational procedure presented in this study, it was possible to determine the first-order kinetic coefficient in biofilms, $(\mu_m/Y)/K_s$.

3. First-order kinetic coefficient, $(\mu_m/Y)/K_s$ for oxygen utilization in the biofilm of RBC different treatment stages was in the range of (0.36-5.55) $\times 10^{-5}$ $cm^3/gVS \cdot s$. The estimated first-order kinetic coefficient in this study was found to differ from the same parameter in activated sludge system, which shows the need for more experimental data on the biofilm kinetic parameters.

4.5 References

Beyenal, H., and Z. Lewandowski. 2000. Combined effect of substrate concentration and flow velocity on effective diffusivity in biofilms. *Water Research* 34 (2):528-538.

Beyenal, H., and Z. Lewandowski. 2002. Internal and external mass transfer in biofilms grown at various flow velocities. *Biotechnol Prog* 18 (1):55-61.

Bishop, P. L. 1997. Biofilm structure and kinetics. *Water Science and Technology* 36 (1):287-294.

Bishop, P. L., and B. E. Rittmann. 1995. Modelling heterogeneity in biofilms: Report of the discussion session. *Water Science and Technology* 32 (8):263-265.

Carvallo, L., J. Carrera, and R. Chamy. 2002. Nitrifying activity monitoring and kinetic parameters determination in a biofilm airlift reactor by respirometry. *Biotechnology Letters* 24 (24):2063-2066.

Gao, X. P., J. Lee, and H. S. White. 1995. Natural-Convection at Microelectrodes. *Analytical Chemistry* 67 (9):1541-1545.

Hibiya, K., J. Nagai, S. Tsuneda, and A. Hirata. 2004. Simple prediction of oxygen penetration depth in biofilms for wastewater treatment. *Biochemical Engineering Journal* 19 (1):61-68.

Horn, H., and D. C. Hempel. 1997. Growth and decay in an auto-/heterotrophic biofilm. *Water Research* 31 (9):2243-2252.

Horn, H., S. Wäsche, and D.C. Hempel. 2002. Simulation of biofilm growth, substrate conversion and mass transfer under different hydrodynamic conditions. *Water Science and Technology* 46 (1-2):249-252.

Hsien, T. Y., and Y. H. Lin. 2005. Biodegradation of phenolic wastewater in a fixed biofilm reactor. *Biochemical Engineering Journal* 27 (2):95-103.

Kappeler, J., and W. Gujer. 1992. Estimation of kinetic-parameters of heterotrophic biomass under aerobic conditions and characterization of waste-water for activated-sludge modeling. *Water Science and Technology* 25 (6):125-139.

Lewandowski, Z., G. Walser, and W. G. Characklis. 1991. Reaction-kinetics in biofilms. *Biotechnology and Bioengineering* 38 (8):877-882.

Lewandowski, Z., P. Stoodley, S. Altobelli, and E. Fukushima. 1994. Hydrodynamics and kinetics in bioifilm kinetics in biofilm systems - recent advances and new problems. *Water Science and Technology* 29 (10-11):223-229.

Lorenzen, J., L. H. Larsen, T. Kjær, and N-P. Revsbech. 1998. Biosensor determination of the microscale distribution of nitrate, nitrate assimilation, nitrification, and denitrification in a diatom-inhabited freshwater sediment. *Applied and Environmental Microbiology* 64 (9):3264-3264.

Lu, C. 2001. A field study on oxygen penetration into wastewater biofilm. M.Sc.Thesis. University of Alberta, Edmonton, Canada.

Meyer, R. L., T. Kjær, and N.P. Revsbech. 2001. Use of NO_x^- microsensors to estimate the activity of sediment nitrification and NO_x^- consumption along an estuarine salinity, nitrate, and light gradient. *Aquatic Microbial Ecology* 26 (2):181-193.

Namkung, E., and B. E. Rittmann. 1987. Modeling bisubstrate removal by biofilms. *Biotechnology and Bioengineering* 29 (2):269-78.

Namkung, E., and B. E. Rittmann. 1987. Estimating volatile organic compound emissions from publicly owned treatment works. *Journal Water Pollution Control* 59 (7):670-678.

Nishidome, K., T. Kusuda, Y. Watanabe, M. Yamauchi, and M. Mihara. 1994. Determination of oxygen-transfer rate to a rotating biological contactor by microelectrode measurement. *Water Science and Technology* 29 (10-11):471-477.

Plattes, M., D. Fiorelli, S. Gille, C. Girard, E. Henry, F. Minette, O. O'Nagy, and P. M. Schosseler. 2007. Modelling and dynamic simulation of a moving bed bioreactor using respirometry for the estimation of kinetic parameters. *Biochemical Engineering Journal* 33 (3):253-259.

Revsbech, N. P. 1989. An oxygen microsensor with a guard cathode. *Limnology and Oceanography* 34 (2):474-478.

Revsbech, N. P., B. Madsen, and B. B. Jørgensen. 1986. Oxygen production and consumption in sediments determined at high spatial-resolution by computer-simulation of oxygen microelectrode Data. *Limnology and Oceanography* 31 (2):293-304.

Revsbech, P. R., L. R. Nielsen, P.B. Christensen, and J. Sørensen. 1988. Combined oxygen and nitrous oxide microsensor for denifrication studies. *Applied and Environmental Microbiology* 54 (9):2245-2245.

Riefler, R. G., D. P. Ahlfeld, and B. F. Smets. 1998. Respirometric assay for biofilm kinetics estimation: parameter identifiability and retrievability. *Biotechnology and Bioengineering* 57 (1):35-45.

Riefler, R. G., and B. F. Smets. 2003. Comparison of a type curve and a least-squared errors method to estimate biofilm kinetic parameters. *Water Research* 37 (13):3279-3285.

Rittmann, B. E., and P. L. McCarty. 1980. Model of steady-state-biofilm kinetics. *Biotechnology and Bioengineering* 22 (11):2343-2357.

Vieira, M.J, and L.F. Melo. 1999. Intrinsic kinetics of biofilms formed under turbulent flow and low substrate concentrations *Bioprocess Engineering* 20(4):369-375.

Yurt, N., H. Beyenal, J. Sears, and Z. Lewandowski. 2003. Quantifying selected growth parameters of Leptothrix discophora SP-6 in biofilms from oxygen concentration profiles. *Chemical Engineering Science* 58 (20):4557-4566.

Zhang, T. C., and P. L. Bishop. 1994. Density, Porosity, and Pore Structure of Biofilms. *Water Research* 28 (11):2267-2277.

Chapter 5

CONCLUSIONS AND FUTURE WORK

5.1 Conclusions

Kinetic parameters for the design of activated sludge reactors are available in many handbooks and literature due to many previous studies in this area. To design activated sludge reactors, we can easily obtain the required kinetic parameters from handbook or literature. However, we cannot do the same for the design of biofilm reactors because of lack of biofilm kinetic parameters. Some previous researchers have tried to obtain biofilm kinetic parameters and have made important progress. Based on this background, the main objective of this thesis was to obtain kinetic parameters in biofilm based on the modification of exiting computational procedures. Conclusions from this study are described below:

- Kinetic parameters in wastewater biofilms were successfully measured using the computational procedure presented in this study. The calculated values of Monod's half-saturation coefficient (K_s) for oxygen consumption and maximum utilization rate of oxygen (μ_m/Y) in MABs were 2.01 mg O_2/cm^3 and 6.50×10^{-8} $mgO_2/gVS\cdot s$, respectively.

- Oxygen mass transfer limitation was encountered in several measurements. It allowed first-order relationship, a special case of Monod kinetic model, which limited the number of kinetic parameter estimate to one. And, the values of first-order kinetic coefficient, $(\mu_m/Y)/K_s$, in MABs and RBC biofilms were in the range of $(0.62\times\text{-}1.43)\times10^{-6}$ and $(0.36\times\text{-}5.55)\times 10^{-5} cm^3/gVS\cdot s$, respectively. The results of this study suggest the need for improved measurements based on the experimental design that minimizes the effects of oxygen transfer limitation on biofilm kinetics. This will help in the current research efforts to accumulate more experimental data on biofilm kinetic parameters required for successful modeling and design of biofilm reactors for effective wastewater treatment.

- The range of values for the Monod half-saturation coefficient, K_s, for the activated sludge process of 0.24 – 0.25 mgO_2/L is smaller than values of K_s

obtained in this study, which was 2.01 mgO_2/L in MABs. In the same vein, the range of values of specific maximum rate of oxygen utilization rate, $\frac{\mu_m}{Y}$ for the activated sludge process of (0.56-2.44) $\times 10^{-2}$ $mgO_2/gSS \cdot s$ is higher than value of $\frac{\mu_m}{Y}$ obtained in this study, which was 6.5 $\times 10^{-8}$ $mgO_2/gVS \cdot s$ for MABs. Also, the range of values for the first-order kinetic coefficient, $(\mu_m/Y)/K_s$ for the activated sludge process of (2.31- 4.63 $cm^3/gVSS \cdot s$) is higher than the values of $(\mu_m/Y)/K_s$ obtained in this study, which were in the range of (0.62-1.43)$\times 10^{-6}$ and (0.36 -5.55)$\times 10^{-5}$ $cm^3/gVS \cdot s$ for MABs and RBC biofilms, respectively. It is obvious that kinetic parameters in biofilms estimated in this study differ from the reported numbers in activated sludge systems, suggesting that physiology and microbial species composition of biofilm systems are different from activated sludge systems. This means that parameters from activated sludge systems cannot be used in biofilms and therefore, more experimental data for kinetic parameters in biofilms are required for the calibration and improvement of biofilm models.

- The value of K_s for oxygen consumption in MABs of 2.01 mgO_2/L was higher than K_s values in other biofilm systems, which were in the range of 0.16 – 0.33 mgO_2/L. Other kinetic parameters MABs obtained in this study such as $\frac{\mu_m}{Y}$ and $(\mu_m/Y)/K_s$ were found to be different from reported numbers in the activated sludge systems. Pure oxygen was used in the MAB while the activated sludge and other biofilm systems used air. Therefore, the difference between our kinetic parameters in MABs and reported numbers in the activated sludge and other biofilm systems can also be attributed to the use of pure oxygen in MABs.

5.2 Recommendations for future work

- The main benefit of research efforts described in this thesis is determining biokinetic parameters in one-dimensional model of mixed organism population in the biofilms such as RBC biofilms and MABs. At this stage, future work should focus on obtaining more experimental data for kinetic parameters to verify the results of this study and accumulating more data for different types of biofilms. The resulting information can then be used in the process of modeling, designing and scaling-up of biofilm reactors for effective wastewater treatment processes.

- In this study, it was observed that oxygen mass transfer limitations in biofilms could be an important factor affecting the determination of kinetic parameters of wastewater biofilms from oxygen concentration profiles. Therefore, for future work to determine kinetic parameters in biofilm from oxygen concentration profiles, efforts should be made to minimize oxygen mass transfer limitations in biofilms.

- Develop a better experimental technique for kinetic parameter measurements in biofilms such as fabrication of organic substrate microsensors. The organic substrate microsensor can be used concurrently with oxygen microsensors to measure organic substrate and oxygen concentration profiles in biofilms, respectively. This approach will lead to better understanding of the relationship between the kinetics of organic substrate biodegradation and oxygen consumption in biofilms.

- A further work with more focus on correct estimation of biofilm density is also suggested. This can be achieved by using oxygen microsensor to first obtain spatial distribution of aerobic and anaerobic layers in the biofilms. The biofilms can then be cut into slices using a microslicing technique and accumulated sliced pieces of the biofilm corresponding to the thickness of the each layer should be subjected for measurements to determine biofilm density.

APPENDIX A
DATA FOR FIGURES IN CHAPTER 2
A1. Figure 2.4

Time	Influent COD	Effluent COD	Time	Influent COD	Effluent COD
Days	mg/L	mg/L	Days	mg/L	mg/L
3	254.75	92.25	119	226	65.5
4	274.75	207.25	128	209.25	39.25
5	212.25	42.25	136	223	74.25
7	237.25	89.75	136	223	74.25
9	262	122	142	230.5	104.25
10	270	141	149	271.269	83.655
11	247	73	156	268.291	119.391
14	241	51	163	295.093	92.589
16	286	58	169	253.401	77.699
18	218.8	34.8	196	220.643	68.765
22	210.8	46.8	198	247.445	116.413
23	220.8	60.8	200	283.287	67.4264
25	214.8	86.8	202	259.6314	58.555
31	224.8	48.8	205	262.5884	96.9964
35	226.8	36.8	221	242.66	31.59
36	221.8	68.8	225	219.95	19.96
37	207.8	42.8	227	265.78	37.01
39	228.8	107.8	228	197.75	10.56
42	238.8	68.8	234	342.38	85.83
44	240.25	85.25	239	342.38	4.26
51	287.75	95.25	240	289.20	4.82
56	242.75	127.75	249	230.08	65.38
59	298.2	96.02	252	191.49	38.69
63	246.2	94.2	254	252.36	75.15
64	214.2	64.2	257	265.49	73.88
65	212.2	72.2	263	242.81	105.04
67	218.2	58.2	273	257.56	110.11
70	212.2	98.2	277	293.72	59.26
71	257.00	92.70	279	242.08	59.26
72	275.91	119.89	283	190.77	61.35
73	271.18	39.51	286	244.66	74.12
74	284.19	52.51	288	226.60	80.66
75	232.18	25.33	290	216.31	78.47
78	262.91	103.34	293	183.18	69.82
85	265.27	118.71	295	208.62	27.68
92	258.6	62.6	297	234.33	22.16
105	254.6	96.6	300	195.85	49.02
109	260.6	106.6	302	239.50	22.16
113	277.6	86.6			
115	224.6	64.6			

A2. Figure 2.5

Time	Influent COD	Effluent COD	Time	Influent COD	Effluent COD	Time	Influent COD	Effluent COD
Days	mg/L	mg/L	Days	mg/L	mg/L	Days	mg/L	mg/L
1	284.75	84.75	105	208.60	68.60	283	216.31	55.13
2	292.25	114.75	107	258.60	146.60	286	213.74	57.19
3	269.75	92.25	109	246.60	110.60	288	280.84	15.02
4	259.75	97.25	113	224.60	65.60	290	224.02	23.98
5	274.75	117.25	114	212.60	106.60	293	229.18	55.13
7	274.75	69.75	120	259.25	111.75	297	229.18	138.59
8	302.25	144.75	122	219.25	66.75	300	296.29	126.58
9	279.00	232.00	126	300.00	119.25	302	234.33	126.58
10	250.00	90.00	128	180.50	58.00			
11	230.00	134.00	133	244.00	121.00			
14	246.00	86.00	134	281.75	79.25			
15	256.00	84.00	137	209.25	89.25			
16	276.00	78.00	140	244.25	43.00			
17	188.80	80.80	142	296.75	109.25			
18	220.80	32.80	155	250.42	86.63			
22	184.80	60.80	164	250.42	12.18			
25	222.80	66.80	170	256.38	131.30			
31	220.80	80.80	197	268.29	95.57			
32	212.80	80.80	199	280.20	110.46			
35	207.80	37.54	200	298.07	120.65			
36	232.80	45.80	202	262.59	167.96			
37	207.80	63.80	205	386.78	108.82			
38	233.80	54.80	207	224.15	46.73			
39	236.80	55.80	210	265.55	85.17			
43	232.75	27.75	219	268.70	85.80			
50	267.75	117.75	227	248.41	6.54			
51	252.75	97.75	228	254.18	8.64			
52	267.75	87.75	232	121.06	3.63			
53	280.25	92.75	234	312.80	248.41			
56	202.75	60.25	235	254.18	16.12			
57	230.20	116.20	239	259.97	4.26			
58	226.20	88.20	240	336.47	5.68			
59	226.20	92.20	242	216.46	56.10			
63	238.20	88.20	245	189.97	67.28			
64	296.20	60.20	247	197.80	59.76			
65	210.20	96.20	249	268.01	56.10			
67	226.20	88.20	252	219.16	79.00			
70	226.20	102.20	254	227.33	83.02			
71	216.81	121.07	257	242.81	102.49			
73	239.27	60.79	259	192.31	38.28			
74	217.99	90.34	261	240.54	32.99			
75	255.82	90.34	263	248.49	94.79			
79	265.27	116.34	273	242.81	60.51			
86	240.45	121.07	275	265.35	43.03			
93	258.60	80.60	277	257.59	57.19			
95	228.60	62.60	279	226.60	98.57			

A3. Figure 2.6

Time	Influent SO_4^{2-}	Effluent SO_4^{2-}	Time	Influent SO_4^{2-}	Effluent SO_4^{2-}	Time	Influent SO_4^{2-}	Effluent SO_4^{2-}
Days	mg/L	mg/L	Days	mg/L	mg/L	Days	mg/L	mg/L
2	204.86	84.46	98	236.19	67.05	249	214.53	51.69
4	244.06	205.94	99	227.41	65.74	252	213.98	51.64
8	307.54	260.56	105	239.79	58.75	254	226.93	49.50
9	289.27	111.87	106	267.86	134.24	257	218.58	44.84
10	403.38	117.89	113	243.14	86.44	259	219.83	42.41
15	220.42	165.65	114	214.61	79.91	261	217.18	44.93
18	228.52	147.81	115	202.24	71.58	263	217.37	45.93
24	227.02	137.60	116	204.62	55.28	273	223.04	38.07
25	232.16	127.81	119	196.60	60.34	275	223.65	51.99
28	236.30	117.66	123	202.74	35.26	277	223.30	49.54
29	228.32	130.58	126	205.08	73.63	279	237.35	56.54
31	260.05	139.83	136	233.67	61.20	283	223.25	62.66
32	259.85	127.92	137	225.74	59.38	286	232.23	47.94
35	227.82	95.90	142	232.31	90.13	288	227.93	31.20
36	233.30	128.82	151	231.35	59.93	307	222.75	110.70
37	232.57	92.41	154	237.19	61.29	310	217.56	84.41
38	238.24	100.91	156	226.13	46.02			
39	239.01	119.80	163	231.85	31.78			
42	236.88	99.22	169	227.45	57.08			
43	237.98	107.25	196	207.53	82.78			
44	237.95	105.38	205	214.52	56.56			
46	237.38	116.15	210	219.26	63.12			
49	214.46	89.66	220	218.59	37.72			
50	217.83	85.06	221	221.41	49.16			
51	215.52	70.68	225	207.41	60.94			
52	216.52	68.10	227	207.93	56.61			
53	212.55	66.39	228	209.24	57.54			
56	222.89	109.23	232	217.09	63.21			
71	222.47	71.49	234	214.90	56.68			
72	222.68	65.91	235	213.87	46.76			
73	222.46	114.39	239	225.68	52.13			
86	227.52	56.75	240	225.88	113.15			
91	237.28	102.79	242	224.42	68.02			
93	240.66	79.23	245	222.87	58.74			
95	239.34	55.56	247	221.43	50.08			

A4. Figure 2.4

Time	Influent SO_4^{2-}	Effluent SO_4^{2-}	Time	Influent SO_4^{2-}	Effluent SO_4^{2-}	Time	Influent SO_4^{2-}	Effluent SO_4^{2-}
Days	mg/L	mg/L	Days	mg/L	mg/L	Days	mg/L	mg/L
2	245.57	183.21	114	204.21	69.56	273	224.17	13.57
3	221.89	163.10	119	204.30	55.59	275	219.81	39.59
4	221.40	148.01	120	201.74	40.75	277	217.49	48.56
5	222.71	168.62	122	201.77	53.05	279	234.93	26.40
7	220.13	150.45	123	197.67	47.52	283	230.56	101.42
8	218.77	124.76	126	196.11	58.39	307	230.25	125.08
9	263.70	211.50	127	197.21	54.27	310	219.70	115.98
14	202.23	107.89	128	194.94	47.65			
15	223.32	119.78	129	184.56	75.30			
16	293.80	223.44	133	208.58	49.79			
18	229.52	145.95	136	100.11	62.99			
22	322.61	214.80	137	217.24	131.21			
24	226.29	133.82	140	277.42	236.61			
25	234.76	122.67	141	233.57	99.88			
28	235.33	110.90	144	220.12	161.07			
29	225.57	110.14	149	230.56	88.82			
31	242.25	121.71	151	229.25	80.65			
32	245.20	135.87	154	246.92	76.3			
35	240.48	207.56	156	220.39	72.78			
36	240.77	92.89	169	237.95	83.85			
37	237.41	117.42	196	213.53	45.01			
38	229.68	114.81	198	213.53	38.64			
39	241.81	97.66	200	218.44	55.16			
42	236.09	117.95	205	212.75	27.12			
43	212.87	157.02	210	219.26	63.12			
44	212.86	130.98	220	217.01	39.27			
46	212.75	133.58	221	219.34	n.a			
49	220.67	93.09	225	201.11	38.55			
50	220.93	86.18	227	203.07	34.45			
51	221.14	81.38	228	195.34	31.35			
52	221.48	76.48	232	202.96	31.28			
53	218.95	74.14	234	198.75	53.68			
58	213.07	153.87	235	197.65	49.35			
59	214.55	70.66	239	227.68	55.45			
70	226.25	88.11	240	229.92	49.08			
71	240.66	79.23	242	225.65	22.25			
72	231.35	123.14	245	220.79	49.56			
73	221.37	65.74	247	223.02	35.33			
77	236.27	145.40	249	223.18	32.05			
91	252.66	80.17	252	224.98	38.60			
95	369.90	207.29	254	219.10	22.68			
98	217.21	56.77	257	227.29	22.70			
105	236.27	145.40	259	233.97	23.78			
106	252.66	80.17	261	233.78	23.75			
113	217.21	56.77	263	232.82	23.34			

APPENDIX B

B1. Figure 3.3

CALIBRATION PROCESS FOR OXYGEN MICROSENSOR USED IN MABRs

B1.1. Membrane Aerated Biofilm (Hollow-Fiber)

Table B1.1-1: Data from calibration process of oxygen microelectrode in the reactor sample

	Conditions*		
Time	**O2-free (1st Cycle)**	**Air-saturated (1st Cycle)**	**Pure Oxygen (100% O_2)**
Seconds	**nA**		
0	0.03	0.53	5.24
30		0.82	5.25
60		1.10	5.25
90		1.25	
120		1.33	
150		1.36	
180		1.35	
Selected value	**0.03**	**1.35**	**5.25**
* Reading under stagnant water at room temperature			

Table B1.1-2: Summary of calibration process of oxygen microelectrode in the reactor sample

Conditions	**Pure Oxygen Concentration (mg/L)**	**Sensor Limiting Current Signal (nA)**
Oxygen-free	0	0.03
Saturated air	8.6	1.35
Pure Oxygen	40.95**	5.25

** *At room temperature, dissolved oxygen concentration of air-saturated sample (21% O_2) is approximately 8.6mg/L and therefore pure oxygen (100% O_2 will give [8.6mg/L×(100%/21%)] = 40.95mg/L.*

B1.2. Membrane Aerated Biofilm (Flat-Sheet)

Table B1.2-1: Data from calibration process of oxygen microelectrode in the reactor sample

	Conditions*				
Time	**O_2-free (1st Cycle)**	**Air-saturated (1st Cycle)**	**O_2-free (2nd Cycle)**	**Air-saturated (2nd Cycle)**	**Pure Oxygen (100% O_2)**
Seconds	**nA**				
0	0.09	1.03	1.63	0.09	1.60
30		1.30	0.87	0.67	2.82
60		1.48	0.61	1.01	3.32
90		1.56	0.41	1.26	3.94
120		1.60	0.29	1.41	4.48
150		1.62	0.22	1.52	5.04
180		1.63	0.16	1.56	5.36
210			0.12	1.58	5.64
240			0.10	1.59	5.98
270			0.09	1.60	6.25
300				1.61	6.26
Selected value			**0.09**	**1.61**	**6.26**

* Reading under stagnant water at room temperature

Table B1.2-2: Summary of calibration process of oxygen microelectrode in the reactor sample

Conditions	**Pure Oxygen Concentration (mg/L)**	**Sensor Limiting Current Signal (nA)**
Oxygen-free	0	0.09
Saturated air	8.6	1.61
Pure Oxygen	40.95**	6.26

** *At room temperature, dissolved oxygen concentration of air-saturated sample (21% O_2) is approximately 8.6mg/L and therefore pure oxygen (100% O_2 will give [8.6mg/L×(100%/21%)] = 40.95mg/L.*

B2. Figure 3.4(0 hour)

0 hour					
z	**DO**	**z**	**DO**	**z**	**DO**
[μm]	**[mg/L]**	**[μm]**	**[mg/L]**	**[μm]**	**[mg/L]**
-3025	0	375	2.90	1275	28.61
-2525	0	400	3.46	1300	29.17
-2025	0	425	5.29	1325	29.57
-1525	0	450	6.16	1350	30.13
-1025	0	475	6.96	1375	30.84
-525	0	500	7.75	1400	31.64
-500	0	525	8.47	1425	34.11
-475	0	550	9.03	1450	36.34
-450	0	575	9.51	1475	37.13
-425	0	600	10.14	1500	38.01
-375	0	625	10.86	1525	38.57
-325	0	650	11.42	1550	38.41
-225	0	675	11.89	1575	38.09
-200	0	700	12.37	1600	37.93
-175	0	725	12.77	1625	38.73
-150	0	750	13.89	1650	40.56
-125	0	775	14.52		
-100	0	800	15.08		
-75	0	825	15.56		
-50	0	850	16.04		
-25	0	875	16.51		
0	0.03	900	16.91		
25	0.03	925	17.23		
50	0.03	950	17.87		
75	0.03	975	18.82		
100	0.03	1000	19.30		
125	0.03	1025	19.86		
150	0.03	1050	20.33		
175	0.11	1075	20.81		
200	0.19	1100	21.37		
225	0.43	1125	21.69		
250	0.75	1150	22.17		
275	1.31	1175	22.64		
300	1.62	1200	27.34		
325	1.94	1225	27.74		
350	2.42	1250	28.06		

B2. Figure 3.4(12 hours)

12 hours					
z	DO	z	DO	z	DO
[μm]	[mg/L]	[μm]	[mg/L]	[μm]	[mg/L]
-3025	0	350	0.00	1250	26.07
-2525	0	375	0.75	1275	26.70
-2025	0	400	1.31	1300	27.26
-1525	0	425	1.46	1325	27.98
-1025	0	450	1.86	1350	28.38
-1000	0	475	2.42	1375	29.01
-975	0	500	2.82	1400	30.05
-950	0	525	3.14	1425	30.92
-925	0	550	3.69	1450	31.72
-875	0	575	6.32	1475	34.27
-825	0	600	7.12	1500	36.34
-725	0	625	7.83	1525	37.13
-625	0	650	8.39	1550	37.61
-525	0	675	9.03		
-425	0	700	9.75		
-325	0	725	10.86		
-225	0	750	11.97		
-125	0	775	12.61		
-100	0	800	13.25		
-75	0	825	14.28		
-50	0	850	14.76		
-25	0	875	15.48		
0	0	900	16.11		
25	0	925	16.91		
50	0	950	17.55		
75	0	975	18.18		
100	0	1000	18.82		
125	0	1025	19.54		
150	0	1050	20.41		
175	0	1075	21.13		
200	0	1100	21.69		
225	0	1125	22.48		
250	0	1150	22.96		
275	0	1175	23.68		
300	0	1200	24.71		
325	0	1225	25.35		

B2. Figure 3.4(24hours)

24 hours							
z	**DO**	**z**	**DO**	**z**	**DO**	**z**	**DO**
[µm]	**[mg/L]**	**[µm]**	**[mg/L]**	**[µm]**	**[mg/L]**	**[µm]**	**[mg/L]**
-2375	0	-1000	0	-100	0	800	8.15
-1875	0	-975	0	-75	0	825	9.90
-1850	0	-950	0	-50	0	850	10.46
-1825	0	-925	0	-25	0	875	11.34
-1800	0	-900	0	0	0	900	12.05
-1775	0	-875	0	25	0	925	12.93
-1750	0	-850	0	50	0	950	13.49
-1725	0	-825	0	75	0	975	14.20
-1700	0	-800	0	100	0	1000	15.08
-1675	0	-775	0	125	0	1025	16.04
-1650	0	-750	0	150	0	1050	16.75
-1625	0	-725	0	175	0	1075	17.63
-1600	0	-700	0	200	0	1100	18.66
-1575	0	-675	0	225	0	1125	19.78
-1550	0	-650	0	250	0	1150	21.05
-1525	0	-625	0	275	0	1175	21.77
-1500	0	-600	0	300	0	1200	22.80
-1475	0	-575	0	325	0	1225	23.76
-1450	0	-550	0	350	0	1250	25.19
-1425	0	-525	0	375	0	1275	25.99
-1400	0	-500	0	400	0	1300	27.26
-1375	0	-475	0	425	0	1325	28.38
-1350	0	-450	0	450	0	1350	29.49
-1325	0	-425	0	475	0	1375	30.68
-1300	0	-400	0	500	0	1400	32.12
-1275	0	-375	0	525	0	1425	32.83
-1250	0	-350	0	550	0.03	1450	34.03
-1225	0	-325	0	575	0.19	1475	35.54
-1200	0	-300	0	600	0.51	1500	36.34
-1175	0	-275	0	625	0.67	1525	37.21
-1150	0	-250	0	650	4.57	1550	37.93
-1125	0	-225	0	675	5.13	1575	38.73
-1100	0	-200	0	700	5.84	1600	39.36
-1075	0	-175	0	725	6.40	1625	40.72
-1050	0	-150	0	750	7.04		
-1025	0	-125	0	775	7.60		

B3. Figure 3.5 (Location HF#1)

HF #1							
z	**DO**	**z**	**DO**	**z**	**DO**	**z**	**DO**
[µm]	**[mg/L]**	**[µm]**	**[mg/L]**	**[µm]**	**[mg/L]**	**[µm]**	**[mg/L]**
-275	0.00	625	4.89	1525	22.32	2425	40.64
-250	0.00	650	5.05	1550	22.64	2450	40.80
-150	0.00	750	5.61	1650	24.39		
-125	0.00	775	5.76	1675	24.79		
-100	0.00	800	6.00	1700	25.43		
-75	0.00	825	6.00	1725	25.99		
-50	0.00	850	6.96	1750	26.62		
-25	0.00	875	7.28	1775	27.02		
0	**0.51**	900	8.87	1800	27.26		
25	0.51	925	9.27	1825	27.58		
50	0.59	950	9.67	1850	28.06		
75	0.67	975	9.98	1875	28.38		
100	0.83	1000	10.22	1900	28.61		
125	0.91	1025	10.62	1925	29.09		
150	1.15	1050	11.66	1950	32.20		
175	1.23	1075	12.77	1975	32.52		
200	1.46	1100	13.25	2000	32.68		
225	1.54	1125	13.65	2025	32.83		
250	1.70	1150	14.60	2050	32.99		
275	1.86	1175	14.84	2075	33.31		
300	2.02	1200	15.16	2100	33.79		
325	2.18	1225	15.48	2125	34.11		
350	2.42	1250	16.19	2150	34.35		
375	2.58	1275	16.99	2175	35.38		
400	2.74	1300	17.39	2200	36.66		
425	2.90	1325	17.87	2225	37.77		
450	3.06	1350	18.26	2250	38.17		
475	3.38	1375	18.82	2275	38.49		
500	3.46	1400	19.30	2300	39.12		
525	3.61	1425	19.78	2325	39.52		
550	3.85	1450	20.18	2350	39.84		
575	6.80	1475	21.85	2375	40.48		
600	4.81	1500	22.01	2400	40.56		

B3. Figure 3.5 (Location HF#2)

HF #2					
z	**DO**	**z**	**DO**	**z**	**DO**
[µm]	**[mg/L]**	**[µm]**	**[mg/L]**	**[µm]**	**[mg/L]**
-275	0	625	4.33	1525	24.55
-250	0	650	4.73	1550	25.03
-225	0	675	4.89	1575	25.19
-200	0	700	5.21	1600	25.67
-175	0	725	5.53	1625	26.07
-150	0	750	5.84	1650	26.62
-125	0	775	6.80	1675	27.50
-100	0	800	7.36	1700	30.61
-75	0	825	8.63	1725	30.68
-50	0	850	9.35	1750	31.08
-25	0	875	9.75	1775	31.32
0	0.03	900	10.30	1800	31.64
25	0.11	925	10.62	1825	32.68
50	0.27	950	11.50	1850	33.07
75	0.43	975	11.89	1875	33.15
100	0.51	1000	12.61	1900	33.71
125	0.67	1025	13.09	1925	34.43
150	0.83	1050	13.57	1950	34.75
175	0.99	1075	14.04	1975	35.14
200	1.15	1100	14.44	2000	35.54
225	1.23	1125	14.76	2025	35.94
250	1.46	1150	15.16	2050	36.34
275	1.62	1175	17.55	2075	36.97
300	1.70	1200	18.34	2100	37.61
325	1.78	1225	18.82	2125	37.93
350	2.02	1250	19.22	2150	38.41
375	2.10	1275	19.54	2175	39.36
400	2.34	1300	20.10	2200	39.68
425	2.42	1325	20.41	2225	39.44
450	2.58	1350	21.05	2250	38.81

B3. Figure 3.5 (Location HF#3)

HF #3					
z	DO	z	DO	z	DO
[µm]	[mg/L]	[µm]	[mg/L]	[µm]	[mg/L]
-275	0	625	3.85	1525	16.51
-250	0	650	4.17	1550	16.67
-225	0	675	4.33	1575	16.99
-200	0	700	4.49	1600	17.31
-175	0	725	4.73	1625	17.47
-150	0	750	4.89	1650	17.71
-125	0	775	5.13	1675	18.18
-100	0	800	5.29	1700	18.66
-75	0	825	5.53	1725	18.98
-50	0	850	5.76	1750	19.46
-25	0	875	6.00	1775	20.41
0	0.03	900	6.08	1800	21.53
25	0.11	925	6.32	1825	22.01
50	0.19	950	6.48	1850	23.28
75	0.35	975	9.51	1875	24.79
100	0.51	1000	9.98	1900	27.58
125	0.59	1025	10.38	1925	28.22
150	0.67	1050	10.70	1950	29.01
175	0.83	1075	11.02	1975	29.81
200	0.99	1100	11.26	2000	30.76
225	1.15	1125	11.74	2025	31.40
250	1.31	1150	11.97	2050	31.80
275	1.46	1175	12.29		
300	1.62	1200	12.45		
325	1.78	1225	12.69		
350	1.94	1250	13.01		
375	2.10	1275	13.41		
400	2.26	1300	14.04		
425	3.38	1325	14.28		
450	2.74	1350	14.44		
475	2.90	1375	14.68		
500	2.90	1400	14.84		
525	3.14	1425	15.00		
550	3.38	1450	15.24		
575	3.54	1475	15.56		
600	3.69	1500	16.19		

B3. Figure 3.5 (Location HF#4)

HF #4					
z	**DO**	**z**	**DO**	**z**	**DO**
[µm]	**[mg/L]**	**[µm]**	**[mg/L]**	**[µm]**	**[mg/L]**
-275	0.00	825	9.96	1725	34.14
-225	0.00	850	10.45	1750	34.00
-125	0.00	875	10.87	1775	33.72
-25	0.00	900	11.28	1800	33.58
0	0.03	925	11.63	1825	34.28
50	0.10	950	12.60	1850	35.88
75	0.17	975	13.16		
100	0.31	1000	13.65		
125	0.31	1025	14.06		
150	0.38	1050	14.48		
175	0.45	1075	14.90		
200	0.51	1100	15.24		
225	0.51	1125	15.52		
250	0.51	1150	16.08		
275	0.51	1175	16.91		
300	0.51	1200	17.33		
325	0.51	1225	17.81		
350	0.51	1250	18.23		
375	0.58	1275	18.65		
400	0.65	1300	19.13		
425	0.86	1325	19.41		
450	1.14	1350	19.83		
475	1.63	1375	20.25		
500	1.90	1400	24.34		
525	2.18	1425	24.69		
550	2.60	1450	24.97		
575	3.02	1475	25.46		
600	3.50	1500	25.94		
625	5.10	1525	26.29		
650	5.86	1550	26.78		
675	6.56	1575	27.40		
700	7.25	1600	28.10		
725	7.88	1625	30.25		
750	8.37	1650	32.19		
775	8.78	1675	32.89		
800	9.34	1700	33.65		

B3. Figure 3.5 (Location FS#1)

FS #1					
z	**DO**	**z**	**DO**	**z**	**DO**
[µm]	**[mg/L]**	**[µm]**	**[mg/L]**	**[µm]**	**[mg/L]**
-200	0	520	9.43	1240	32.59
-180	0	540	9.84	1260	33.29
-160	0	560	10.34	1280	33.49
-140	0	580	10.74	1300	33.96
-120	0	600	10.98	1320	34.90
-100	0	620	11.38	1340	35.04
-80	0	640	11.52	1360	35.64
-60	0	660	11.72	1380	37.12
-40	0	680	12.19	1400	38.13
-20	0	700	12.59	1420	38.26
0	0.36	720	13.20	1440	39.14
20	0.63	740	13.67	1460	40.08
40	0.90	760	14.21	1480	40.35
60	1.17	780	14.81	1500	40.75
80	1.64	800	15.08	1520	41.02
200	3.79	920	16.83		
220	3.99	940	17.10		
240	4.46	960	17.50		
260	4.66	980	18.04		
280	4.93	1000	18.78		
300	5.20	1020	18.84		
320	5.47	1040	19.31		
340	5.74	1060	19.58		
360	6.07	1080	19.92		
380	6.68	1100	20.32		
400	6.95	1120	20.66		
420	7.49	1140	20.93		
440	7.69	1160	21.33		
460	7.96	1180	21.93		
480	8.76	1200	30.20		
500	9.10	1220	31.54		

B3. Figure 3.5 (Location FS#2)

FS #2					
z	DO	z	DO	z	DO
[µm]	[mg/L]	[µm]	[mg/L]	[µm]	[mg/L]
-420	0.00	660	2.82	1380	18.77
-220	0.00	680	2.98	1400	18.93
-20	0.00	700	3.15	1420	19.20
0	0.00	720	3.42	1440	19.52
20	0.01	740	3.58	1460	19.74
40	0.01	760	3.74	1480	20.55
60	0.01	780	4.17	1500	21.25
80	0.01	800	4.28	1520	21.52
100	0.06	820	4.66	1540	21.85
120	0.17	840	4.82	1560	23.42
140	0.17	860	5.04	1580	23.96
160	0.23	880	5.25	1600	24.33
180	0.33	900	5.58	1620	25.09
200	0.33	920	6.12	1640	25.90
220	0.39	940	6.28	1660	26.82
240	0.39	960	6.66	1680	27.74
260	0.39	980	6.93	1700	28.39
280	0.44	1000	7.20	1720	28.71
300	0.50	1020	9.09	1740	29.31
320	0.50	1040	9.47	1760	29.36
340	0.55	1060	9.90	1780	30.01
360	0.60	1080	10.39	1800	30.23
380	0.66	1100	10.60	1820	30.55
400	0.71	1120	10.87	1840	30.93
420	0.77	1140	11.36	1860	31.31
440	0.87	1160	11.63	1880	31.52
460	0.93	1180	12.33	1900	31.79
480	1.04	1200	13.04	1920	32.50
500	1.09	1220	13.25	1940	32.93
520	1.15	1240	13.79	1960	33.15
540	1.79	1260	14.66	1980	33.63
560	1.96	1280	15.09		
580	2.12	1300	17.15		
600	2.23	1320	17.79		
620	2.44	1340	18.28		
640	2.66	1360	18.55		

B3. Figure 3.5 (Location FS#3)

FS #3					
z	**DO**	**z**	**DO**	**z**	**DO**
[µm]	**[mg/L]**	**[µm]**	**[mg/L]**	**[µm]**	**[mg/L]**
-220	0	520	6.07	1240	32.28
-200	0	540	6.21	1260	34.03
-180	0	560	6.54	1280	34.30
-160	0	580	6.75	1300	34.30
-140	0	600	7.01	1320	35.64
-120	0	620	7.49	1340	35.78
-80	0	640	7.89	1360	35.58
-60	0	660	8.09	1380	35.91
-40	0	680	8.36	1400	36.32
-20	0	700	8.63	1420	36.58
0	0.03	720	14.00	1440	36.85
20	0.23	740	20.12	1460	36.99
40	0.36	760	20.59	1480	37.32
60	0.50	780	21.06	1500	38.33
80	0.70	800	20.99	1520	38.67
100	0.83	820	21.13	1540	39.68
120	0.97	840	21.19	1560	39.68
140	1.10	860	21.26	1580	39.74
160	1.37	880	21.40	1600	40.48
180	1.50	900	21.40	1620	40.75
440	4.60	1160	30.54		
460	4.86	1180	31.07		
480	5.47	1200	31.34		
500	5.67	1220	31.75		

B3. Figure 3.5 (Location FS#4)

FS #4					
z	DO	z	DO	z	DO
[µm]	[mg/L]	[µm]	[mg/L]	[µm]	[mg/L]
-220	0	520	10.91	1240	27.98
-200	0	540	11.05	1260	28.12
-180	0	560	11.25	1280	28.39
-160	0	580	11.38	1300	28.86
-140	0	600	11.85	1320	28.79
-120	0	620	12.12	1340	29.39
-80	0	640	12.79	1360	29.86
-60	0	660	13.40	1380	30.27
-40	0	680	13.60	1400	30.27
-20	0	700	13.74	1420	30.33
0	0.03	720	14.27	1440	30.94
20	0.09	740	14.34	1460	31.28
40	0.36	760	14.94	1480	32.15
60	0.70	780	15.28	1500	32.75
80	0.97	800	15.75	1520	33.76
100	1.37	820	15.75	1540	36.99
120	1.64	840	16.15	1560	37.93
140	1.64	860	16.56	1580	38.47
160	1.84	880	16.63	1600	39.41
180	2.31	900	17.36	1620	39.68
200	2.58	920	18.04	1640	40.75
220	2.98	940	18.17		
240	3.39	960	18.31		
260	4.53	980	20.12		
280	5.54	1000	20.19		
300	6.21	1020	20.72		
320	6.75	1040	23.35		
340	7.28	1060	24.22		
360	7.96	1080	24.49		
380	8.49	1100	24.62		
400	8.96	1120	24.96		
420	9.17	1140	25.56		
440	9.64	1160	25.56		
460	10.11	1180	25.76		
480	10.24	1200	27.04		
500	10.51	1220	27.71		

B4. Figure 3.6 (Location HF#1)

HF # 1					
Depth, z	**D^*_{fz}**	**Depth, z**	**D^*_{fz}**	**Depth, z**	**D^*_{fz}**
[cm]	**Nil**	**[cm]**	**Nil**	**[cm]**	**Nil**
0	0.1600036	0.0850	0.160018	0.1700	0.1600593
0.0025	0.1600036	0.0875	0.1600187	0.1725	0.1600605
0.005	0.1600037	0.0900	0.1600222	0.1750	0.1600619
0.0075	0.1600039	0.0925	0.1600231	0.1775	0.1600628
0.01	0.1600043	0.0950	0.160024	0.1800	0.1600634
0.0125	0.1600044	0.0975	0.1600247	0.1825	0.1600641
0.015	0.160005	0.1000	0.1600253	0.1850	0.1600651
0.0175	0.1600052	0.1025	0.1600262	0.1875	0.1600658
0.02	0.1600057	0.1050	0.1600285	0.1900	0.1600664
0.0225	0.1600059	0.1075	0.160031	0.1925	0.1600675
0.025	0.1600062	0.1100	0.160032	0.1950	0.1600744
0.0275	0.1600066	0.1125	0.1600329	0.1975	0.1600751
0.03	0.1600069	0.1150	0.1600351	0.2000	0.1600755
0.0325	0.1600073	0.1175	0.1600356	0.2025	0.1600758
0.035	0.1600078	0.1200	0.1600363	0.2050	0.1600762
0.0375	0.1600082	0.1225	0.160037	0.2075	0.1600769
0.04	0.1600085	0.1250	0.1600386	0.2100	0.160078
0.0425	0.1600089	0.1275	0.1600404	0.2125	0.1600787
0.045	0.1600093	0.1300	0.1600413	0.2150	0.1600792
0.0475	0.16001	0.1325	0.1600424	0.2175	0.1600815
0.05	0.1600101	0.1350	0.1600432	0.2200	0.1600844
0.0525	0.1600105	0.1375	0.1600445	0.2225	0.1600868
0.055	0.160011	0.1400	0.1600456	0.2250	0.1600877
0.0575	0.1600176	0.1425	0.1600466	0.2275	0.1600885
0.06	0.1600132	0.1450	0.1600475	0.2300	0.1600899
0.0625	0.1600133	0.1475	0.1600513	0.2325	0.1600908
0.065	0.1600137	0.1500	0.1600516	0.2350	0.1600915
0.0675	0.1600139	0.1525	0.1600523	0.2375	0.1600929
0.07	0.1600194	0.1550	0.160053	0.2400	0.1600931
0.0725	0.1600142	0.1575	0.1600537	0.2425	0.1600933
0.075	0.1600149	0.1600	0.1600548	0.2450	0.1600936
0.0775	0.1600153	0.1625	0.1600555		
0.08	0.1600158	0.1650	0.1600569		
0.0825	0.1600158	0.1675	0.1600578		

B4. Figure 3.6 (Location HF#2)

Depth, z [cm]	D^*_{fz} Nil	Depth, z [cm]	D^*_{fz} Nil	Depth, z [cm]	D^*_{fz} Nil
0.0000	0.1600025	0.0875	0.1600242	0.1750	0.1600719
0.0025	0.1600027	0.0900	0.1600254	0.1775	0.1600724
0.0050	0.160003	0.0925	0.1600262	0.1800	0.1600731
0.0075	0.1600034	0.0950	0.1600281	0.1825	0.1600755
0.0100	0.1600036	0.0975	0.160029	0.1850	0.1600763
0.0125	0.1600039	0.1000	0.1600306	0.1875	0.1600765
0.0150	0.1600043	0.1025	0.1600317	0.1900	0.1600778
0.0175	0.1600046	0.1050	0.1600327	0.1925	0.1600794
0.0200	0.160005	0.1075	0.1600338	0.1950	0.1600801
0.0225	0.1600052	0.1100	0.1600347	0.1975	0.160081
0.0250	0.1600057	0.1125	0.1600354	0.2000	0.1600819
0.0275	0.1600061	0.1150	0.1600363	0.2025	0.1600828
0.0300	0.1600062	0.1175	0.1600416	0.2050	0.1600836
0.0325	0.1600064	0.1200	0.1600434	0.2075	0.1600851
0.0350	0.1600069	0.1225	0.1600445	0.2100	0.1600865
0.0375	0.1600071	0.1250	0.1600454	0.2125	0.1600872
0.0400	0.1600077	0.1275	0.1600461	0.2150	0.1600883
0.0425	0.1600078	0.1300	0.1600473	0.2175	0.1600904
0.0450	0.1600082	0.1325	0.1600481	0.2200	0.1600911
0.0475	0.1600087	0.1350	0.1600495	0.2225	0.1600906
0.0500	0.1600091	0.1375	0.1600502	0.2250	0.1600892
0.0525	0.1600094	0.1400	0.1600507		
0.0550	0.1600100	0.1425	0.1600518		
0.0575	0.1600107	0.1450	0.1600534		
0.0600	0.1600112	0.1475	0.1600552		
0.0625	0.1600121	0.1500	0.1600559		
0.0650	0.160013	0.1525	0.1600573		
0.0675	0.1600133	0.1550	0.1600584		
0.0700	0.1600141	0.1575	0.1600587		
0.0725	0.1600148	0.1600	0.1600598		
0.0750	0.1600155	0.1625	0.1600607		
0.0775	0.1600176	0.1650	0.1600619		
0.0800	0.1600189	0.1675	0.1600639		
0.0825	0.1600217	0.1700	0.1600708		
0.0850	0.1600233	0.1725	0.160071		

B4. Figure 3.6 (Location HF#3)

HF # 3					
Depth, z	**D^*_{fz}**	**Depth, z**	**D^*_{fz}**	**Depth, z**	**D^*_{fz}**
[cm]	**Nil**	**[cm]**	**Nil**	**[cm]**	**Nil**
0.0000	0.1600025	0.0825	0.1600148	0.1675	0.1600431
0.0025	0.1600027	0.0850	0.1600153	0.1700	0.1600441
0.0050	0.1600028	0.0875	0.1600158	0.1725	0.1600448
0.0075	0.1600032	0.0900	0.160016	0.1750	0.1600459
0.0100	0.1600036	0.0950	0.1600169	0.1775	0.1600481
0.0125	0.1600037	0.0975	0.1600237	0.1800	0.1600505
0.0150	0.1600039	0.1000	0.1600247	0.1825	0.1600516
0.0175	0.1600043	0.1025	0.1600256	0.1850	0.1600545
0.0200	0.1600046	0.1050	0.1600263	0.1875	0.1600578
0.0225	0.160005	0.1075	0.1600271	0.1900	0.1600641
0.0250	0.1600053	0.1100	0.1600276	0.1925	0.1600655
0.0275	0.1600057	0.1125	0.1600287	0.1950	0.1600673
0.0300	0.1600061	0.1150	0.1600292	0.1975	0.1600691
0.0325	0.1600064	0.1175	0.1600299	0.2000	0.1600712
0.0350	0.1600068	0.1200	0.1600303	0.2025	0.1600726
0.0375	0.1600071	0.1225	0.1600308	0.2050	0.1600735
0.0400	0.1600075	0.1250	0.1600315		
0.0425	0.16001	0.1275	0.1600324		
0.0450	0.1600085	0.1300	0.1600338		
0.0475	0.1600089	0.1325	0.1600343		
0.0500	0.1600089	0.1350	0.1600347		
0.0525	0.1600094	0.1375	0.1600352		
0.0550	0.16001	0.1400	0.1600356		
0.0575	0.1600103	0.1425	0.1600359		
0.0600	0.1600107	0.1450	0.1600365		
0.0625	0.160011	0.1475	0.1600372		
0.0650	0.1600117	0.1500	0.1600386		
0.0675	0.1600121	0.1525	0.1600393		
0.0700	0.1600125	0.1550	0.1600397		
0.0725	0.160013	0.1575	0.1600404		
0.0750	0.1600133	0.1600	0.1600411		
0.0775	0.1600139	0.1625	0.1600415		
0.0800	0.1600142	0.1650	0.160042		

B4. Figure 3.6 (Location HF#4)

HF # 4			
Depth, z	**D^*_{fz}**	**Depth, z**	**D^*_{fz}**
[cm]	**Nil**	**[cm]**	**Nil**
0	0.1600025	0.0825	0.1600383
0.0025	0.1600025	0.0850	0.1600393
0.0050	0.1600025	0.0875	0.1600402
0.0075	0.1600025	0.0900	0.1600409
0.0100	0.1600025	0.0950	0.1600424
0.0125	0.1600025	0.0975	0.1600445
0.0150	0.1600025	0.1000	0.1600456
0.0175	0.1600027	0.1025	0.1600468
0.0200	0.1600028	0.1050	0.1600479
0.0225	0.1600034	0.1075	0.1600489
0.0250	0.1600041	0.1100	0.1600502
0.0275	0.1600053	0.1125	0.1600509
0.0300	0.1600061	0.1150	0.160052
0.0325	0.1600068	0.1175	0.160053
0.0350	0.1600078	0.1200	0.1600635
0.0375	0.1600089	0.1225	0.1600644
0.0400	0.1600101	0.1250	0.1600651
0.0425	0.1600142	0.1275	0.1600664
0.0450	0.1600162	0.1300	0.1600676
0.0475	0.160018	0.1325	0.1600685
0.0500	0.1600198	0.1350	0.1600698
0.0525	0.1600214	0.1375	0.1600714
0.0550	0.1600226	0.1400	0.1600731
0.0575	0.1600237	0.1425	0.1600787
0.0600	0.1600251	0.1450	0.1600836
0.0625	0.1600267	0.1475	0.1600854
0.0650	0.1600279	0.1500	0.1600874
0.0675	0.160029	0.1525	0.1600886
0.0700	0.1600301	0.1550	0.1600883
0.0725	0.160031	0.1575	0.1600876
0.0750	0.1600335	0.1600	0.1600872
0.0775	0.1600349	0.1625	0.160089
0.0800	0.1600361	0.1650	0.1600931

B5. Figure 3.6 (Location FS#1)

FS # 1					
Depth, z	D^*_{fz}	Depth, z	D^*_{fz}	Depth, z	D^*_{fz}
[cm]	Nil	[cm]	Nil	[cm]	Nil
0	0.1600445	0.068	0.1603577	0.136	0.1609788
0.002	0.1600516	0.07	0.1603684	0.138	0.161018
0.004	0.1600587	0.072	0.1603844	0.14	0.1610447
0.006	0.1600658	0.074	0.1603969	0.142	0.1610482
0.008	0.1600783	0.076	0.1604111	0.144	0.1610714
0.01	0.1600908	0.078	0.1604271	0.146	0.1610963
0.012	0.160105	0.08	0.1604342	0.148	0.1611034
0.014	0.1601121	0.082	0.1604449	0.15	0.1611141
0.016	0.1601228	0.084	0.160452	0.152	0.1611212
0.018	0.1601264	0.086	0.1604574		
0.02	0.1601353	0.088	0.1604645		
0.022	0.1601406	0.09	0.1604716		
0.024	0.1601531	0.092	0.1604805		
0.026	0.1601584	0.094	0.1604876		
0.028	0.1601655	0.096	0.1604983		
0.03	0.1601726	0.098	0.1605125		
0.032	0.1601797	0.1	0.1605321		
0.034	0.1601869	0.102	0.1605339		
0.036	0.1601958	0.104	0.1605464		
0.038	0.1602118	0.106	0.1605535		
0.04	0.1602189	0.108	0.1605624		
0.042	0.1602331	0.11	0.1605731		
0.044	0.1602385	0.112	0.160582		
0.046	0.1602456	0.114	0.1605891		
0.048	0.160267	0.116	0.1605998		
0.05	0.1602759	0.118	0.1606158		
0.052	0.1602847	0.12	0.1608347		
0.054	0.1602954	0.122	0.1608703		
0.056	0.1603088	0.124	0.1608979		
0.058	0.1603195	0.126	0.1609165		
0.06	0.1603257	0.128	0.1609219		
0.062	0.1603364	0.13	0.1609343		
0.064	0.1603399	0.132	0.1609593		
0.066	0.1603453	0.134	0.1609628		

B5. Figure 3.7(Location FS#2)

FS # 2					
Depth, z	**D^*_{fz}**	**Depth, z**	**D^*_{fz}**	**Depth, z**	**D^*_{fz}**
[cm]	**Nil**	**[cm]**	**Nil**	**[cm]**	**Nil**
0	0.1600356	0.068	0.1602563	0.136	0.160977
0.002	0.1600409	0.07	0.1602634	0.138	0.1609859
0.004	0.1600445	0.072	0.1604058	0.14	0.1609966
0.006	0.1600481	0.074	0.1605677	0.142	0.1610037
0.008	0.1600534	0.076	0.1605802	0.144	0.1610109
0.01	0.1600569	0.078	0.1605926	0.146	0.1610144
0.012	0.1600605	0.08	0.1605909	0.148	0.1610233
0.014	0.1600641	0.082	0.1605944	0.15	0.16105
0.016	0.1600712	0.084	0.1605962	0.152	0.1610589
0.018	0.1600747	0.086	0.160598	0.154	0.1610856
0.02	0.1600801	0.088	0.1606015	0.156	0.1610856
0.022	0.1600872	0.09	0.1606015	0.158	0.1610874
0.024	0.1600925	0.092	0.1606051	0.16	0.161107
0.026	0.1600979	0.094	0.1606104	0.162	0.161114
0.028	0.1601032	0.096	0.160751		
0.03	0.1601103	0.098	0.1607653		
0.032	0.1601157	0.1	0.1607955		
0.034	0.160121	0.102	0.1608062		
0.036	0.1601281	0.104	0.1608062		
0.038	0.1601335	0.106	0.1608062		
0.04	0.1601424	0.108	0.1608115		
0.042	0.1601495	0.11	0.1608187		
0.044	0.1601566	0.112	0.1608222		
0.046	0.1601637	0.114	0.1608365		
0.048	0.1601797	0.116	0.1608436		
0.05	0.1601851	0.118	0.1608578		
0.052	0.1601958	0.12	0.1608649		
0.054	0.1601993	0.122	0.1608756		
0.056	0.1602082	0.124	0.1608898		
0.058	0.1602136	0.126	0.1609361		
0.06	0.1602207	0.128	0.1609432		
0.062	0.1602331	0.13	0.1609432		
0.064	0.1602438	0.132	0.1609788		
0.066	0.1602492	0.134	0.1609824		

B5. Figure 3.7 (Location FS#3)

Depth, z [cm]	D^*_{fz} Nil	Depth, z [cm]	D^*_{fz} Nil	Depth, z [cm]	D^*_{fz} Nil
0	0.1600356	0.068	0.1602563	0.136	0.160977
0.002	0.1600409	0.07	0.1602634	0.138	0.1609859
0.004	0.1600445	0.072	0.1604058	0.14	0.1609966
0.006	0.1600481	0.074	0.1605677	0.142	0.1610037
0.008	0.1600534	0.076	0.1605802	0.144	0.1610109
0.01	0.1600569	0.078	0.1605926	0.146	0.1610144
0.012	0.1600605	0.08	0.1605909	0.148	0.1610233
0.014	0.1600641	0.082	0.1605944	0.15	0.16105
0.016	0.1600712	0.084	0.1605962	0.152	0.1610589
0.018	0.1600747	0.086	0.160598	0.154	0.1610856
0.02	0.1600801	0.088	0.1606015	0.156	0.1610856
0.022	0.1600872	0.09	0.1606015	0.158	0.1610874
0.024	0.1600925	0.092	0.1606051	0.16	0.161107
0.026	0.1600979	0.094	0.1606104	0.162	0.1611141
0.028	0.1601032	0.096	0.160751		
0.03	0.1601103	0.098	0.1607653		
0.032	0.1601157	0.1	0.1607955		
0.034	0.160121	0.102	0.1608062		
0.036	0.1601281	0.104	0.1608062		
0.038	0.1601335	0.106	0.1608062		
0.04	0.1601424	0.108	0.1608115		
0.042	0.1601495	0.11	0.1608187		
0.044	0.1601566	0.112	0.1608222		
0.046	0.1601637	0.114	0.1608365		
0.048	0.1601797	0.116	0.1608436		
0.05	0.1601851	0.118	0.1608578		
0.052	0.1601958	0.12	0.1608649		
0.054	0.1601993	0.122	0.1608756		
0.056	0.1602082	0.124	0.1608898		
0.058	0.1602136	0.126	0.1609361		
0.06	0.1602207	0.128	0.1609432		
0.062	0.1602331	0.13	0.1609432		
0.064	0.1602438	0.132	0.1609788		
0.066	0.1602492	0.134	0.1609824		

B5. Figure 3.7 (Location FS#4)

Depth, z	D^*_{fz}	Depth, z	D^*_{fz}	Depth, z	D^*_{fz}
[cm]	Nil	[cm]	Nil	[cm]	Nil
0	0.1600356	0.06	0.1603951	0.128	0.1608258
0.002	0.1600374	0.062	0.1603986	0.13	0.1608365
0.004	0.1600445	0.064	0.1604129	0.132	0.1608365
0.006	0.1600534	0.074	0.1604147	0.134	0.1608382
0.008	0.1600605	0.076	0.1604307	0.136	0.1608542
0.01	0.1600712	0.078	0.1604396	0.138	0.1608631
0.012	0.1600783	0.08	0.160452	0.14	0.1608863
0.014	0.1600783	0.082	0.160452	0.142	0.1609023
0.016	0.1600836	0.084	0.1604627	0.144	0.160929
0.018	0.1600961	0.086	0.1604734	0.146	0.1610144
0.02	0.1601032	0.088	0.1604752	0.148	0.1610393
0.022	0.1601139	0.09	0.1604948	0.15	0.1610536
0.024	0.1601246	0.092	0.1605125	0.152	0.1610785
0.026	0.1601548	0.094	0.1605161	0.154	0.1610856
0.028	0.1601815	0.096	0.1605197	0.156	0.1611141
0.03	0.1602598	0.098	0.1606763		
0.032	0.1602723	0.1	0.1606834		
0.034	0.1602776	0.102	0.160687		
0.036	0.1602901	0.104	0.1606959		
0.038	0.1603025	0.106	0.1607119		
0.04	0.1603061	0.108	0.1607119		
0.042	0.1603132	0.11	0.1607172		
0.044	0.1603239	0.112	0.160751		
0.046	0.1603275	0.114	0.1607688		
0.048	0.1603328	0.116	0.1607759		
0.05	0.1603364	0.118	0.1607795		
0.052	0.1603488	0.12	0.1607866		
0.054	0.1603559	0.122	0.1607991		
0.056	0.1603737	0.124	0.1607973		
0.058	0.1603898	0.126	0.1608133		

B6. Polynomial curve fitting for oxygen concentration profiles in HF-MABs

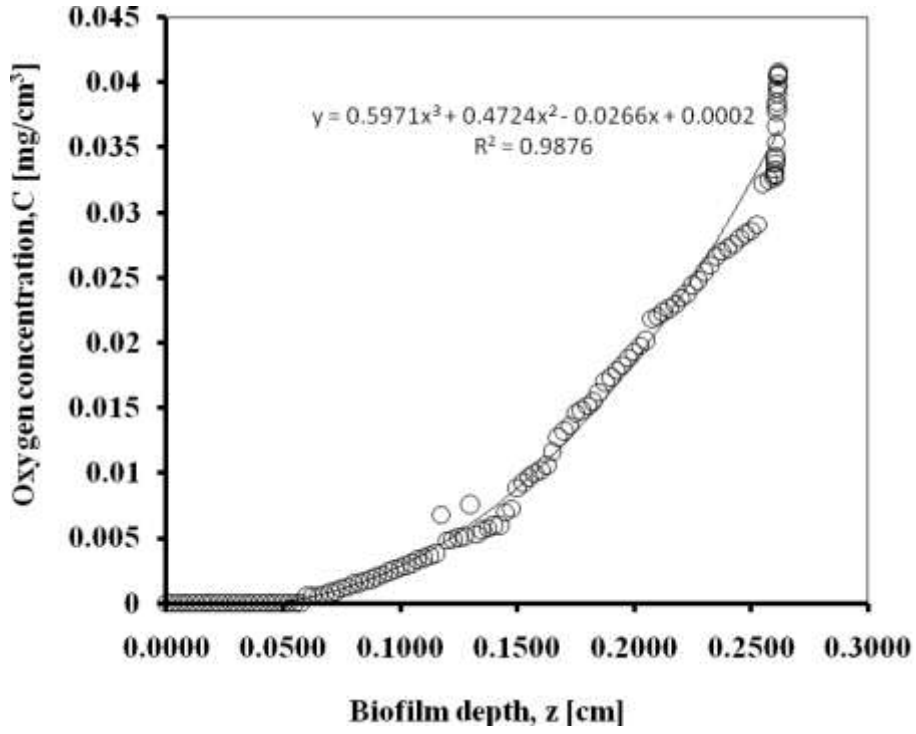

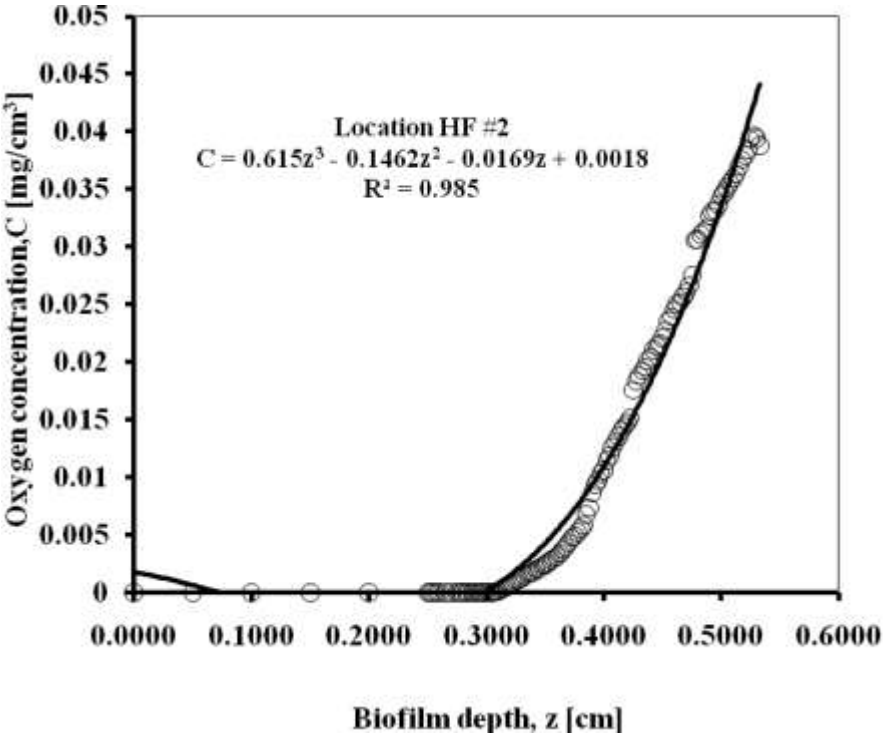

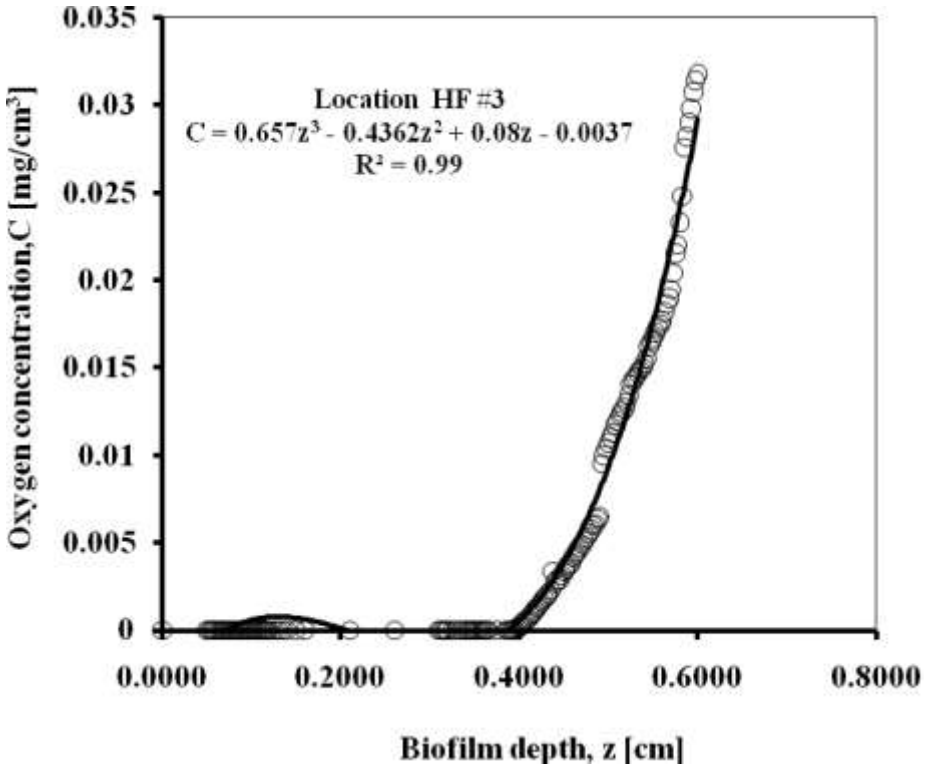
Location HF #3
C = 0.657z³ - 0.4362z² + 0.08z - 0.0037
R² = 0.99
Oxygen concentration,C [mg/cm³]
0.035
0.03
0.025
0.02
0.015
0.01
0.005
0
0.0000
0.2000
0.4000
0.6000
0.8000
Biofilm depth, z [cm]

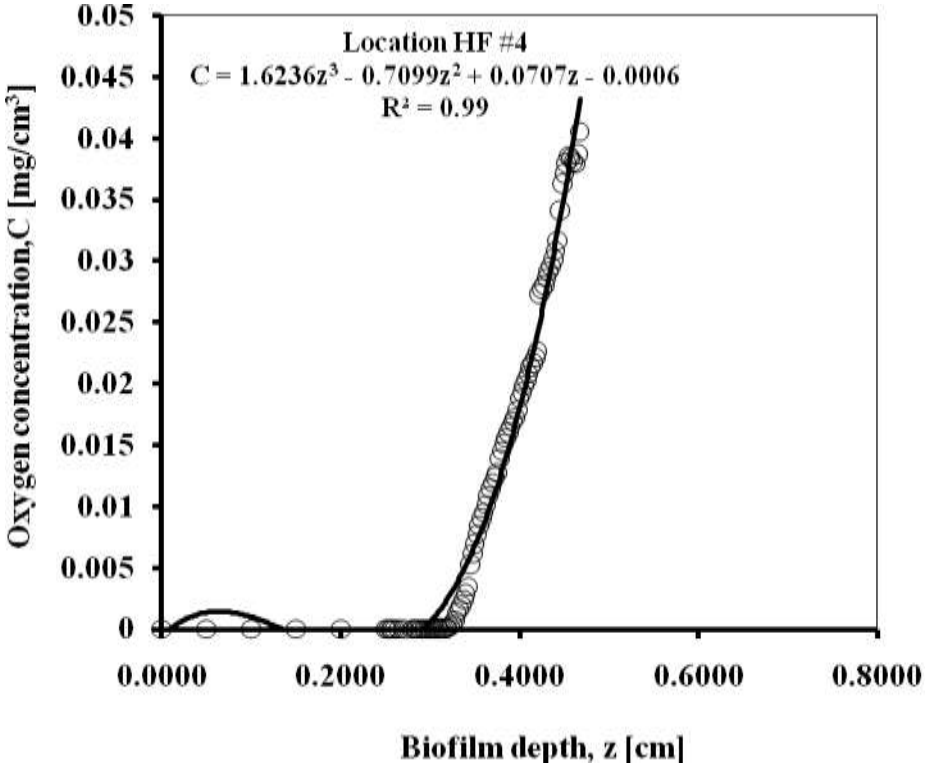
Location HF #4
C = 1.6236z³ - 0.7099z² + 0.0707z - 0.0006
R² = 0.99
Oxygen concentration,C [mg/cm³]
0.05
0.045
0.04
0.035
0.03
0.025
0.02
0.015
0.01
0.005
0
0.0000
0.2000
0.4000
0.6000
0.8000
Biofilm depth, z [cm]

B7. Polynomial curve fitting for oxygen concentration profiles in FS-MABs

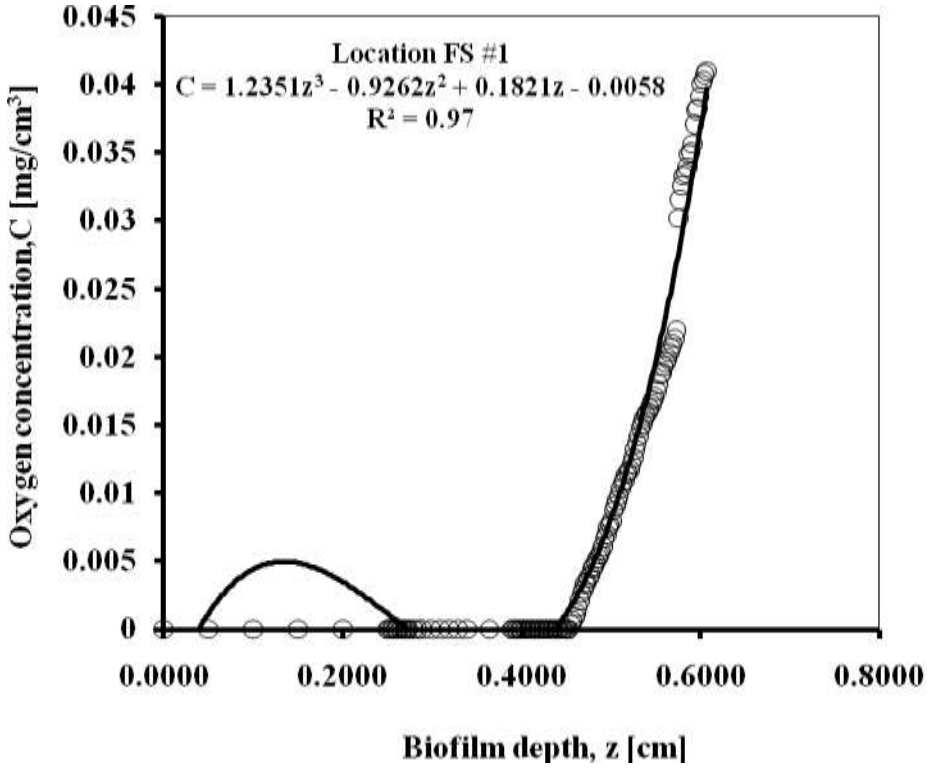

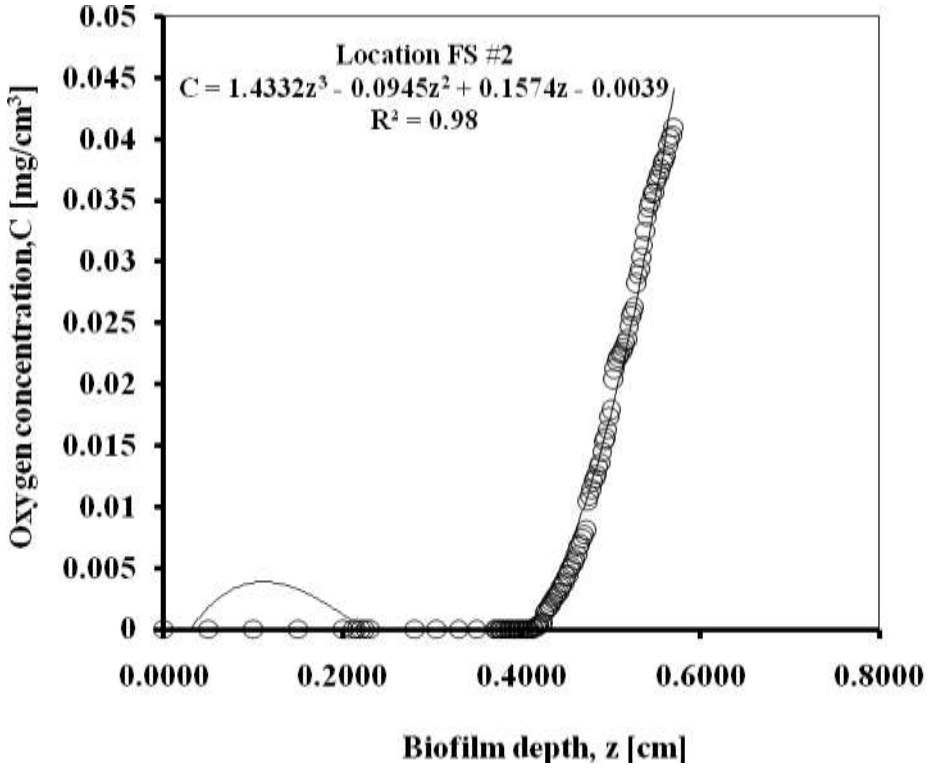

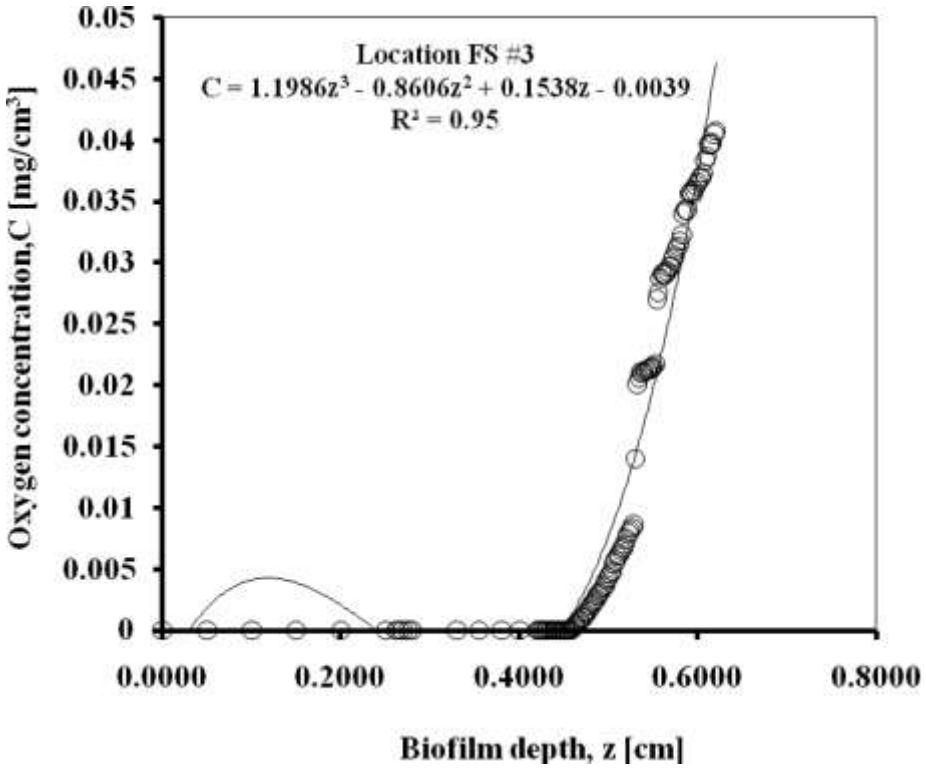
Location FS #3
C = 1.1986z³ - 0.8606z² + 0.1538z - 0.0039
R² = 0.95
Oxygen concentration,C [mg/cm³]
0.05
0.045
0.04
0.035
0.03
0.025
0.02
0.015
0.01
0.005
0
0.0000
0.2000
0.4000
0.6000
0.8000
Biofilm depth, z [cm]

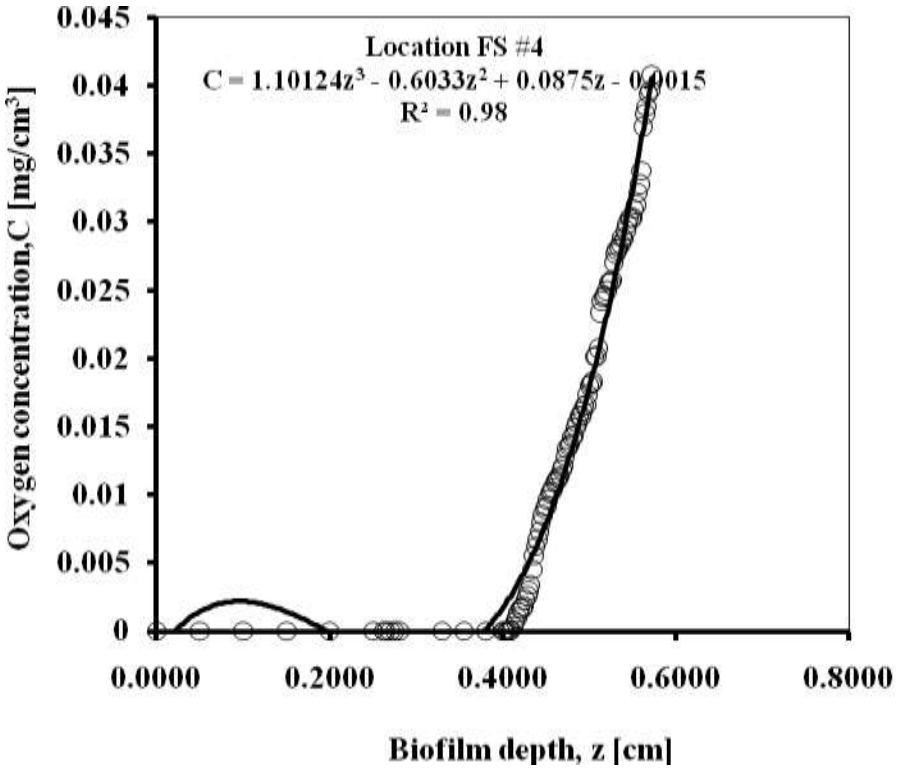
Location FS #4
C = 1.10124z³ - 0.6033z² + 0.0875z - 0.0015
R² = 0.98
Oxygen concentration,C [mg/cm³]
0.045
0.04
0.035
0.03
0.025
0.02
0.015
0.01
0.005
0
0.0000
0.2000
0.4000
0.6000
0.8000
Biofilm depth, z [cm]

B8. Figure 3.8

Location HF#1					
DO	**Rs**	**DO**	**Rs**	**DO**	**Rs**
[$mgcm^{-3}$]	**[$mgcm^{-3}s^{-1}$]**	**[$mgcm^{-3}$]**	**[$mgcm^{-3}s^{-1}$]**	**[$mgcm^{-3}$]**	**[$mgcm^{-3}s^{-1}$]**
0.00051	5.85E-06	0.00967	7.56E-06	0.02861	9.28E-06
0.00051	5.89E-06	0.00998	7.61E-06	0.02909	9.33E-06
0.00059	5.94E-06	0.01022	7.65E-06	0.03220	9.37E-06
0.00067	5.98E-06	0.01062	7.70E-06	0.03252	9.42E-06
0.00083	6.03E-06	0.01166	7.74E-06	0.03268	9.46E-06
0.00091	6.07E-06	0.01277	7.79E-06	0.03283	9.46E-06
0.00115	6.12E-06	0.01325	7.83E-06	0.03299	9.46E-06
0.00123	6.16E-06	0.01365	7.88E-06	0.03331	9.47E-06
0.00146	6.21E-06	0.01460	7.92E-06	0.03379	9.47E-06
0.00154	6.25E-06	0.01484	7.97E-06	0.03411	9.47E-06
0.00170	6.30E-06	0.01516	8.02E-06	0.03435	9.47E-06
0.00186	6.34E-06	0.01548	8.06E-06	0.03538	9.47E-06
0.00202	6.39E-06	0.01619	8.11E-06	0.03666	9.48E-06
0.00218	6.43E-06	0.01699	8.15E-06	0.03777	9.48E-06
0.00242	6.48E-06	0.01739	8.20E-06	0.03817	9.48E-06
0.00258	6.52E-06	0.01787	8.24E-06	0.03849	9.48E-06
0.00274	6.57E-06	0.01826	8.29E-06	0.03912	9.48E-06
0.00290	6.61E-06	0.01882	8.33E-06	0.03952	9.48E-06
0.00306	6.66E-06	0.01930	8.38E-06	0.03984	9.49E-06
0.00338	6.71E-06	0.01978	8.42E-06	0.04048	9.49E-06
0.00346	6.75E-06	0.02018	8.47E-06	0.04056	9.49E-06
0.00361	6.80E-06	0.02185	8.51E-06	0.04064	9.49E-06
0.00385	6.84E-06	0.02201	8.56E-06	0.04080	9.49E-06
0.00680	6.89E-06	0.02232	8.60E-06		
0.00481	6.93E-06	0.02264	8.65E-06		
0.00489	6.98E-06	0.02296	8.69E-06		
0.00505	7.02E-06	0.02344	8.74E-06		
0.00513	7.07E-06	0.02376	8.78E-06		
0.00760	7.11E-06	0.02439	8.83E-06		
0.00529	7.16E-06	0.02479	8.87E-06		
0.00561	7.20E-06	0.02543	8.92E-06		
0.00576	7.25E-06	0.02599	8.96E-06		
0.00600	7.29E-06	0.02662	9.01E-06		
0.00600	7.34E-06	0.02702	9.05E-06		
0.00696	7.38E-06	0.02726	9.10E-06		
0.00728	7.43E-06	0.02758	9.14E-06		
0.00887	7.47E-06	0.02806	9.19E-06		
0.00927	7.52E-06	0.02838	9.24E-06		

B9. Figure 3.9

Location HF#2		Location HF#3		Location HF#4	
DO	Rs	DO	Rs	DO	Rs
[$mgcm^{-3}$]	[$mgcm^{-3}s^{-1}$]	[$mgcm^{-3}$]	[$mgcm^{-3}s^{-1}$]	[$mgcm^{-3}$]	[$mgcm^{-3}s^{-1}$]
0.00003	4.25E-06	0.00031	3.17E-06	0.00003	7.70E-06
0.00011	4.29E-06	0.00039	3.22E-06	0.00003	7.82E-06
0.00027	4.34E-06	0.00047	3.27E-06	0.00003	7.95E-06
0.00043	4.39E-06	0.00063	3.31E-06	0.00003	8.07E-06
0.00051	4.43E-06	0.00086	3.36E-06	0.00003	8.19E-06
0.00067	4.48E-06	0.00094	3.40E-06	0.00003	8.32E-06
0.00083	4.53E-06	0.00102	3.45E-06	0.00003	8.44E-06
0.00099	4.57E-06	0.00118	3.50E-06	0.00011	8.56E-06
0.00115	4.62E-06	0.00133	3.54E-06	0.00019	8.68E-06
0.00123	4.67E-06	0.00141	3.59E-06	0.00043	8.81E-06
0.00146	4.71E-06	0.00149	3.64E-06	0.00075	8.93E-06
0.00162	4.76E-06	0.00165	3.68E-06	0.00131	9.05E-06
0.00170	4.81E-06	0.00180	3.73E-06	0.00162	9.18E-06
0.00178	4.85E-06	0.00196	3.77E-06	0.00194	9.30E-06
0.00202	4.90E-06	0.00212	3.82E-06	0.00242	9.42E-06
0.00210	4.95E-06	0.00228	3.87E-06	0.00290	9.54E-06
0.00234	4.99E-06	0.00243	3.91E-06	0.00346	9.67E-06
0.00242	5.04E-06	0.00259	3.96E-06	0.00529	9.79E-06
0.00258	5.08E-06	0.00275	4.01E-06	0.00616	9.91E-06
0.00282	5.13E-06	0.00290	4.05E-06	0.00696	1.00E-05
0.00298	5.18E-06	0.00306	4.10E-06	0.00775	1.02E-05
0.00314	5.22E-06	0.00416	4.14E-06	0.00847	1.03E-05
0.00338	5.27E-06	0.00353	4.19E-06	0.00903	1.04E-05
0.00369	5.32E-06	0.00369	4.24E-06	0.00951	1.05E-05
0.00393	5.36E-06	0.00369	4.28E-06	0.01014	1.06E-05
0.00433	5.41E-06	0.00392	4.33E-06	0.01086	1.08E-05
0.00473	5.46E-06	0.00416	4.38E-06	0.01142	1.09E-05
0.00489	5.50E-06	0.00431	4.42E-06	0.01189	1.10E-05
0.00521	5.55E-06	0.00447	4.47E-06	0.01237	1.11E-05
0.00553	5.60E-06	0.00463	4.51E-06	0.01277	1.13E-05
0.00584	5.64E-06	0.00494	4.56E-06	0.01389	1.14E-05
0.00680	5.69E-06	0.00510	4.61E-06	0.01452	1.15E-05
0.00736	5.74E-06	0.00526	4.65E-06	0.01508	1.16E-05
0.00863	5.78E-06	0.00549	4.70E-06	0.01556	1.18E-05
0.00935	5.83E-06	0.00565	4.75E-06	0.01604	1.19E-05
0.00975	5.88E-06	0.00588	4.79E-06	0.01651	1.20E-05
0.01030	5.92E-06	0.00604	4.84E-06	0.01691	1.21E-05
0.01062	5.97E-06	0.00628	4.89E-06	0.01723	1.22E-05

B9. Figure 3.9 (continued)

Figure 3.9 continued					
Location HF#2		Location HF#3		Location HF#4	
DO	Rs	DO	Rs	DO	Rs
[$mgcm^{-3}$]	[$mgcm^{-3}s^{-1}$]	[$mgcm^{-3}$]	[$mgcm^{-3}s^{-1}$]	[$mgcm^{-3}$]	[$mgcm^{-3}s^{-1}$]
0.01150	6.02E-06	0.00651	4.93E-06	0.01787	1.24E-05
0.01189	6.06E-06	0.00675	4.98E-06	0.01882	1.25E-05
0.01261	6.11E-06	0.00683	5.02E-06	0.01930	1.26E-05
0.01309	6.16E-06	0.00706	5.07E-06	0.01986	1.27E-05
0.01357	6.20E-06	0.00722	5.12E-06	0.02033	1.29E-05
0.01404	6.25E-06	0.01020	5.16E-06	0.02081	1.30E-05
0.01444	6.29E-06	0.01067	5.21E-06	0.02137	1.31E-05
0.01476	6.34E-06	0.01106	5.26E-06	0.02169	1.32E-05
0.01516	6.39E-06	0.01138	5.30E-06	0.02217	1.34E-05
0.01755	6.43E-06	0.01169	5.35E-06	0.02264	1.35E-05
0.01834	6.48E-06	0.01192	5.39E-06	0.02734	1.36E-05
0.01882	6.53E-06	0.01239	5.44E-06	0.02774	1.37E-05
0.01922	6.57E-06	0.01263	5.49E-06	0.02806	1.38E-05
0.01954	6.62E-06	0.01294	5.53E-06	0.02861	1.40E-05
0.02010	6.67E-06	0.01310	5.58E-06	0.02917	1.41E-05
0.02041	6.71E-06	0.01334	5.63E-06	0.02957	1.42E-05
0.02105	6.76E-06	0.01365	5.67E-06	0.03013	1.43E-05
0.02137	6.81E-06	0.01404	5.72E-06	0.03084	1.45E-05
0.02161	6.85E-06	0.01467	5.76E-06	0.03164	1.46E-05
0.02209	6.90E-06	0.01491	5.81E-06	0.03411	1.47E-05
0.02280	6.95E-06	0.01506	5.86E-06	0.03634	1.48E-05
0.02360	6.99E-06	0.01530	5.90E-06	0.03713	1.50E-05
0.02392	7.04E-06	0.01545	5.95E-06	0.03801	1.51E-05
0.02455	7.09E-06	0.01561	6.00E-06	0.03857	1.52E-05
0.02503	7.13E-06	0.01585	6.04E-06	0.03841	1.53E-05
0.02519	7.18E-06	0.01616	6.09E-06	0.03809	1.54E-05
0.02567	7.23E-06	0.01679	6.13E-06	0.03793	1.56E-05
0.02607	7.27E-06	0.01710	6.18E-06	0.03873	1.57E-05
0.02662	7.32E-06	0.01726	6.23E-06	0.04056	1.58E-05
0.02750	7.37E-06	0.01757	6.27E-06		
0.03061	7.41E-06	0.01789	6.32E-06		
0.03068	7.46E-06	0.01804	6.37E-06		
0.03108	7.50E-06	0.01828	6.41E-06		
0.03132	7.55E-06	0.01875	6.46E-06		
0.03164	7.60E-06	0.01922	6.50E-06		
0.03268	7.64E-06	0.01953	6.55E-06		
0.03307	7.69E-06	0.02000	6.60E-06		
0.03315	7.74E-06	0.02095	6.64E-06		

B9. Figure 3.9 (continued)

Figure 3.9 continued			
Location HF#2		Location HF#3	
DO	Rs	DO	Rs
[$mgcm^{-3}$]	[$mgcm^{-3}s^{-1}$]	[$mgcm^{-3}$]	[$mgcm^{-3}s^{-1}$]
0.03371	7.78E-06	0.02204	6.69E-06
0.03443	7.83E-06	0.02251	6.74E-06
0.03475	7.88E-06	0.02377	6.78E-06
0.03514	7.92E-06	0.02526	6.83E-06
0.03554	7.97E-06	0.02801	6.87E-06
0.03594	8.02E-06	0.02863	6.92E-06
0.03634	8.06E-06	0.02942	6.97E-06
0.03697	8.11E-06	0.03020	7.01E-06
0.03761	8.16E-06	0.03114	7.06E-06
0.03793	8.20E-06	0.03177	7.11E-06
0.03841	8.25E-06	0.03216	7.15E-06
0.03936	8.30E-06	0.00230	3.62E-06
0.03968	8.34E-06	0.00250	3.66E-06
0.03944	8.39E-06	0.00340	3.70E-06
0.03881	8.44E-06	0.00290	3.74E-06
		0.00300	3.78E-06
		0.00300	3.83E-06
		0.00320	3.87E-06
		0.00340	3.91E-06
		0.00360	3.95E-06
		0.00370	3.99E-06
		0.00380	4.03E-06
		0.00410	4.08E-06
		0.00430	4.12E-06
		0.00440	4.16E-06
		0.00460	4.20E-06
		0.00480	4.24E-06
		0.00500	4.28E-06
		0.00510	4.33E-06
		0.00530	4.37E-06
		0.00550	4.41E-06
		0.00570	4.45E-06
		0.00580	4.49E-06
		0.00600	4.54E-06
		0.00610	4.58E-06
		0.00880	4.62E-06
		0.00920	4.66E-06
		0.00950	4.70E-06

B10. Figure 3.10

Location FS#1		Location FS#2		Location FS#3		Location FS#4	
DO	Rs	DO	Rs	DO	Rs	DO	Rs
[$mgcm^{-3}$]	[$mgcm^{-3}s^{-1}$]	[$mgcm^{-3}$]	[$mgcm^{-3}s^{-1}$]	[$mgcm^{-3}$]	[$mgcm^{-3}s^{-1}$]	[$mgcm^{-3}$]	[$mgcm^{-3}s^{-1}$]
0.0003616	7.79E-06	0.00003	8.42E-06	0.00003	8.02E-06	0.00003	7.58E-06
0.0006304	7.87E-06	0.00009	8.51E-06	0.00023	8.09E-06	0.00009	7.64E-06
0.0008992	7.95E-06	0.00023	8.60E-06	0.00036	8.17E-06	0.00036	7.71E-06
0.001168	8.02E-06	0.00029	8.69E-06	0.00050	8.24E-06	0.00070	7.78E-06
0.0016384	8.10E-06	0.00043	8.77E-06	0.00070	8.32E-06	0.00097	7.85E-06
0.0021089	8.17E-06	0.00050	8.86E-06	0.00083	8.39E-06	0.00137	7.91E-06
0.0026465	8.25E-06	0.00056	8.95E-06	0.00097	8.46E-06	0.00164	7.98E-06
0.0029153	8.33E-06	0.00137	9.04E-06	0.00110	8.54E-06	0.00164	8.05E-06
0.0033185	8.40E-06	0.00157	9.13E-06	0.00137	8.61E-06	0.00184	8.12E-06
0.003453	8.48E-06	0.00177	9.21E-06	0.00150	8.68E-06	0.00231	8.18E-06
0.003789	8.55E-06	0.00191	9.30E-06	0.00171	8.76E-06	0.00258	8.25E-06
0.0039906	8.63E-06	0.00218	9.39E-06	0.00197	8.83E-06	0.00298	8.32E-06
0.004461	8.71E-06	0.00244	9.48E-06	0.00218	8.90E-06	0.00339	8.39E-06
0.0046626	8.78E-06	0.00265	9.57E-06	0.00238	8.98E-06	0.00453	8.45E-06
0.0049315	8.86E-06	0.00285	9.65E-06	0.00258	9.05E-06	0.00554	8.52E-06
0.0052003	8.93E-06	0.00305	9.74E-06	0.00285	9.13E-06	0.00621	8.59E-06
0.0054691	9.01E-06	0.00339	9.83E-06	0.00305	9.20E-06	0.00675	8.66E-06
0.0057379	9.09E-06	0.00359	9.92E-06	0.00325	9.27E-06	0.00728	8.72E-06
0.0060739	9.16E-06	0.00379	1.00E-05	0.00352	9.35E-06	0.00796	8.79E-06
0.0066788	9.24E-06	0.00433	1.01E-05	0.00372	9.42E-06	0.00849	8.86E-06
0.0069476	9.32E-06	0.00446	1.02E-05	0.00406	9.49E-06	0.00896	8.93E-06
0.0074852	9.39E-06	0.00493	1.03E-05	0.00433	9.57E-06	0.00917	8.99E-06
0.0076868	9.47E-06	0.00513	1.04E-05	0.00460	9.64E-06	0.00964	9.06E-06
0.0079556	9.54E-06	0.00540	1.04E-05	0.00486	9.72E-06	0.01011	9.13E-06
0.0087621	9.62E-06	0.00567	1.05E-05	0.00547	9.79E-06	0.01024	9.20E-06
0.0090981	9.70E-06	0.00607	1.06E-05	0.00567	9.86E-06	0.01051	9.26E-06
0.0094341	9.77E-06	0.00675	1.07E-05	0.00607	9.94E-06	0.01091	9.33E-06
0.0098374	9.85E-06	0.00695	1.08E-05	0.00621	1.00E-05	0.01105	9.40E-06
0.0103414	9.92E-06	0.00742	1.09E-05	0.00654	1.01E-05	0.01125	9.47E-06
0.0107446	1.00E-05	0.00775	1.10E-05	0.00675	1.02E-05	0.01138	9.53E-06
0.0109798	1.01E-05	0.00809	1.11E-05	0.00701	1.02E-05	0.01185	9.60E-06
0.0113831	1.02E-05	0.01044	1.12E-05	0.00749	1.03E-05	0.01212	9.67E-06
0.0115175	1.02E-05	0.01091	1.12E-05	0.00789	1.04E-05	0.01279	9.74E-06
0.0117191	1.03E-05	0.01145	1.13E-05	0.00809	1.05E-05	0.01340	9.80E-06
0.0121895	1.04E-05	0.01206	1.14E-05	0.00836	1.05E-05	0.01360	9.87E-06
0.0125927	1.05E-05	0.01232	1.15E-05	0.00863	1.06E-05	0.01374	9.94E-06
0.0131976	1.05E-05	0.01266	1.16E-05	0.01400	1.07E-05	0.01427	1.00E-05
0.013668	1.06E-05	0.01326	1.17E-05	0.02012	1.07E-05	0.01434	1.01E-05

B10. Figure 3.10 (continued)

Location FS#1		Location FS#2		Location FS#3		Location FS#4	
DO	Rs	DO	Rs	DO	Rs	DO	Rs
[$mgcm^{-3}$]	[$mgcm^{-3}s^{-1}$]	[$mgcm^{-3}$]	[$mgcm^{-3}s^{-1}$]	[$mgcm^{-3}$]	[$mgcm^{-3}s^{-1}$]	[$mgcm^{-3}$]	[$mgcm^{-3}s^{-1}$]
0.01421	1.07E-05	0.01360	1.18E-05	0.02059	1.08E-05	0.01494	1.01E-05
0.01481	1.08E-05	0.01447	1.19E-05	0.02106	1.09E-05	0.01528	1.02E-05
0.01508	1.08E-05	0.01535	1.19E-05	0.02099	1.10E-05	0.01575	1.03E-05
0.01548	1.09E-05	0.01562	1.20E-05	0.02113	1.10E-05	0.01575	1.03E-05
0.01575	1.10E-05	0.01629	1.21E-05	0.02119	1.11E-05	0.01615	1.04E-05
0.01595	1.11E-05	0.01736	1.22E-05	0.02126	1.12E-05	0.01656	1.05E-05
0.01622	1.11E-05	0.01790	1.23E-05	0.02140	1.13E-05	0.01663	1.05E-05
0.01649	1.12E-05	0.02046	1.24E-05	0.02140	1.13E-05	0.01736	1.06E-05
0.01683	1.13E-05	0.02126	1.25E-05	0.02153	1.14E-05	0.01804	1.07E-05
0.01710	1.14E-05	0.02187	1.26E-05	0.02173	1.15E-05	0.01817	1.07E-05
0.01750	1.14E-05	0.02220	1.27E-05	0.02704	1.16E-05	0.01831	1.08E-05
0.01804	1.15E-05	0.02247	1.27E-05	0.02758	1.16E-05	0.02012	1.09E-05
0.01878	1.16E-05	0.02267	1.28E-05	0.02872	1.17E-05	0.02019	1.10E-05
0.01884	1.17E-05	0.02301	1.29E-05	0.02913	1.18E-05	0.02072	1.10E-05
0.01931	1.18E-05	0.02341	1.30E-05	0.02913	1.19E-05	0.02335	1.11E-05
0.01958	1.18E-05	0.02368	1.31E-05	0.02913	1.19E-05	0.02422	1.12E-05
0.01992	1.19E-05	0.02469	1.32E-05	0.02933	1.20E-05	0.02449	1.12E-05
0.02032	1.20E-05	0.02556	1.33E-05	0.02960	1.21E-05	0.02462	1.13E-05
0.02066	1.21E-05	0.02590	1.34E-05	0.02973	1.22E-05	0.02496	1.14E-05
0.02093	1.21E-05	0.02630	1.34E-05	0.03027	1.22E-05	0.02556	1.14E-05
0.02133	1.22E-05	0.02825	1.35E-05	0.03054	1.23E-05	0.02556	1.15E-05
0.02193	1.23E-05	0.02892	1.36E-05	0.03107	1.24E-05	0.02576	1.16E-05
0.03020	1.24E-05	0.02939	1.37E-05	0.03134	1.24E-05	0.02704	1.16E-05
0.03154	1.24E-05	0.03033	1.38E-05	0.03175	1.25E-05	0.02771	1.17E-05
0.03259	1.25E-05	0.03134	1.39E-05	0.03228	1.26E-05	0.02798	1.18E-05
0.03329	1.26E-05	0.03249	1.40E-05	0.03403	1.27E-05	0.02812	1.18E-05
0.03349	1.27E-05	0.03363	1.41E-05	0.03430	1.27E-05	0.02839	1.19E-05
0.03396	1.27E-05	0.03443	1.42E-05	0.03430	1.28E-05	0.02886	1.20E-05
0.03490	1.28E-05	0.03484	1.42E-05	0.03564	1.29E-05	0.02879	1.20E-05
0.03504	1.29E-05	0.03558	1.43E-05	0.03578	1.30E-05	0.02939	1.21E-05
0.03564	1.30E-05	0.03564	1.44E-05	0.03558	1.30E-05	0.02986	1.22E-05
0.03712	1.30E-05	0.03645	1.45E-05	0.03591	1.31E-05	0.03027	1.22E-05
0.03813	1.31E-05	0.03672	1.46E-05	0.03632	1.32E-05	0.03027	1.23E-05
0.03826	1.32E-05	0.03712	1.47E-05	0.03658	1.33E-05	0.03033	1.24E-05
0.03914	1.33E-05	0.03759	1.48E-05	0.03685	1.33E-05	0.03094	1.24E-05
0.04008	1.34E-05	0.03806	1.49E-05	0.03699	1.34E-05	0.03128	1.25E-05
0.04035	1.34E-05	0.03833	1.49E-05	0.03732	1.35E-05	0.03215	1.26E-05
0.04075	1.35E-05	0.03867	1.50E-05	0.03833	1.36E-05	0.03275	1.26E-05
0.04102	1.36E-05	0.0395417	1.51E-05	0.03867	1.36E-05	0.0337621	1.27E-05
		0.0400793	1.52E-05	0.03968	1.37E-05	0.0369879	1.28E-05
		0.0403481	1.53E-05	0.03968	1.38E-05	0.0379288	1.28E-05
		0.040953	1.54E-05	0.03974	1.39E-05	0.0384664	1.29E-05
				0.04048	1.39E-05	0.0394073	1.30E-05
				0.04075	1.40E-05	0.0396761	1.30E-05
						0.0407513	1.31E-05

APPENDIX C

C1: Statistical analysis of first-order kinetic parameter in MABs

The statistical analysis was performed using 2007 Microsoft Excel and the results are summarized below:

Summary of statistical analysis to investigate the effects of MABR module configurations on first-order kinetic parameter

F-test for k' values	Since F < F critical (6.12 < 19) and p value > α (0.14> 0.05), the null hypothesis of equal variances was validated and t-test assuming equal variances was applied.
T-test for k' values	Since the t statistic < t critical (-2.17 < 2.78) and p value < α (0.09< 0.05) , the alternative hypothesis of unequal means was validated

Since the null hypothesis is that the mean difference (μ_1- μ_2) is equal to zero, this is a two-sided test. Therefore, the two-tail values were used for the t-test analysis.

APPENDIX D

D1 Figure 4.3
OXYGEN MICROELECTRODE CALIBRATION FOR RBCs

D1-1. RBC Biofilm (Stage#2)

Table D1-1-1: Data from calibration process of oxygen microelectrode

pA	mg/L
25	0
925.5	Air-saturated water (8.6)

B2. RBC Biofilm (Stage#4)

Table D1-1-2: Data from calibration process of oxygen microelectrode

pA	mg/L
5	0
2360	Air-saturated water (8.6)

D2. Figure 4.6

Location S2#1		Location S2#2		Location S2#3		Location S2#4	
z	**DO**	***z***	**DO**	***z***	**DO**	***z***	**DO**
[µm]	**[mg/L]**	**[µm]**	**[mg/L]**	**[µm]**	**[mg/L]**	**[µm]**	**[mg/L]**
-500	7.03	-550	6.77	-500	6.64	-500	6.29
-400	7.01	-450	6.72	-400	6.63	-400	6.24
-300	6.92	-350	6.71	-300	6.59	-300	6.26
-200	6.84	-250	6.71	-250	6.59	-200	6.29
-100	6.53	-200	6.74	-200	6.69	-100	6.2
-50	6.39	-150	6.71	-150	6.54	0	5.82
0	6.13	-100	6.56	-100	6.38	50	5.6
50	5.78	-50	6.41	-50	6.39	100	5.7
100	5.41	0	5.73	0	6.36	150	5.45
150	4.98	50	5.82	0	5.47	200	5.35
200	4.68	100	5.67	50	5.43	250	4.71
250	4.13	150	5.4	100	5.42	300	4.37
300	3.29	200	5.2	150	5.38	350	4.47
350	2.9	250	4.94	200	5.8	400	4.44
400	1.83	300	4.24	250	5.26	450	3.95
450	1.18	350	3.56	300	5.44	500	3.68
500	0.72	400	2.61	350	5.3	550	3.47
550	0.23	450	1.54	400	5.09	600	2.98
600	0.01	500	0.71	450	5.03	650	3.06
650	0	550	0	500	4.99	700	2.48
700	0	600	0	550	4.68	750	2.3
750	0			600	4.33	800	1.93
				650	4.08	850	1.29
				700	4.16	900	1.16
				750	3.52	950	0.71
				800	2.8	1000	0.51
				850	2.56	1050	0.28
				900	2.03	1100	0.04
				950	1.87	1150	0.01
				1000	1.51		
				1050	1.17		
				1100	0.95		
				1150	0.5		
				1200	0.33		
				1250	0.19		
				1300	0.05		
				1350	0.01		
				1400	0		

D2. Figure 4.6

Location S4#1		Location S4#2		Location S4#3		Location S4#4	
z	DO	z	DO	z	DO	z	DO
[µm]	[mg/L]	[µm]	[mg/L]	[µm]	[mg/L]	[µm]	[mg/L]
-500	7.22	-500	7.32	-500	7.32	-500	6.55
-450	7.22	-450	7.41	-400	7.28	-450	6.66
-400	7.26	-400	7.41	-300	7.35	-400	6.71
-350	7.11	-350	7.39	-200	7.24	-350	6.72
-300	7.26	-300	7.43	-150	6.81	-300	6.73
-250	7.2	-250	7.11	-100	6.4	-250	6.74
-200	7	-200	6.91	-50	6.11	-200	6.75
-150	6.89	-150	6.74	0	5.25	-150	6.71
-100	6.78	-100	6.5	50	4.82	-100	6.63
-50	6.57	-50	6.09	100	4.6	-50	6.53
0	6.14	0	6.12	150	4.02	0	6.18
50	5.77	50	5.71	200	3.02	50	5.93
100	4.67	100	5.49	250	1.88	100	5.72
150	3.57	150	4.17	300	1.43	150	4.92
200	3	200	3.83	350	0.58	200	4.12
250	2.05	250	2.46	400	0.09	250	3.38
300	1.56	300	1.62	450	0	300	2.64
350	0.56	350	0.61			350	1.47
400	0.04	400	0.26			400	1.02
450	0	450	0.04			450	0.24
		500	0			500	0.02
						550	0.02

D3. Polynomial curve fitting for oxygen concentration profiles in RBC biofilms

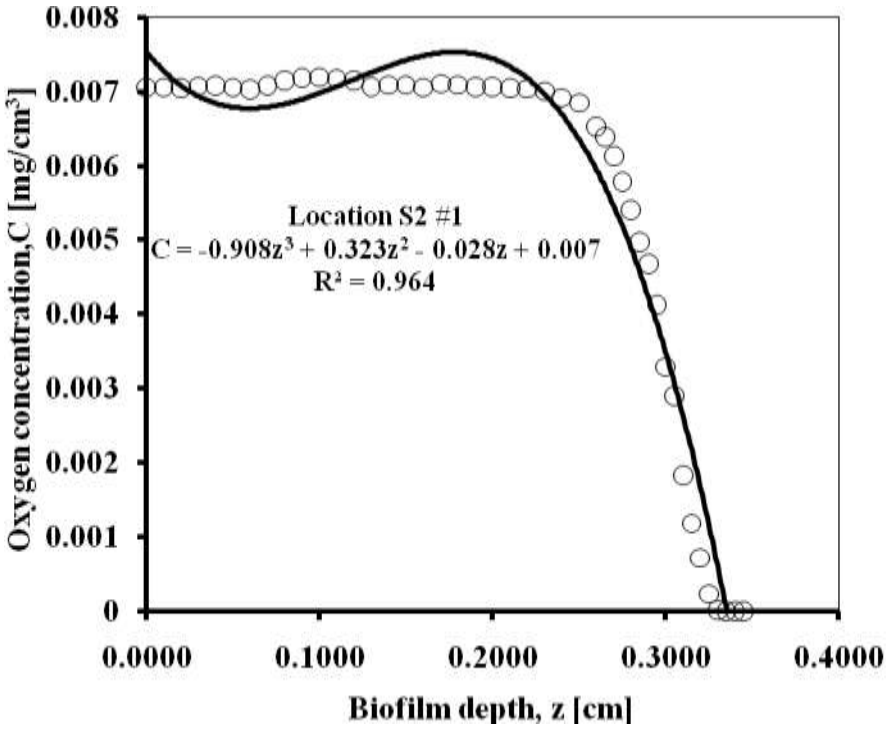

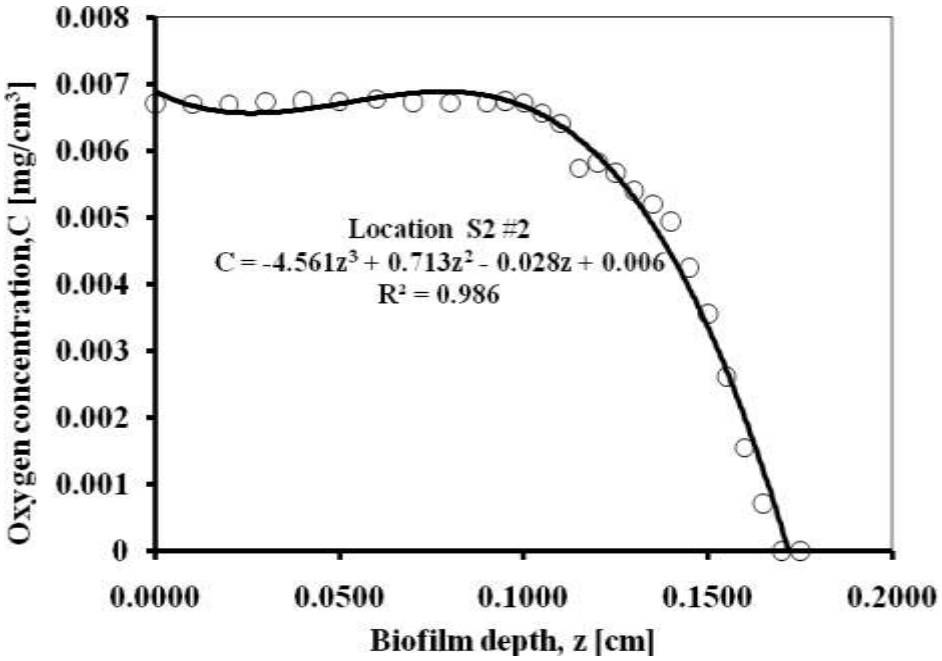

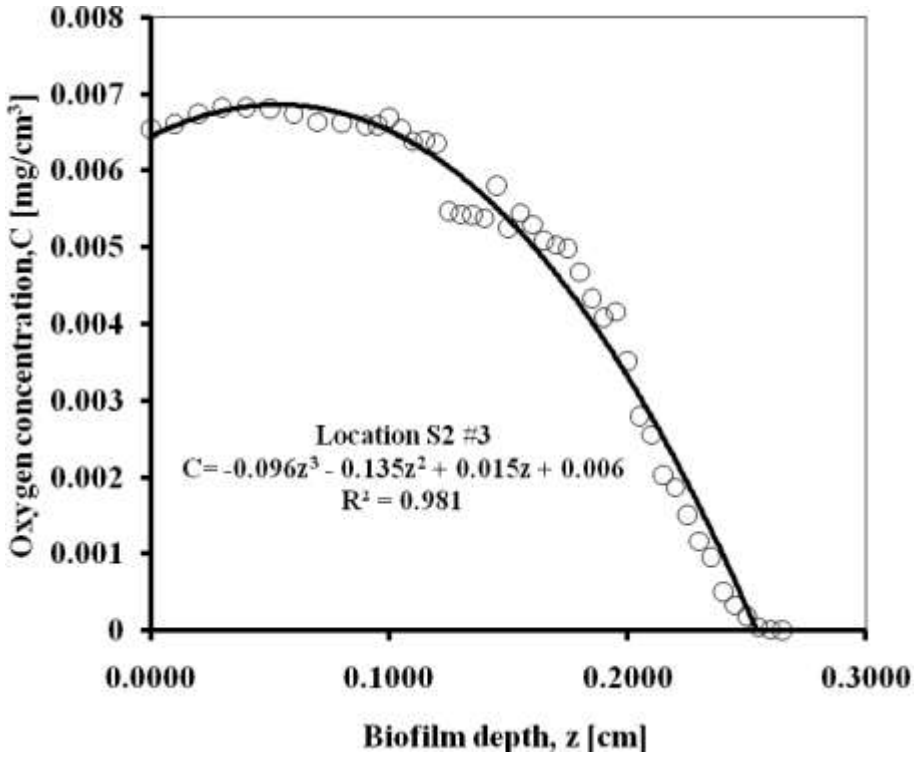
0.008
0.007
0.006
0.005
0.004
0.003
0.002
0.001
0
Oxygen concentration,C [mg/cm³]
Location S2 #3
C= -0.096z³ - 0.135z² + 0.015z + 0.006
R² = 0.981
0.0000
0.1000
0.2000
0.3000
Biofilm depth, z [cm]

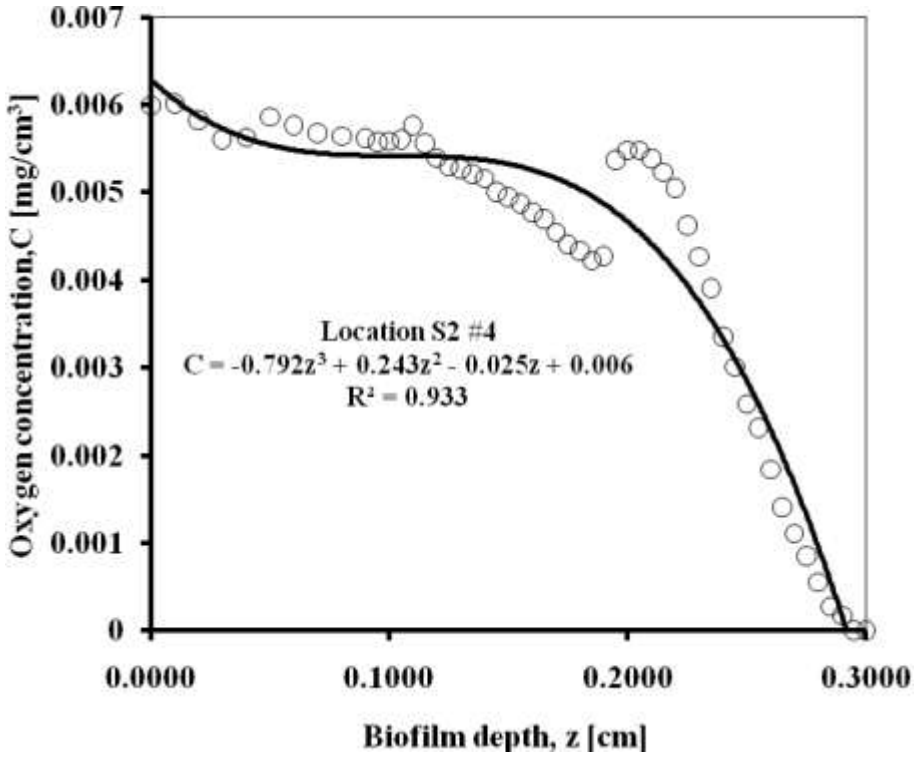
0.007
0.006
0.005
0.004
0.003
0.002
0.001
0
Oxygen concentration,C [mg/cm³]
Location S2 #4
C = -0.792z³ + 0.243z² - 0.025z + 0.006
R² = 0.933
0.0000
0.1000
0.2000
0.3000
Biofilm depth, z [cm]

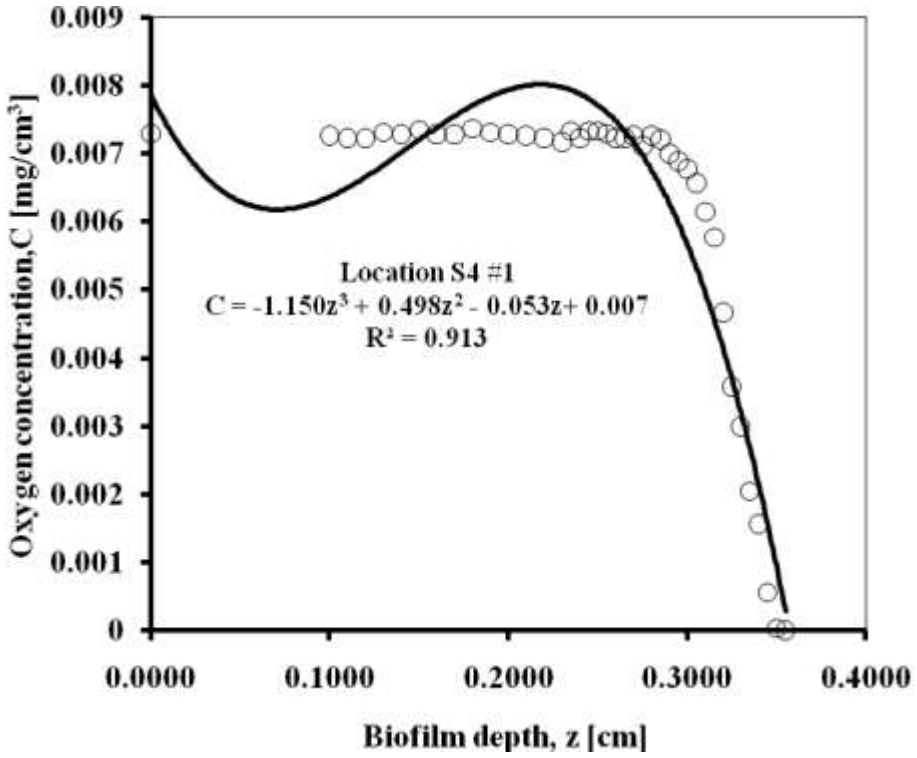
0.009
0.008
0.007
0.006
0.005
0.004
0.003
0.002
0.001
0
Oxygen concentration,C [mg/cm³]
Location S4 #1
C = -1.150z³ + 0.498z² - 0.053z+ 0.007
R² = 0.913
0.0000
0.1000
0.2000
0.3000
0.4000
Biofilm depth, z [cm]

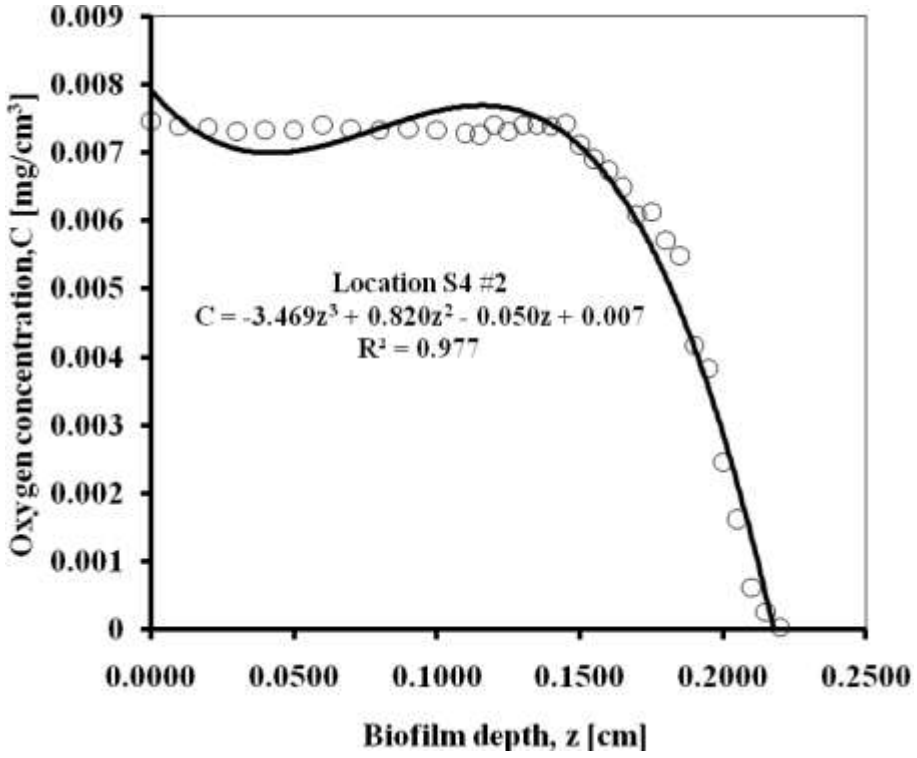
0.009
0.008
0.007
0.006
0.005
0.004
0.003
0.002
0.001
0
Oxygen concentration,C [mg/cm³]
Location S4 #2
C = -3.469z³ + 0.820z² - 0.050z + 0.007
R² = 0.977
0.0000
0.0500
0.1000
0.1500
0.2000
0.2500
Biofilm depth, z [cm]

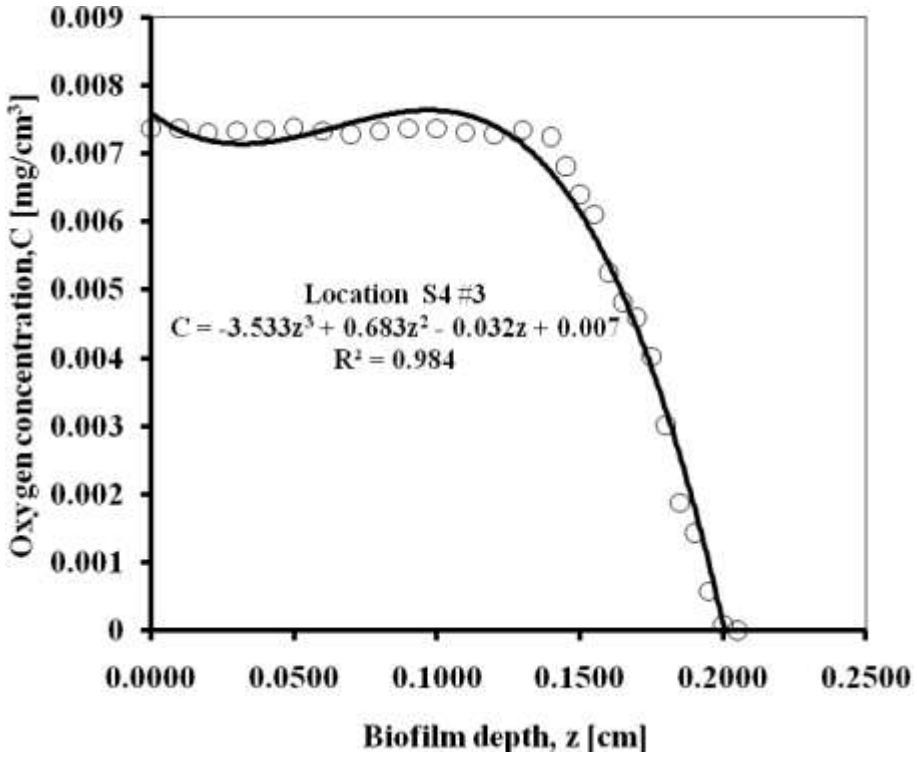
0.009
0.008
0.007
0.006
0.005
0.004
0.003
0.002
0.001
0
Oxygen concentration,C [mg/cm³]
Location S4 #3
C = -3.533z³ + 0.683z² - 0.032z + 0.007
R² = 0.984
0.0000
0.0500
0.1000
0.1500
0.2000
0.2500
Biofilm depth, z [cm]

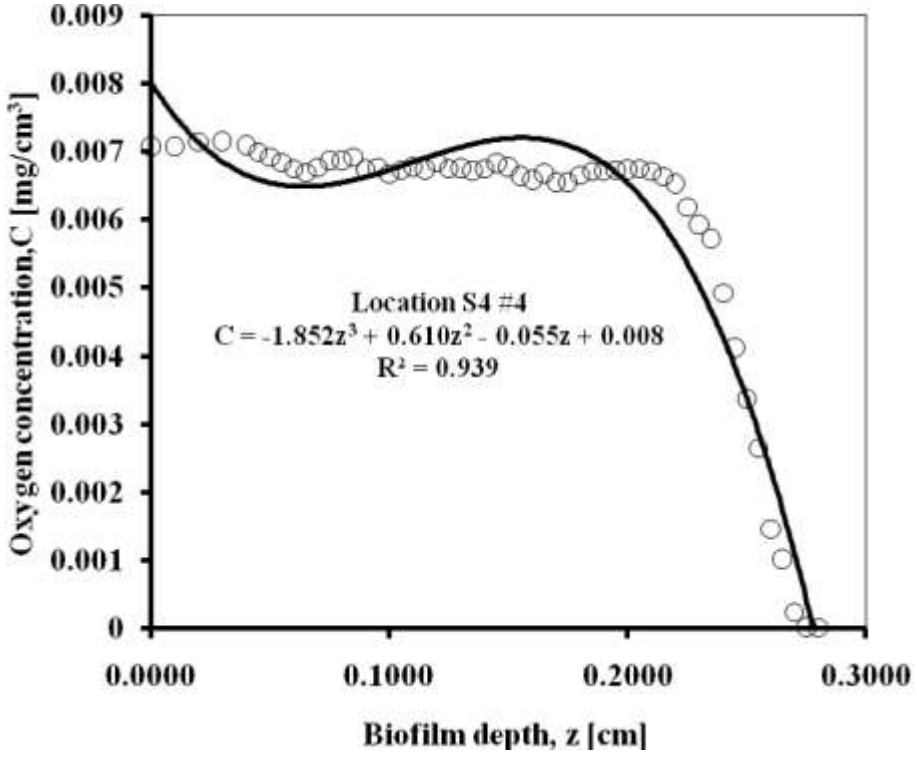
0.009
0.008
0.007
0.006
0.005
0.004
0.003
0.002
0.001
0
Oxygen concentration,C [mg/cm³]
Location S4 #4
C = -1.852z³ + 0.610z² - 0.055z + 0.008
R² = 0.939
0.0000
0.1000
0.2000
0.3000
Biofilm depth, z [cm]

D4. Figure 4.7

33 h		37 h		37 h	
Depth	**DO**	**Depth**	**DO**	**Depth**	**DO**
[µm]	**[mg/L]**	**[µm]**	**[mg/L]**	**[µm]**	**[mg/L]**
-500	6.12	-500	6.2	-500	6.52
-400	6.11	-400	6.11	-400	6.48
-350	6.13	-350	6.21	-350	6.54
-300	6.09	-300	6.11	-300	6.45
-250	6.1	-250	6.07	-250	6.48
-200	6.11	-200	6.21	-200	6.48
-150	6	-150	6.14	-150	6.3
-100	5.87	-100	6.11	-100	6.36
-50	5.71	-50	5.82	-50	6.12
0	5.42	0	5.63	0	5.89
50	5.01	50	5.35	50	5.43
100	4.28	100	4.29	100	4.73
150	3.64	150	3.61	150	3.86
200	2.94	200	2.83	200	2.65
250	2.13	250	2.23	250	2.07
300	1.3	300	1.7	300	1.54
350	0.39	350	0.67	350	0.53
400	0.11	400	0.13	400	0.01
450	0.01	450	0.03	450	0.01
500	0	500	0	500	0
***Time is defined as zero when the reactor was operated**					

D5. Figure 4.8

Location S2#1		Location S2#2		Location S2#3		Location S2#4	
Depth,z	D^*_{fz}	Depth,z	D^*_{fz}	Depth,z	D^*_{fz}	Depth,z	D^*_{fz}
[cm]	[Nil]	[cm]	[Nil]	[cm]	[Nil]	[cm]	[Nil]
0	0.1601193	0	0.1601119	0	0.160107	0	0.1601071
0.005	0.1601127	0.005	0.1601135	0.005	0.1601062	0.005	0.1601071
0.01	0.1601057	0.01	0.1601107	0.01	0.1601061	0.01	0.1601054
0.015	0.1600977	0.015	0.1601055	0.015	0.1601053	0.015	0.1601025
0.02	0.1600922	0.02	0.1601018	0.02	0.1601132	0.02	0.160099
0.025	0.1600818	0.025	0.160097	0.025	0.160103	0.025	0.1600911
0.03	0.160066	0.03	0.1600839	0.03	0.1601064	0.03	0.1600844
0.035	0.1600587	0.035	0.1600711	0.035	0.1601037	0.035	0.1600778
0.04	0.1600387	0.04	0.1600533	0.04	0.1600998	0.04	0.1600673
0.045	0.1600266	0.045	0.1600334	0.045	0.1600986	0.045	0.1600609
0.05	0.1600179	0.05	0.1600177	0.05	0.1600979	0.05	0.1600529
				0.055	0.1600921	0.055	0.1600479
				0.06	0.1600856	0.06	0.1600389
				0.065	0.1600809	0.065	0.1600308
				0.07	0.1600823	0.07	0.1600252
				0.075	0.1600704	0.075	0.1600204
				0.08	0.1600569	0.08	0.1600149
				0.085	0.1600523	0.085	0.1600096
				0.09	0.1600424	0.09	0.1600077
				0.095	0.1600395		
				0.1	0.1600327		
				0.105	0.1600263		
				0.11	0.1600223		
				0.115	0.1600139		
				0.12	0.1600106		
				0.125	0.1600079		
				0.13	0.1600053		
				0.135	0.1600047		

D6. Figure 4.9

Location S4#1		Location S4#2		Location S4#3		Location S4#4	
Depth,z	**D^*_{fz}**	**Depth,z**	**D^*_{fz}**	**Depth,z**	**D^*_{fz}**	**Depth,z**	**D^*_{fz}**
[cm]	**[Unitless]**	**[cm]**	**[Unitless]**	**[cm]**	**[Unitless]**	**[cm]**	**[Unitless]**
0.000	0.1603025	0.000	0.1603017	0.000	0.1602598	0.000	0.1601594
0.005	0.1602847	0.005	0.1602821	0.005	0.1602394	0.005	0.1601531
0.010	0.1602322	0.010	0.1602714	0.010	0.1602287	0.010	0.1601479
0.015	0.1601797	0.015	0.1602082	0.015	0.1602011	0.015	0.1601279
0.020	0.1601522	0.020	0.1601922	0.020	0.1601531	0.020	0.1601078
0.025	0.1601068	0.025	0.1601264	0.025	0.1600988	0.025	0.1600891
0.030	0.1600836	0.030	0.1600863	0.030	0.1600774	0.030	0.1600707
0.035	0.1600356	0.035	0.1600383	0.035	0.1600365	0.035	0.1600412
0.040	0.1600107	0.040	0.1600214	0.040	0.1600133	0.040	0.16003
		0.045	0.1600107			0.045	0.1600105
						0.050	0.1600051
						0.055	0.1600049

D7. Figure 4.10

Location S2#1		Location S2#2		Location S2#3		Location S2#4	
C	Rs	C	Rs	C	Rs	C	Rs
[$mgcm^{-3}$]	[$mgcm^{-3}s^{-1}$]	[$mgcm^{-3}$]	[$mgcm^{-3}s^{-1}$]	[$mgcm^{-3}$]	[$mgcm^{-3}s^{-1}$]	[$mgcm^{-3}$]	[$mgcm^{-3}s^{-1}$]
0.00578	-4.29E-06	0.00578	-4.29E-06	0.00547	-1.73E-06	0.0055	-2.34E-06
0.00541	-4.43E-06	0.00541	-4.43E-06	0.00543	-1.74E-06	0.0055	-2.46E-06
0.00498	-4.57E-06	0.00498	-4.57E-06	0.00542	-1.75E-06	0.0054	-2.58E-06
0.00468	-4.71E-06	0.00468	-4.71E-06	0.00538	-1.77E-06	0.0052	-2.70E-06
0.00413	-4.84E-06	0.00413	-4.84E-06	0.00580	-1.78E-06	0.0050	-2.82E-06
0.00329	-4.98E-06	0.00329	-4.98E-06	0.00526	-1.80E-06	0.0046	-2.94E-06
0.00290	-5.12E-06	0.00290	-5.12E-06	0.00544	-1.81E-06	0.0043	-3.06E-06
0.00183	-5.26E-06	0.00183	-5.26E-06	0.00530	-1.83E-06	0.0039	-3.18E-06
0.00118	-5.40E-06	0.00118	-5.40E-06	0.00509	-1.84E-06	0.0034	-3.30E-06
0.00072	-5.53E-06	0.00072	-5.53E-06	0.00503	-1.86E-06	0.0030	-3.42E-06
0.00023	-5.67E-06	0.00023	-5.67E-06	0.00499	-1.87E-06	0.0026	-3.54E-06
0.00001	-5.81E-06	0.00001	-5.81E-06	0.00468	-1.89E-06	0.0023	-3.66E-06
				0.00433	-1.90E-06	0.0018	-3.78E-06
				0.00408	-1.91E-06	0.0014	-3.90E-06
				0.00416	-1.93E-06	0.0011	-4.02E-06
				0.00352	-1.94E-06	0.0009	-4.14E-06
				0.00280	-1.96E-06	0.0006	-4.26E-06
				0.00256	-1.97E-06	0.0003	-4.38E-06
				0.00203	-1.99E-06	0.0002	-4.50E-06
				0.00187	-2.00E-06		
				0.00151	-2.02E-06		
				0.00117	-2.03E-06		
				0.00095	-2.05E-06		
				0.00050	-2.06E-06		
				0.00033	-2.07E-06		
				0.00019	-2.09E-06		
				0.00005	-2.10E-06		
				0.00001	-2.12E-06		

D8. Figure 4.11

Location S4#1		Location S4#2		LocationS4#3		LocationS4#4	
C	**Rs**	**C**	**Rs**	**C**	**Rs**	**C**	**Rs**
[$mgcm^{-3}$]	**[$mgcm^{-3}s^{-1}$]**	**[$mgcm^{-3}$]**	**[$mgcm^{-3}s^{-1}$]**	**[$mgcm^{-3}$]**	**[$mgcm^{-3}s^{-1}$]**	**[$mgcm^{-3}$]**	**[$mgcm^{-3}s^{-1}$]**
0.00614	-2.18E-06	0.00612	-1.01E-05	0.00525	-1.02E-05	0.00618	**-6.46E-06**
0.00577	-2.25E-06	0.00571	-1.06E-05	0.00482	-1.08E-05	0.00593	-6.74E-06
0.00467	-2.31E-06	0.00549	-1.12E-05	0.00460	-1.13E-05	0.00572	-7.02E-06
0.00357	-2.37E-06	0.00417	-1.17E-05	0.00402	-1.18E-05	0.00492	-7.30E-06
0.00300	-2.44E-06	0.00383	-1.22E-05	0.00302	-1.24E-05	0.00412	-7.58E-06
0.00205	-2.50E-06	0.00246	-1.27E-05	0.00188	-1.29E-05	0.00338	-7.86E-06
0.00156	-2.56E-06	0.00162	-1.33E-05	0.00143	-1.34E-05	0.00264	-8.14E-06
0.00056	-2.62E-06	0.00061	-1.38E-05	0.00058	-1.40E-05	0.00147	-8.42E-06
0.00004	-2.69E-06	0.00026	-1.43E-05	0.00009	-1.45E-05	0.00102	-8.70E-06
		0.00004	-1.48E-05			0.00024	-8.99E-06
						0.00002	-9.27E-06
						0.00002	-9.55E-06

APPENDIX E

E1: Statistical analysis of kinetic parameters in RBC biofilms

The statistical analysis was performed using 2007 Microsoft Excel and the results are summarized below:

Summary of statistical analysis to investigate the effects of different treatment stages of RBC biofilm systems

F-Test for $(u_m/Y)/K_s$values	Since F < F critical (0.13< 0.11) and p value > α (0.06> 0.05), the alternative hypothesis of unequal variances was validated and t-test assuming unequal variances was applied .
T-test for $(u_m/Y)/K_s$ values	Since the t statistic < t critical (-1.77 < 2.78) and p value < α (0.15> 0.05) , the alternative hypothesis of unequal means was validated